Analysis and Validation of an Artifact Resistant Design for Oxygen Saturation Measurement Using Photo Pletyhsmographic Ring Sensors

by

Phillip Andrew Shaltis

Bachelor of Arts in Physics
Albion College, 1999

Bachelor of Science in Mechanical Engineering
University of Michigan, 2000

Submitted to the Departments of Electrical Engineering and Computer Science and Mechanical Engineering in Partial Fulfillment of the Requirements for the Degrees of

Master of Science in Electrical Engineering and Computer Science
Master of Science in Mechanical Engineering

at the

Massachusetts Institute of Technology
June 2004

Signature of Author: .....
Department of Mechanical Engineering
May 9, 2004

Certified by: .....
H. Harry Asada
Ford Professor of Mechanical Engineering
Thesis Supervisor

Accepted by: .....
Ain A. Sonin
Chairman, Department Committee on Graduate Students
Department of Mechanical Engineering

Accepted by: .....
Arthur C. Smith
Chairman, Department Committee on Graduate Students
Department of Electrical Engineering and Computer Science

Analysis and Validation of an Artifact Resistant Design for Oxygen Saturation Measurement Using Photo Pletyhsmographic Ring Sensors

by

Phillip Andrew Shaltis

Submitted to the Departments of Electrical Engineering and Computer Science and Mechanical Engineering on May 9, 2004 in Partial Fulfillment of the Requirements for the Degrees of
Master of Science in Electrical Engineering and Computer Science
Master of Science in Mechanical Engineering

ABSTRACT

Recent advances in continuous noninvasive health monitoring technologies provide clinicians and researchers with a previously unrealistic opportunity for closely tracking the developments and treatments of various pathologies both within and outside of a clinical setting. At the same time, miniaturized, wireless communication technologies have greatly enhanced the transmission of sensor data while reducing the size requirements for traditional, wearable sensors. The synergism of these innovations has led to the development of the Ring Sensor, a miniaturized, telemetric, photo plethysmograph sensor for continuous health monitoring. Previous work on the Ring Sensor has led to significant power savings in regards to data acquisition and transmission. Additionally, early long-term monitoring tests have indicated that the Ring Sensor is capable of acquiring a reliable waveform nearly 30% of the time. However, the utility of the Ring Sensor has remained somewhat limited. This thesis addresses several of the remaining issues associated with the Ring Sensor.

The main design consideration associated with the Ring Sensor is achieving minimal power consumption while maintaining high signal quality. To this end, significant effort has been channeled to the development of an appropriate motion artifact model, representing the complex interplay between internal hemodynamics and external influences. Additionally, an artifact resistant, power-efficient, high-speed modulation scheme has been incorporated into the design of the Ring Sensor. It has been shown that this design significantly reduces the amount of data corrupted by motion while also minimizing the power consumed by the LEDs (one of the single largest power consuming elements).

This thesis also details the refinement of both the analog signal processing circuit and the redesigning of the sensor band for a more secure device interface. In particular, the order and type of filtering utilized by the Ring Sensor have been optimized for signal quality and stability. An improved sensor unit assembly provides a secure, pressurized contact with the patient's skin while protecting the optical components and wires from the external environment., while additional sensors, incorporated into both the sensor band and the ring unit, provide temperature and light feedback for signal quality assurance. In addition to these advancements, preliminary work towards sensor calibration for oxygen saturation measurements is provided. The thesis concludes with promising results obtained from field testing work conducted in the Massachusetts General Hospital's Pulmonary Function Testing Lab.

Thesis Supervisor: H. Harry Asada
Title: Ford Professor of Mechanical Engineering
Director, d'Arbeloff Laboratory for Information Systems and Technology

Acknowledgements

This thesis would not have been possible without the guidance, support, and friendship of the following people.

I would first like to thank my thesis advisor, Professor Harry Asada, for his tireless commitment to my growth as both a scholar and a researcher. I am grateful for his willingness to continually push the bounds of my abilities and for never letting me be satisfied with "good enough." His faith in my abilities has been a source of strength throughout the project.

I would also like to thank Dr. Andrew Reisner for his friendship and support throughout this project. His insights and unique medical perspective have not only enhanced my understanding and appreciation of the underlying physiology of the plethysmograph signal, but have helped me to better understand how essential it is for an engineer to be able to visualize their work from both a clinician's and a patient's perspective.

Dr. Sokwoo Rhee and Dr. Yi Zhang have been extraordinary mentors, role models, and friends. I would like to thank Sokwoo for helping me along with the project when I was first getting started and for always being willing to answer my questions, no matter how trivial. Yi has been an amazing person to know and with whom to work. Your insights, attention to detail, and wonderful spirit have been an inspiration. Most importantly, though, I thank you for your friendship and support both within and outside of the lab.

To the *Asada Group* – you guys are the best. The people may change, but the spirit of the lab always remains. From lunches to volleyball to post-qualifier parties, you guys help to make the days bearable even when there are umpteen sponsor visits scheduled the day before a big homework assignment is due. Thanks for being there and for always making sure that life in the lab is entertaining.

Melissa, what can I say? You are my best friend, my closest companion, my harshest critic (other than myself), and my smile each and every day. You make my life in so many ways. Thank you for your patience, love, and compassion. You mean everything to me.

Finally, I would like to thank my family. I can't begin to express what all of you mean to me. Your unconditional love and support give me strength and keep me sane. Mom – thank you for always listening to me and for always being there, no matter what. Dad – thank you for being such an amazing role model, teacher, and friend. I hope that someday I can be as successful as you. Bill – thanks for putting up with me when we were growing up. You are an incredible guy with amazing talents and someone who I am proud to call my brother.

Table of Contents

List of Figures & Tables

Chapter 1 Introduction

Non-intrusive, reliable vital sign monitoring has become an essential tool for enabling independent lifestyles for the growing numbers of elderly adults. Additionally, both minimally invasive and noninvasive sensor technologies have received growing interest from both medical and military interests because of their increasing reliability and richness of real-time sensor information [1]. Continuous monitoring both within and outside of a clinical setting provides clinicians and researchers with a previously unrealizable opportunity for closely monitoring the developments and treatments of various pathologies. At the same time, miniaturized, wireless communication technologies have greatly enhanced the transmission of sensor data while reducing the size requirements for traditional, wearable sensors (WS). In the end, reliable, wearable sensors are the key to improved diagnosis and treatment of all levels of patient care.

1.1 Wearable Sensor Technologies

1.1.1 Wearable Sensor Design Paradigm

The monitoring environments for out-of-hospital, wearable devices demand a new paradigm in noninvasive sensor design. As has been stated in various publications [2], [3], [4], there are several important challenges associated with wearable sensor designs and implementations. Compactness, stability of signal, motion and other disturbance rejection, durability, data storage and transmission, and low power consumption comprise the major design considerations. Additionally, since wearable sensors are to be worn without direct doctor supervision, it is

imperative that they are simple to use and comfortable to wear for long periods of time. A challenge unique to wearable sensor design is the tradeoff between patient comfort, or long-term wearability, and reliable sensor attachment. While it is nearly needless to say that WS technology must be safe, it should be noted that there have been tragic reports of serious injury resulting from early home monitoring technology [5].

1.1.2 Decision Making Systems

The physiologic information generated by noninvasive technologies must trigger some appropriate system action to improve health outcomes, while differentiating between abnormal patient states and corrupted data. These difficult requirements necessitate carefully designed wearable sensors, as well as innovative post-processing and intelligent data interpretation. Post-processing of sensor data has led to improvements in sensor usability, as illustrated by recent advances in pulse oximetry technology [6], [7], [8]. However, reliable, "intelligent" data interpretation is still in the early stages of development. For example, real-time alarm "algorithms" using simple thresholds for measured parameters, like heart rate and oxygen saturation, have demonstrated high rates of false alarms. [9], [10]. Similarly, algorithms for off-line, retrospective data analysis require further research. Studies of novel automated "triage" software used to interpret hours of continuous non-invasive ECG data of monitored outpatients suggest that the software's diagnostic yield is not equal to a human's when it comes to arrhythmia detection [11], [12]. It will presumably require further improvements in WS hardware, middleware and software in order to fully exploit the promise of wearable ambulatory monitoring systems.

1.1.3 Existing Wearable Sensor Modalities

There are already several wearable sensors, in various stages of technologic maturity, which measure established cardiopulmonary "vital signs," such as: heart rate, arterial blood pressure, arterial oxygen saturation, respiratory rate, temperature, and even cardiac output. Wearable electrocardiogram systems represent the most mature WS technology. Holter and related ambulatory electrophysiologic monitoring solutions have established utility in the diagnosis of cardiac arrhythmias [13], [14], [15]. Alternatively, it has been shown that cardiac output can be extracted from thoracic bioimpedance measurements as well as other information such as, pulsatile blood volumes, respiratory volumes, and intracellular and extracellular fluid balances.

Ambulatory systems for arterial blood pressure measurement also exist. Most standard solutions employ a portable oscillometric cuff that fits around the wrist or upper arm. Unfortunately, these solutions require the wearer to remain still during measurements and provide only discrete waveforms [16]. An alternative ABP monitoring device that is worn on the subject's wrist and fingers is the Portapres®. The Portapres® utilizes the volume clamp technique to continuously measure ABP and is currently capable of storing over 60 hours of data at a time [17], [18].

Various wrist-type and fingertip PPG and pulse oximetry devices have been developed in the past decade. Standard, commercially available PPG and oximetry devices include models made by Seiko (Pulse Graph®) [19] and Nonin (Onyx®) [20]. Although these devices are easier to wear than previous generations, they are limited in terms of data collection and storage. In fact, neither device is capable of wirelessly transferring data for long-term storage or additional analysis. Understanding the aforementioned design considerations and limitations of existing devices has shaped the course the Ring Sensor's overall development. As will be illustrated in

the follow sections, the development of the Ring Sensor has stressed first an understanding of and then the subsequent elimination of front-end signal artifacts. By implementing an electro-mechanical design that is sensitive to the true causes of signal corruption, significant improvements in overall signal quality can be achieved and sensor effectiveness for various environments can be improved.

1.2 Advantages of the Ring Sensor Design

The Ring Sensor is a wireless PPG sensor that is, in many ways, superior to existing fingertip monitoring devices.

1.2.1 Motion Artifact Reduction

Perhaps the most important consideration for any noninvasive continuous monitoring device is its susceptibility to patient motion. Traditional pulse oximeters such as the N-395®, developed by companies such as Nellcor, depend heavily on fingertip capillary pulsations. Although the fingertip is rich in capillary blood, it is also highly susceptive to patient motions. Since pressures in capillaries are much lower than arteries, small external forces can easily occlude or alter normal blood flow. In fact, recent work in the lab based upon this strong motion influence has led to the development of the fingernail sensor [21]. The fingernail sensor uses the significant changes in capillary and tissue blood volume at the fingertip to capture finger motions and actions. The Ring Sensor, however, breaks tradition and utilizes arterial pulsations at the finger base.

The finger base is ideal for patient monitoring because it has fewer degrees of freedom than the wrist and because the effects of finger motions on the vasculature of the base of the finger are far smaller. For example, bending of the finger for actions such as typing have little affect on the

finger base since the magnitude of the motion is much smaller. Additionally, since the base of the finger is rarely used to interact with the patient's environment (touching, feeling, etc.) it should be possible to maintain a more robust waveform.

1.2.2 Early Warning Device

Another important feature of the Ring Sensor is that it is capable of being used as an early warning device for cases of extreme patient trauma. For example, patients with internal bleeding will have certain repeatable indicators of cardiovascular trauma. One of the earliest internal responses to cardiovascular trauma is a significant reduction of blood flow to the periphery [22]. The fingers, toes, and ears are amongst the first areas of the body for flow reduction to occur. However, as cited by recent studies, the finger is perhaps the best location for vital sign monitoring [23]. The primary vasculature of the finger is located near the surface and therefore makes it optimal for monitoring these changes in arterial blood flow using non-invasive optoelectronic sensors. Thus, by monitoring the arterial blood flow of the patient's finger base, the Ring Sensor is capable of detecting these important cardiovascular warning signs. In fact, through sensor fusion, it should be possible to differentiate between cases of vasoconstriction related to the patient's environment (such as temperature changes) and cases of vasoconstriction occurring because of internal response mechanisms.

1.2.3 Acceptable Sensor Location

Finally, and perhaps most importantly to the consumer, the Ring Sensor is designed such that it is acceptable for patient's to wear for long periods of time. Unlike fingertip devices, which are bulky and obstruct tactile interaction, the Ring Sensor is worn by the patient as a finger ring. This unique design is a readily accepted jewelry item for both men and women. Additionally,

unlike watches, people in almost every environment wear finger rings, such as wedding bands. Rings are worn in the shower, at work, and during sporting activities because they are light weight and do not interfere with desired motions. Thus, the Ring Sensor is an ideal design for continuous monitoring applications.

1.3 Disadvantages of the Ring Sensor

Like all sensors, there are certain limitations and disadvantages to the design. The following section details some of the current limitations of the Ring Sensor technology.

1.3.1 Surface Measurements

Like all PPG devices, the Ring Sensor utilizes light absorption to monitor both oxygen saturation and pulse rate. Figure 1-1 shows the typical waveform of a photoplethysmograph signal obtained from a human subject ***at rest.*** The signal consists of a large segment of DC signal and a small, superimposed AC signal. The DC component of photon absorption results from light passing through various non-pulsatile media, including tissue, bones, venous blood, and non-pulsatile arterial blood. Assuming that these are kept constant, a band-pass filter can eliminate this nonpulsatile component.

Unfortunately, noninvasive designs based on light absorption are inherently susceptive to changes in local blood distribution caused by cutaneous and subcutaneous blood flow regulation. These changes in skin blood flow can be initiated by everything from changes in emotional state to external environment temperature fluctuations [24]. Even though the main Ring Sensor signal is from digital artery pulsations, a significant fraction of the detected Ring Sensor PPG signal results from capillary blood flow near the surface of the skin. Therefore, like all noninvasive PPG devices, the Ring Sensor's signal is also susceptible to the aforementioned surface blood

flow changes. Power spectrum analysis reveals that this motion artifact often overlaps with the true pulse signal at a frequency of approximately 1 Hz. Therefore a simple noise filter based on frequency separation does not work for PPG Ring Sensors to eliminate motion artifact.

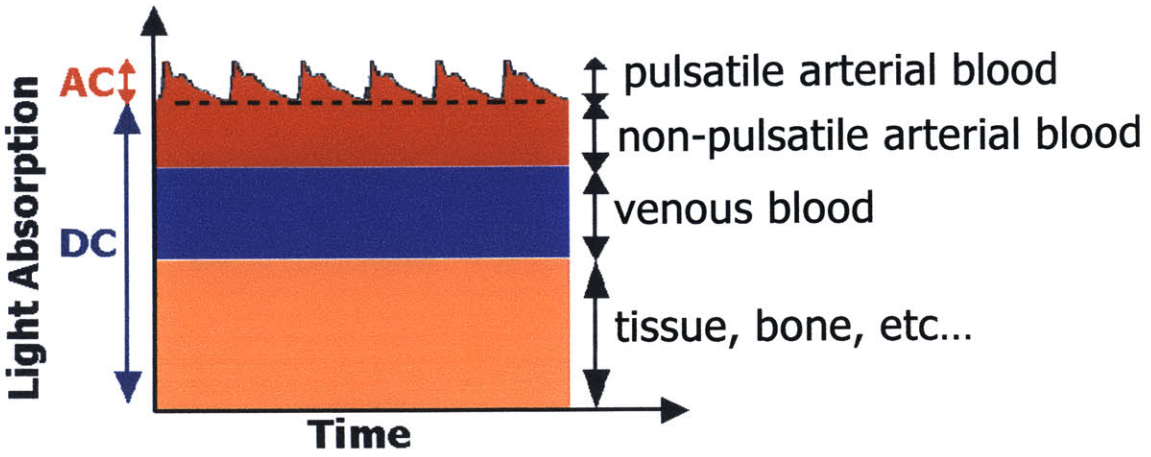

Figure 1-1: Illustrative representation of the relative photon absorbance for various sections of the finger. The DC component is significantly larger than the AC component.

1.3.2 Peripheral Location

Since the Ring Sensor utilizes an LED-photodetector combination for noninvasive health monitoring, it requires a fairly thin layer of skin and tissue for signal measurement. The periphery of the body is ideal for this requirement. Unfortunately, since the sensor is attached at the periphery, it is difficult to directly monitor various components of core cardiovascular function. This means that changes in blood flow to vital internal organs such as the brain, heart, and kidneys cannot be directly monitored, but must be inferred from the available measurements. Even though this is a notable disadvantage of the device, it is important to realize that fingertip PPGs are still widely accepted by medical physicians because of their utility. Ultimately, some information about the performance of the cardiovascular system is better than no information.

1.4 Recent Ring Sensor Advances

Perhaps the main design consideration associated with the Ring Sensor is achieving minimal power consumption while maintaining high signal quality (minimizing both motion and light artifacts). To this end, significant effort has been channeled into the development of an appropriate motion artifact model, representing the complex interplay between internal hemodynamics and external influences. Also, carrying a large battery pack is not acceptable for long-term applications. The whole sensor system must run continually using a small battery. One of the latest advances associated with the design of the Ring Sensor has been the incorporation of an artifact resistant, power-efficient, high-speed modulation design [25]. It has been shown that this design significantly reduces the amount of data corrupted by motion while also minimizing the power consumed by the LEDs (one of the single largest power consuming elements).

Additional work has gone into the refinement of both the analog signal processing circuit and the redesigning of the sensor band for a more secure device interface. In particular, the order and type of filtering utilized by the Ring Sensor have been optimized for signal quality and stability. The improved sensor unit assembly provides a secure, pressurized contact with the patient's skin while protecting the optical components and wires from the external environment. Finally, extra sensors have been incorporated into both the sensor band and the ring unit. The measurements from these additional temperature and light sensors provide environmental feedback for signal quality assurance. The following work details each of these advancements and concludes with promising results obtained from field testing work conducted in the Massachusetts General Hospital's Pulmonary Function Testing Lab.

Chapter 2 History of the Ring Sensor

2.1 Preliminary Ring Design

The Ring Sensor project began in 1996 with the premise of providing a wireless, 24-hour patient monitoring device [26]. In particular, the focus of the project was to combine wireless communication and miniaturization technologies with clinically useful sensor modalities, such as photoplethysmography and pulse oximetry. The basic components of the design consist of optoelectronic modules, a CPU, an RF transmitter, a battery, and a ring chassis (Figure 2-1).

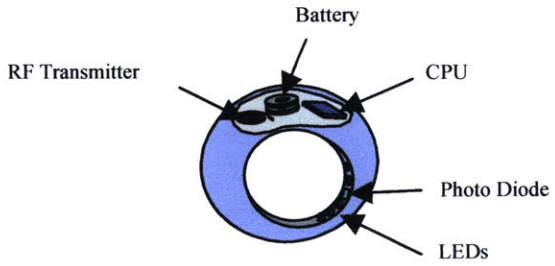

Figure 2-1: Conceptual diagram of the Ring Sensor.

Early design prototypes focused on minimal power consumption and reliable signal acquisition and transmission. Initial findings suggested that, with respect to power consumption, two of the limiting design factors were LED on-time and telemetric baud rate. By implementing a design consisting of PIN photodiodes and a faster transistor for the telemetric transmitter, significant power savings could be realized. Although bulky by commercially acceptable standards, early prototypes demonstrated promising performance during in-lab testing (Figure 2-2).

(a.) (b.)

Figure 2-2: Early versions of the Ring Sensor. (a.) 1997 prototype utilizing 6 circuit boards for data acquisition and transmission. (b.) 1998 prototype with miniaturized electronic components.

2.2 Artifact Resistant Design

Early ring prototypes continued to possess traditional wearable sensor limitations. Like all wearable, optically-based sensors, the Ring Sensor was susceptive to disturbances such as patient motion, physical interactions with the patient's environment, and changes in ambient lighting. Additionally, since the preliminary ring chassis consisted of a solid ring, holding the optical components, issues associated with the potential development of finger tissue necrosis via local ischemia required attention. A tradeoff between the amount of applied pressure and signal fidelity was necessitated. Finally, as described earlier, attention to power consumption optimization continued to be a primary design focus. Significant advances were made through the doctoral work of Dr. Sokwoo Rhee. A new design utilizing a double-ring configuration was developed to lessen the influence of both mechanical and optical disturbances, while avoiding unnecessarily large amounts of local band pressure. Additionally, tremendous progress was realized in the optimization of a minimal power budget for the Ring Sensor [27].

2.2.1 Double-Ring Architecture

As previously mentioned, early models of the Ring Sensor were extremely susceptive to external influences such as interaction with the user's environment and changes in ambient lighting conditions. To resolve several of these issues an isolating ring configuration, which separated the sensor unit from the heavier ring body, was implemented (Figure 2-3).

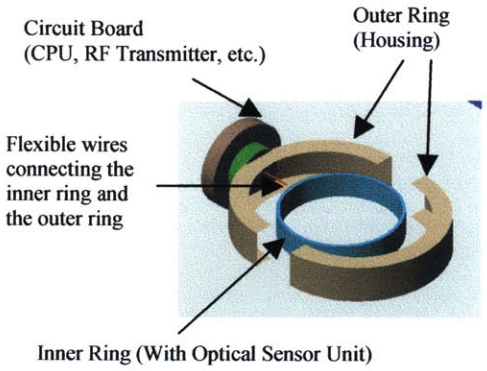

Figure 2-3: Illustration of isolating ring concept [27].

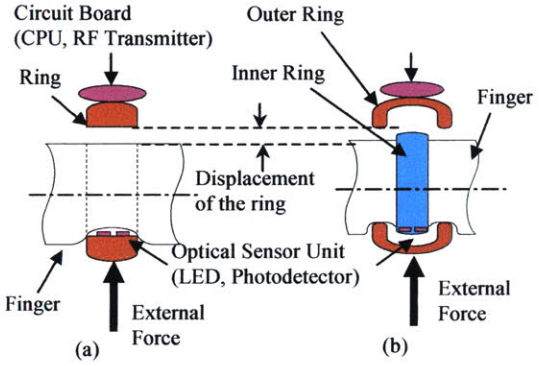

Figure 2-4: Comparison of ring body reactions to external force. (a.) single body ring presses optical components into skin; (b.) isolating ring distributes external force around separated sensors [27].

The isolating ring design consists of a flexible inner ring for the optical components and a mechanically decoupled, solid outer ring that both holds the circuitry and protects the inner ring from ambient light and external forces. Instead of directly transmitting impacts to the optical sensors, as happens for a single ring configuration (Figure 2-4a), the two feet of the bridge-like outer ring surround the sensor band and accordingly distribute all external forces to the bone of the finger (Figure 2-4b). Therefore, this design significantly reduces motion artifact problems arising from both external forces and sudden accelerations linked to the inertia of the outer ring and circuit board. An additional advantage of the double ring design is that it provides a natural shield against ambient light. The feet of the outer ring block much of the light which would

normally impinge upon the photodetectors. Therefore, the effects of changes in ambient lighting were also significantly reduced.

2.2.2 Power Budget Optimization

The basic circuit layout for the Ring Sensor consists of an LED modulation and driving circuit, a signal conditioning circuit for the photodetector, a microprocessor for scheduling, data sampling, and transmission, and an RF transmitter (Figure 2-5).

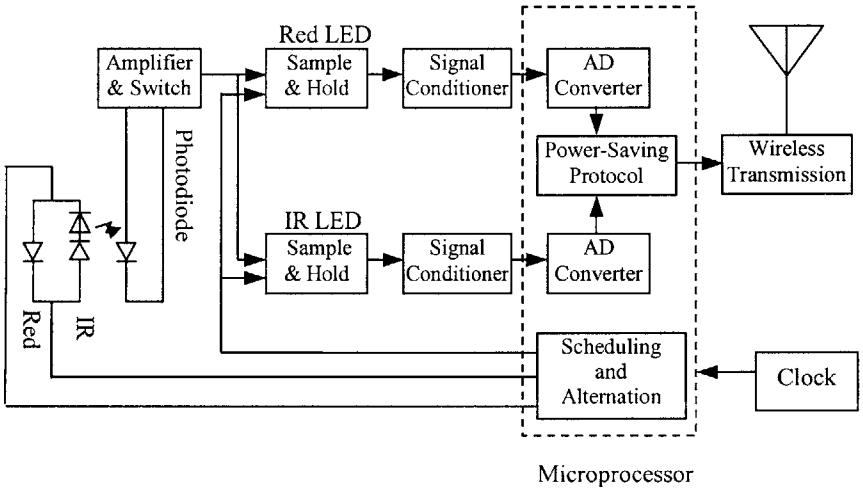

Figure 2-5: Block diagram of photoplethysmography and wireless transmission circuitry used by the Ring Sensor [27].

The circuits used for both the PPG sensor and the wireless transmitter are standard, but optimized for extremely low power consumption. By reducing the power consumed by the LEDs and the RF transmitter, which accounted for nearly 70% of the total power required by the Ring Sensor, Dr. Rhee recognized that significant power savings could be attained. A basic model for each of the devices was developed to optimize the CPU clock speed for minimum power consumption. The derivation of this power consumption model is beyond the scope of this paper, but a detailed summary is available in other publications [28]. Electrical components

for the Ring Sensor were then chosen based on power consumption characteristics and the results of the optimization model.

In addition to the clock optimization, the LEDs were configured in a reflective sensor configuration to further reduce power requirements. We note that LED illumination intensity is directly proportional to the supplied current. Also, according to the Lambert-Beer law the intensity of light passing through a homogenous medium decreases exponentially with distance [29]. Therefore, by reducing the separation distance of the optical sensors the power required to acquire a PPG waveform can be reduced.

The results of the power minimization work led to significant improvements in device lifetime. It was found that the optimized Ring Sensor could run *continuously* for more than 23 days using only a 3V, 220 mAh lithium coin battery. The average total power consumed by the device was reduced to 1/7 of that required by the original design (Figure 2-6).

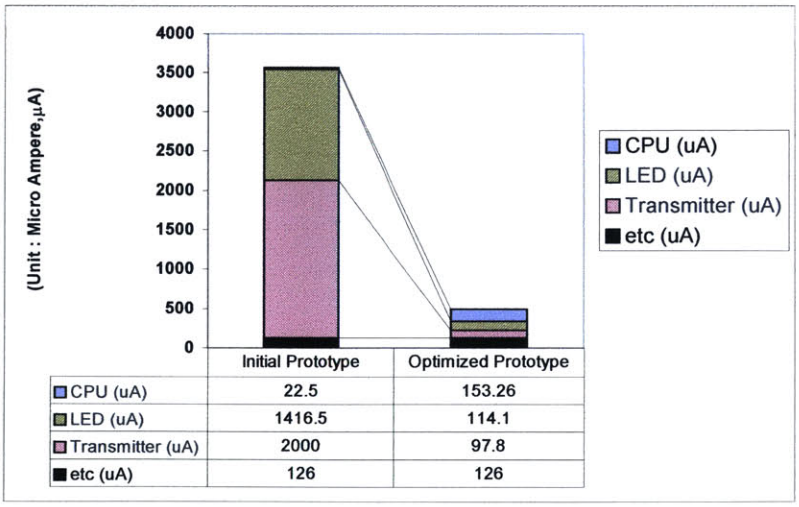

	Initial Prototype	Optimized Prototype
CPU (uA)	22.5	153.26
LED (uA)	1416.5	114.1
Transmitter (uA)	2000	97.8
etc (uA)	126	126

Figure 2-6: Comparison of power requirements for the initial Ring Sensor prototype and the optimized design [27].

2.3 Benchmarking Results

After the redesigning of the Ring Sensor had been completed, several performance tests for benchmarking were performed. The Ring Sensor was first benchmarked using an EKG (AD Instruments Pty, Ltd., NSW, Australia) and an FDA-approved fingertip PPG (IBS Corp., MA, USA). While a volunteer wore each of the devices, waveform data was recorded for both power spectrum analysis and comparisons as well as for heart rate comparisons. It was found that for sensor band pressures as low as 11 mmHg, under static monitoring conditions, the Ring Sensor compared quite favorably to both standard monitoring devices (Figure 2-7). However, it must be noted that measurements obtained at low band pressure during patient motion (hand shaking) displayed complete waveform distortion; a remaining limitation of the design.

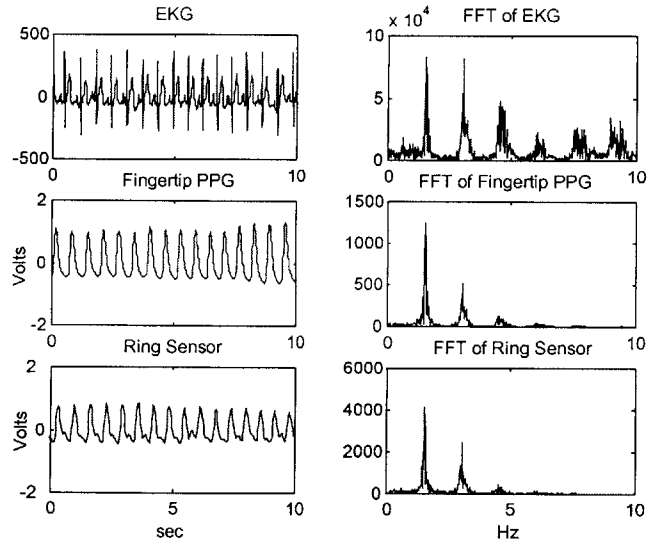

Figure 2-7: Comparison of recorded waveforms and respective power spectra. No external static force with skin pressure of 75 mmHg. "Fingertip PPG" is the photoplethysmograph at the fingertip using FDA-approved device (IBS Corp) [27].

A second benchmarking test focused on the long-term monitoring capabilities of the Ring Sensor. In particular, it is important to have some measure of the Ring Sensor's susceptibility to patient motion over an extended period of time, while normal daily activities are performed. To

this end, a volunteer was monitored throughout a two-hour period. During the experiment, the volunteer attempted to mimic daily activities such as walking, running, writing, typing, and so on. Using conservative motion detection software, which completely rejects signals containing contamination, it was found that the Ring Sensor cleanly monitored the patient over 35% of the total time (Figure 2-8).

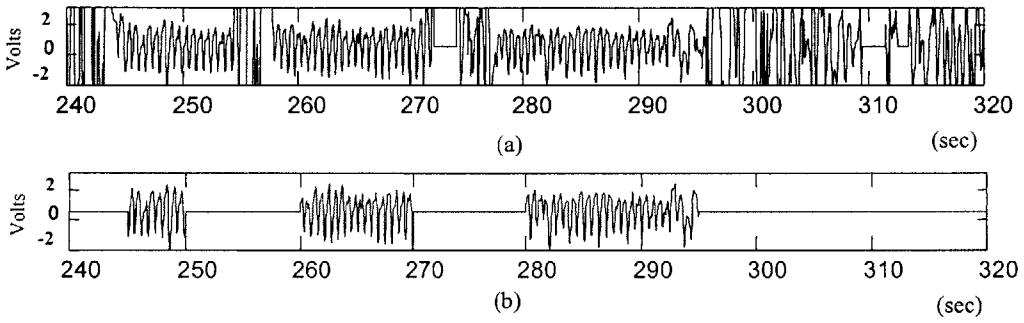

Figure 2-8: A part of the two-hour monitoring test result. The software detected motion artifact and removed the contaminated signal. (a.) Raw data of the Ring Sensor; (b.) Data after artifact detection process [27].

These results indicate that even with an extremely conservative monitoring algorithm, the Ring Sensor is capable of providing valuable physiological information in everyday life.

2.4 Remaining Design Considerations

It is clear that significant advances in both the understanding and the development of wearable sensor designs were achieved in the first four years of the Ring Sensor's development. However, signal corruption due to patient motion continues to be a limiting factor in the usability of the design. Further, there is limited knowledge about the true causes of motion artifacts and other noise components. These design factors must ultimately be better understood and eliminated to enable the best possible sensor design. The sensor band must be optimized for minimal motion artifacts while using low contact pressure and low sensor power. Additionally, only modest work has been done towards calibrating the device for oxygen saturation

measurements. Finally, the Ring Sensor must be tested on actual patients outside of the research lab. The following sections describe improvements and advances which have been made to improve upon Dr. Rhee's Ring Sensor design.

Chapter 3 Motion Artifact Model Development

3.1 Understanding the Limitations of Commercial Pulse Oximeters

3.1.1 Principles of Operation

The pulse oximeter is a non-invasive technology that enables the continuous optically-based measurement of both pulse rate and arterial oxygen saturation. Pulse rate information is obtained directly from the volumetric changes of vessels within the optical path between a source and a detector; as more blood enters the vessel, light from the source is blocked, and consequently a decrease in light intensity is recorded at the detector. Photoplethysmography (PPG) is the nomenclature generally associated with this measurement since it describes a time-dependent volumetric change that is monitored optically. As will be described in more detail in chapter 7, oxygen saturation measurements utilize a similar principle, but rely on two wavelengths of light to obtain spectroscopic information about the absorbers within the light path. In general, it is assumed that there are two main absorbers present within the red to infrared spectrum, i.e. hemoglobin and oxyhemoglobin. Since these two species of hemoglobin are known to absorb different amounts of light as a function of wavelength, it can be shown that a direct measurement of the percentage of oxygenated hemoglobin to the total amount hemoglobin can be derived from

intensity measurements recorded with different wavelengths [30]. Although this assumption is only valid for a first order analysis, it generally, after additional device calibration, enables an estimate that is accurate to within ±2% of the true oxygenation state for saturation levels above 50%. At this point, it must be noted that

> "pulse oximeters differentiate between optical absorption by blood and other anatomical constituents by observation that pulsating arterial blood induces dynamics into the absorption characteristics of well-perfused peripheral sites...and renders that measurement independent of the optical properties of the skin, bone, and nonpulsatile tissue" [6].

This is an important assumption, the ramifications of which will be discussed in detail later. Thus, because of the richness of information provided by the device and the device's relatively unobtrusive design the pulse oximeter has become a recommended standard of care in nearly all areas of the hospital. However, despite the significant success of the device in clinical settings, its incorporation into more routine environments, such as the home, has been minimal to this point. It is reasonable to consider, then, the limiting mechanical factors associated with this sensor's deployment into more rigorous environments.

3.1.2 Commercial Pulse Oximeter Technologies

In general, aside from standard mechanical design features (such as secure sensor attachment through adhesives or pressure, ambient light protection, and protective coverings for the sensor components), most commercial pulse oximeters rely on various signal processing techniques for signal enhancement. To this end, there are several algorithms that have been developed which utilize "black box" methods for the post-processing of acquired signals. Most algorithms incorporate some form of adaptive filtering. However, these methods range from time and frequency domain techniques to a recently developed discrete saturation transform

method [31]. Most time or frequency-based methods utilize a noise reference which is either input from an additional sensor or based upon values in a look-up table (Figure 3-1).

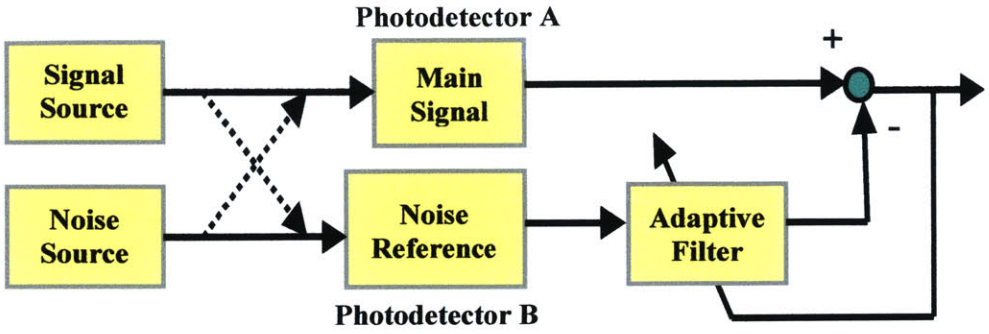

Figure 3-1: Block diagram of standard adaptive noise cancellation algorithm using a second sensor as a noise reference.

The discrete saturation transform utilized by Masimo attempts to better understand the sources of variation within the sensor signal by using a lookup table of Lambert-Beer based saturation ratios. All ratios (representing saturation values from 0-100%) are combined with the measured signal to generate a "noise" reference for an adaptive filter. For each saturation value, the filter outputs essentially a modified correlation signal (i.e.: the larger the magnitude of the output signal, the better the correlation). Typically, two peaks are found with this method as shown in Figure 3-2; one that is assumed to be related to the venous saturation and another that represents the arterial saturation.

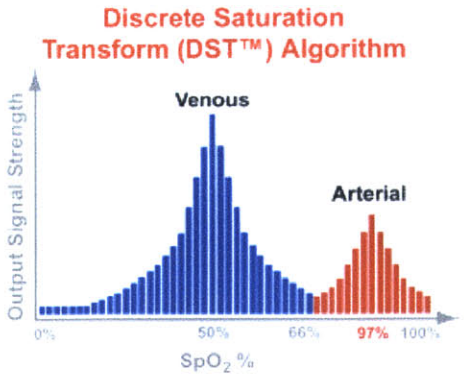

Figure 3-2: Pictorial representation of the information obtained from Masimo's discrete saturation transform algorithm (http://www.masimo.com/technology/systemo.htm).

Alternatively, other groups have produced promising results by attempting to modify the absorption terms in the traditional Lambert-Beer Law to better account for the changes in the distribution of absorbers [6]. This type of statistically-based artifact modeling does acknowledge that traditional monitoring assumptions limit the reliability of oximeter sensors and attempts to improve the calculation by incorporating some of the known deviations from the assumed monitoring conditions. Typically, traditional monitoring assumes the following:

- No measured light comes from sources other than light that has passed through a pulsatile vascular bed
- Pulsatile changes in artery thickness are the same for both wavelengths of light
- Pulsatile signal originates only from varying absorption by arterial oxygenated and reduced hemoglobin (no other pigments, hemoglobin species, or venous pulsations)
- Law is assumed valid for light passing through tissue (absorption dominant is assumed)

These approaches have all improved the quality and reliability of in-hospital oximeters tremendously through relatively modest additional pre-programming. However, they are still very susceptive to false alarms and are often effective for only a limited number of monitoring situations. The question remains: What is the best way to improve the reliability of these sensors in the field? Most of the aforementioned methods post-process the acquired signal without any knowledge about the sources of the disturbance. Perhaps by understanding the interaction between tissue and the intravascular hemodynamics we can not only design better sensors, but we can also improve the information available to post-processing techniques and establish better limits for device performance outside of the hospital.

3.2 Disturbance Modeling

For optically based sensors, the detected signal is a complex superposition of numerous photo-molecular based events (Figure 3-3). This conglomeration of absorbers can be said to exist within a control volume of tissue and can be used to better understand how changes in the PPG signal can occur. By examining how various classes of external disturbances affect the natural internal hemodynamics of the vessels within a finger, important insights into changes in the distribution of absorbers in the illuminated control volume can be realized.

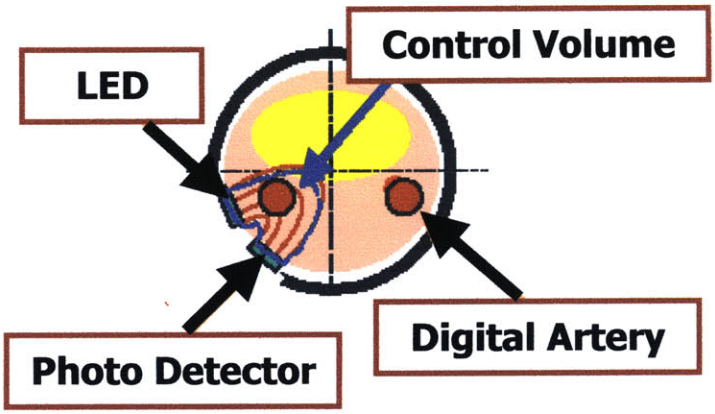

Figure 3-3: Illustration of a finger cross section where an LED is illuminating a control volume of absorbers within the finger that are measured by an optical detector.

It is well known that biological systems are extremely non-linear and time varying. In order to begin an investigation into the *key* contributing factors of internally based motion artifacts, it is therefore necessary to make several initial simplifying assumptions about the anatomical region of interest, which will be revised and validated through experiments.

Outside of the hospital there are many potential sources of disturbance for wearable sensors (Figure 3-4). For this initial work we choose to focus on a particular set of simple, common disturbances that are known to affect sensor performance. In particular, we are interested in characterizing how an external force is propagated through tissue and ultimately to

the vessel wall. This disturbance-type has been chosen because of its relative simplicity and because it is an extremely common interaction for all patients. It is further argued that if a sensor cannot perform reliably under these most basic situations, it has little hope of performing in more rigorous environments.

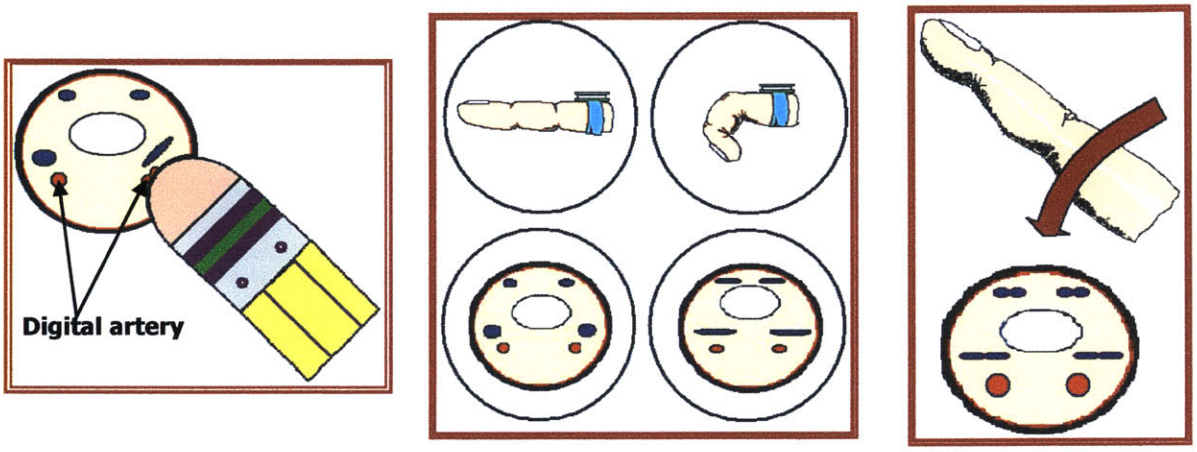

Figure 3-4: Examples of common mechanical disturbances experienced by the Ring Sensor. (a.) Externally applied pressure changes; (b.) Changes in band pressure resulting from finger bending; (c.) Fluidic accelerations resulting from hand movements.

To further our understanding of these complex interactions, it is necessary to focus on the body of work in the area that is available. Several research groups have investigated various aspects of tissue deformation resulting from exogenous forces. Moreover, various finite element models have been constructed including a model developed within our own lab by Dr. Sokwoo Rhee. The results of these analyses indicate that the tissue behavior is indicative of both a solid and a liquid (Figure 3-5a). This observation helps explain why a locally applied pressure appears to radiate out somewhat around the bone. Additionally, we see that the interaction between the tissue and the bone has led to significant deformation of the tissue near the external disturbance force. If we apply these results to a scenario when a pressure is transmitted through tissue to a blood vessel such that the translational motion of the vessel is limited by the presence of a bone we find an interesting situation which must be accounted for by our model. In particular, we

must construct our vascular model such that it will collapse in the direction of the external force and expand in a direction perpendicular to the force (Figure 3-5b). In other words, we must isolate the interplay between the compression of the surrounding tissue matrix and the highly non-linear compliance of the vascular wall.

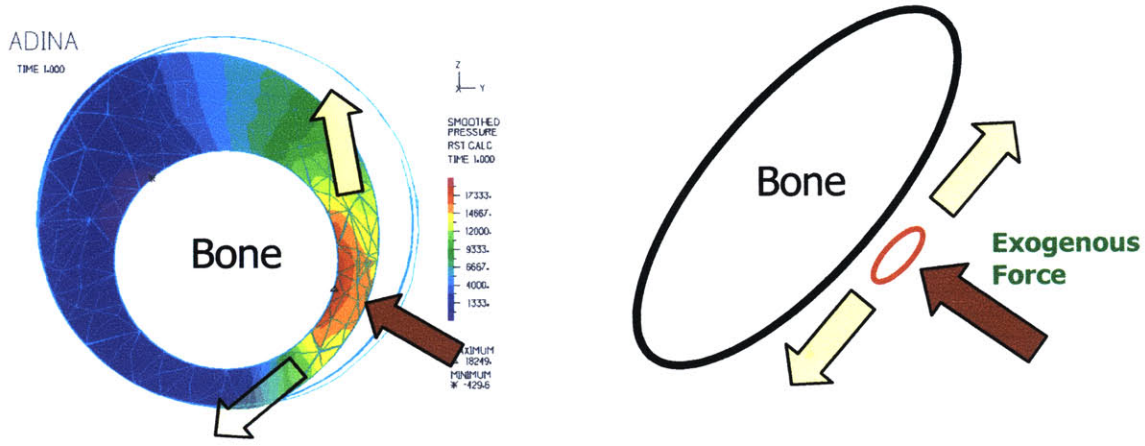

Figure 3-5: Blood vessel-tissue-bone interaction. (a.) FEA model illustrating how an externally applied force radiates around the bone [27]; (b.) Conceptual illustration of exogenous force incident on a vessel's wall.

3.3 Model Derivation

Since our modeling goal is to understand the basic mechanisms of associated with this type of motion artifact, we need the simplest model that is capable of describing the phenomena that have been observed experimentally and with the FEA model. In order to initially investigate how a disturbance is propagated through tissue to a vessel a first-order, lumped parameter model has been developed (Figure 3-6). The model consists of an extremely simplified tissue matrix model (the spring labeled 'k') which, when acted upon by an external force, leads to a decrease in vascular volume. At the same time, as the transmural pressure decreases, the compliance of the vessel increases and the volume is increased in the direction perpendicular to the disturbance. This result is modeled with the temporarily linearized vascular compliance element.

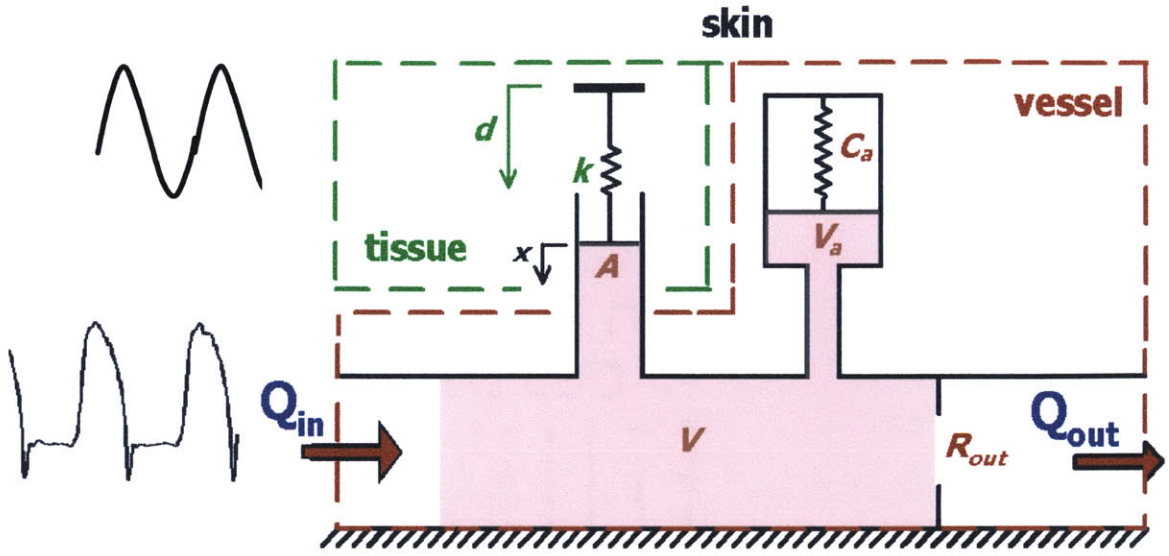

Figure 3-6: Illustration of proposed lumped parameter model.

The justification for the extreme simplification of the true system is to provide a framework for isolating the aforementioned interaction. Since the gross behavior of the tissue is important for proper analysis, a simplified, linear model is deemed acceptable for the current purpose, but must be modified if higher order effects are to be examined. Additionally, as mentioned before, the fluidic inertia has been neglected for this first model. This assumption does limit the number of applicable cases to which the prescribed model can be faithfully applied, but does allow us to more directly consider the first order effects of an external disturbance. Obviously, a more descriptive model must eventually include these important effects.

An equation relating the vessel's change in volume to both a hemodynamic flowrate input and an external disturbance input can be derived as follows. The total volume within the vessel (V_{tot}) is assumed to be the sum of contributions from a static (DC) component (V_o), a pulsatile (AC) component (V_a), and any externally applied disturbances (Ax), such that,

$$V_{tot} = V_o + V_a - Ax \qquad (1)$$

where the pulsatile volume is linearly related to the vessel's internal pressure through a lumped vascular compliance term, C_a, such that,

$$V_a = C_a P \tag{2}$$

Additionally, the propagated disturbance input velocity (v) is transformed into an incident vascular force through a linearized tissue compliance term, k, where,

$$AP = k(v - x) \tag{3}$$

By differentiating equation (1) with respect to time and solving for the pulsatile flowrate term we find that,

$$\frac{dV_a}{dt} = Q - \frac{P}{R} + A\dot{x} \tag{4}$$

where R is the lumped resistance within the vessel and A is the area over which the disturbance is applied. Substituting in our capacitive relation described by equation (2) and taking the standard Laplace transform of both sides of equation (4), we find that,

$$sC_a P = Q - \frac{P}{R} + Axs \tag{5}$$

Finally, combining equations (3) and (5) and solving for the pulsatile volume, we find that the relation becomes,

$$V_a(s) = \frac{R\left(A^2 + kC_a\right)Q - v}{R\left(A^2 + kC_a\right)s + k} \tag{6}$$

Once derived, the lumped parameter model was validated and tuned using experimentally acquired cardiac output and arterial blood pressure data from animal work conducted by our lab

[32]. Figure 3-6 illustrates the tuned model's output when driven by a volumetric flow source input without external disturbances. Although most of the main features and scale of the blood pressure waveform are maintained, it is interesting to note that because of the simplicity of the model, the second peak, resulting from peripheral wave reflections is not visible on the simulated pressure waveform.

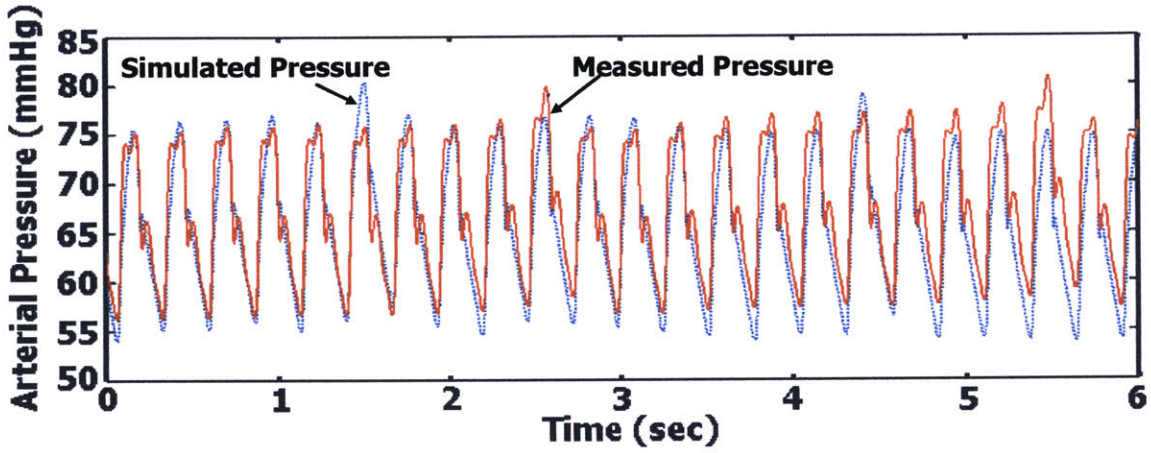

Figure 3-7: Comparison of experimentally measured arterial blood pressure and the blood pressure predicted when using the model under no motion conditions.

One interesting finding from our modeling results is that based on the transfer function derived from the model, it appears that in addition to the well known observation that vascular compliance increases as transmural pressure decreases to 0, the signal to noise ratio (SNR) also increases with the increasing vascular compliance (7).

$$\left| \frac{V/Q_{in}}{V/d} \right| = R(A^2 + kC_a) \qquad (7)$$

For this result, we have defined the SNR to be the ratio of the vascular volume divided by the hemodynamic input (Q_{in}) to the vascular volume divided by an external disturbance. As can be seen from the transfer function of the model, the magnitude of the effects of disturbance is independent of the vascular compliance. Therefore, as the compliance increases, the volumetric

change of the vessel increases due to the hemodynamic input, while the magnitude of the "noise" term associated with the disturbance does not appear to change. These results indicate that for increased external pressures (lower transmural pressures across the vessel's wall) the SNR of the vessel's volumetric changes should increase. Using the tuned model, simulations have been conducted utilizing a low frequency sinusoidal disturbance input (frequency = 0.7 Hz) and the aforementioned volumetric flow input. As predicted, simulation results indicated that increases in transmural pressure actually improve the SNR of the vessel (Figure 3-8). Practically speaking, these results indicate that a higher sensor band pressure should improve a sensor's performance in the presence of external disturbances.

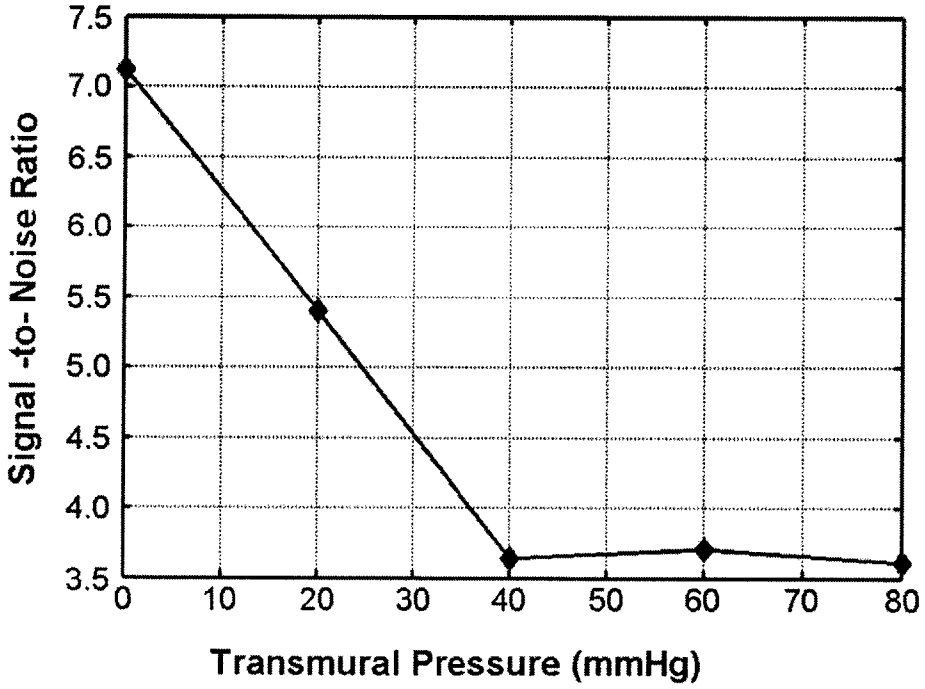

Figure 3-8: Simulation results showing how the signal-to-noise ratio of the volumetric change increases with decreasing transmural pressure.

Based on the results of our modeling analysis, it seems that in order to provide the optimal sensor output, it is necessary to pressurize the sensor band. However, since continuous high pressures can lead to ischemia or tissue necrosis we must either optimize the sensor

pressure for the highest acceptable applied pressure level or incorporate a design which applies only a localized high pressure area near the sensor units. The local pressure technique should make it possible to realize the advantages of the high pressure method while enabling sufficient blood flow to the bulk of the finger.

Chapter 4 Artifact Resistant Transmittance Design

4.1 Understanding the Physiologically-Based Mechanisms of Motion Artifacts

It is well understood that a PPG sensor unit measures changes in blood volume via light absorption [33]. These changes in blood volume (AC component) are relative to the total amount of light absorbed (DC component) along the detected photon paths (Figure 1-1). Since a reflectance sensor configuration monitors a small, local control volume of the finger, any changes in the distribution of blood or tissues within the control volume can significantly affect the sensor measurements. For example, the capillaries are extremely thin-walled vessels and therefore collapse easily if external pressures are applied. Furthermore, it is understood that pressures moving blood through the capillaries are extremely low [34]. This low intravascular pressure and extreme ductility mean that a sudden acceleration of the hand can easily redistribute the volume of blood in the monitored tissues and vessels. The hand's acceleration is essentially an external force, which is applied to the internal elements of the hand and fingers. As the tissues and vessels compress due to the acceleration, the location (or distribution) of the blood within the hand and fingers will change. The new location of the blood will then be related to the magnitude and direction of the applied acceleration. Since the monitored control volume in the reflectance configuration is relatively small, this redistribution of blood can significantly

change the relative influence of the various elements absorbing the light detected by the photodetector (Figure 4-1).

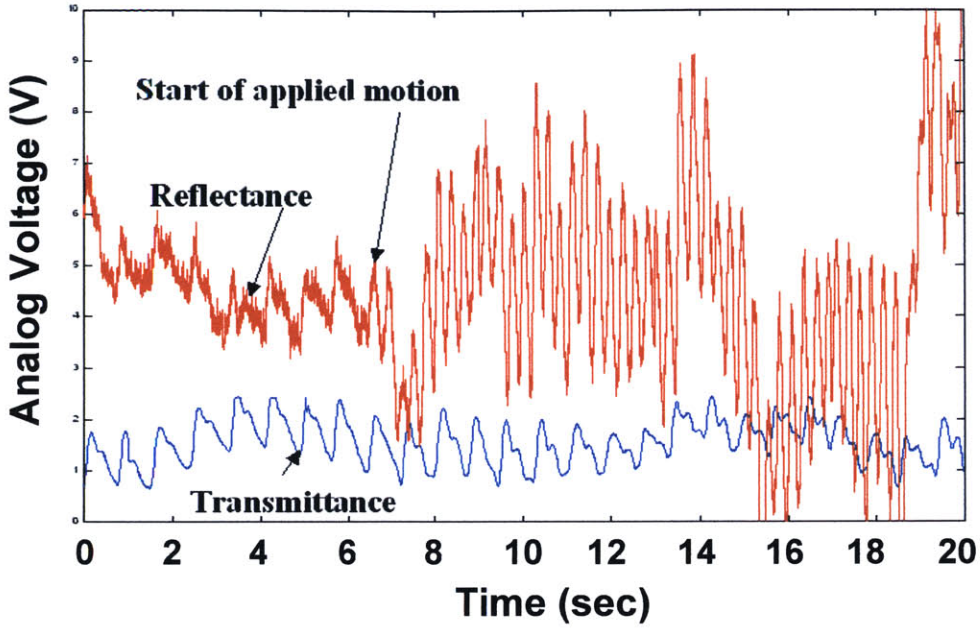

Figure 4-1: Corruption of PPG waveform during the application of a simple chopping motion.

Finger flexion can also easily obstruct blood flow in peripheral vascular beds [35]. As the finger bends, the walls of the capillaries and veins are compressed due to the external tightening of skin and the internal compression of tissue; again, this is related to the low intravascular pressures. As the vessel walls collapse, blood is pushed away from the region of increased pressure. Also, the compression of tissues leads to a redistribution of blood and therefore to a change in the overall light absorbance characteristics of the monitored control volume. These changes in the location of blood lead to an increase in the DC level of the PPG signal and a significant decrease or total loss of the AC component of the PPG signal (Figure 4-2).

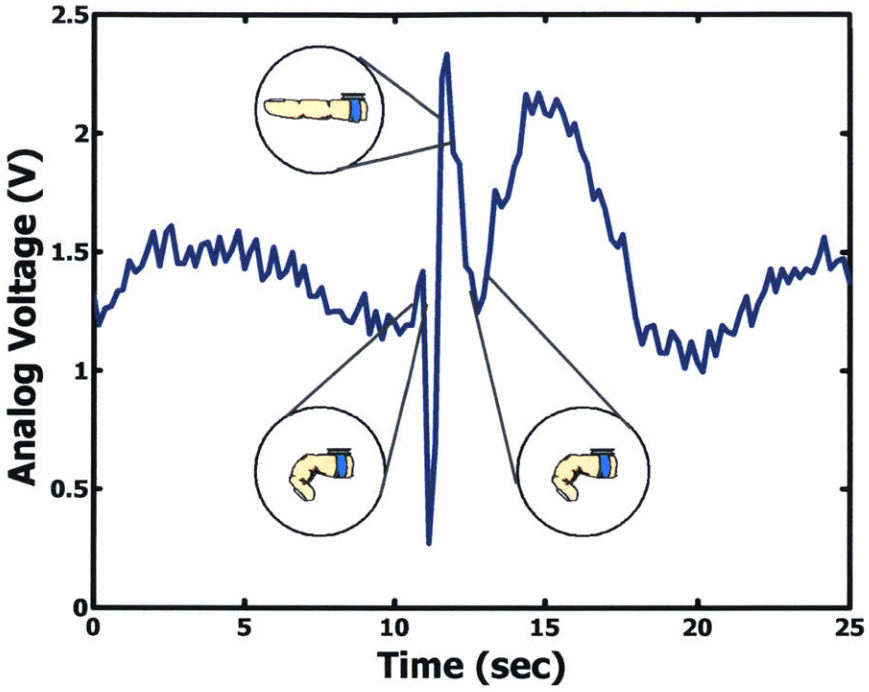

Figure 4-2: Corruption of PPG waveform during simple finger flexion. Note the large change in the DC component of the acquired signal.

This phenomenon can be demonstrated by the slight, visible color change that accompanies finger flexion. Thus, for a given applied motion, the pulsatile component of blood flow found in the peripheral vasculature may be greatly reduced or lost completely as blood is redistributed away from the location of the applied pressure.

4.2 Understanding the Sensor-related Mechanisms of Motion Artifacts

In addition to the internal changes that can occur within the monitored region of interest, external factors can also affect signal quality. One factor that can affect signal stability is a change in the separation distance between the photodetector and the LED [36]. As previously mentioned, the monitored control volume is proportional to the separation distance between the

LED and photodetector. For the Ring Sensor particularly, the optoelectronic sensors are individually mounted and secured onto an elastic band (via double-sided tape), which means that changes in the relative separation distance between the sensors can occur. In a reflectance configuration, it is reasonable to assume that since the driving current for the LED is very low, a large percentage of the DC (or non-pulsatile) signal that reaches the photodetector likely comes from photons that travel through tissues near the surface of the skin. These photons lead to a sort of 'direct lighting' of the photodetector. In other words, these photons pass through the nonvascularized surface epidermal tissue and the slightly vascularized dermal tissue layers before reaching the photodetector. Thus, these photons will mainly contribute to the DC component of the PPG. As noted before, the DC component of the detected signal is much larger than the AC (pulsatile) signal. Therefore, any changes in the DC level can significantly affect the measured AC signal. So, we propose that if the photodetector moves relative to the LED, the amount of lighting contributed to the DC component by the previously described direct lighting method may also change significantly. The resulting change in intensity is caused by a change in the number and location of the photon paths along the skin's surface that reach the photodetector. Since this contribution is likely a significant percentage of the control volume monitored using the reflectance configuration, the changes in the DC signal will lead to changes (or corruption) of the measured AC signal.

A second example of how changes in sensor location can affect the measured PPG signal is found by examining the average location of the photon paths that reach the photodetector. As the LED moves relative to the detector, the average location of the paths that reach the photodetector should change (Figure 4-3). These changes correspond with the changes in size and location of the monitored control volume. Therefore, as the positions of the sensors change,

the relative size of the measured pulsatile waveform as well as the non-pulsatile PPG component should change. Both of these results ultimately lead to changes in the measured signal, which are generally defined to be motion artifacts.

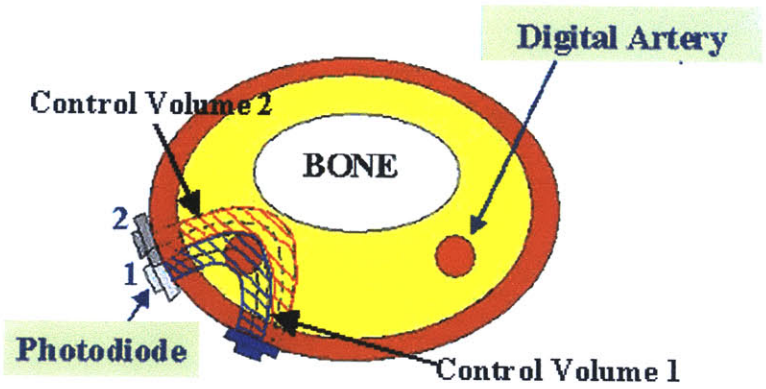

Figure 4-3: Illustration of how sensor position changes can lead to changes in the control volume that is monitored by the PPG.

4.3 Artifact-Resistant Transmittance Sensor Configuration

As previously described, sensor location is a critical factor in signal acquisition for both reflectance and transmittance photoplethysmography. Consequently, sensor position changes resulting from external accelerations of the hand can lead to significant degradation of the pulsatile signal. Since sensor location affects the control volume monitored by the PPG unit, we propose that as the separation distance between the LED and photodetector increases, the affects of small changes in sensor position should be reduced. As discussed in section 4.2, if the separation distance between the LED and photodetector is relatively small, movements of one device relative to another lead to a significant change in the particular photon paths that reach the photodetector. Additionally, small changes in the local distribution of blood caused by external accelerations or pressures significantly affect the distribution of the absorbed blood detected by the photodetector. However, at an increased separation distance, small relative movements of

the LED and photodetector should have a negligible affect on the measured signal since the changes of the photon paths that ultimately reach the detector do not significantly change the relative distribution of the light absorption within the monitored control volume (Figure 4-4).

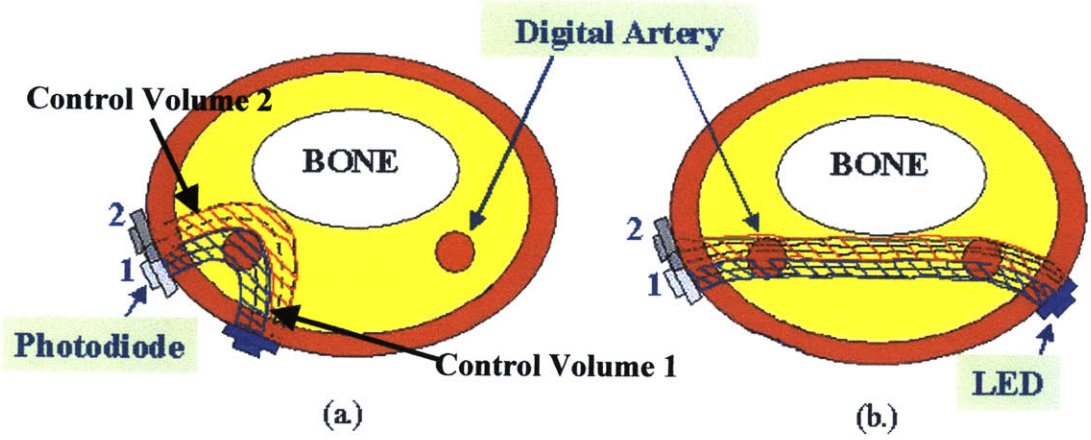

Figure 4-4: (a.) For the reflectance illumination method, movement of the photodetector relative (position 1 to position 2) to the LED leads to a photon path that no longer contains the digital artery. (b.) For the transmittance illumination method, movement of the photodetector relative to the LED still contains photon paths that pass through the digital artery.

Another advantage of the transmittance sensor configuration is that the pulsatile component of the PPG signal is believed to come predominantly from the digital arteries of the finger. The digital arteries are deep to the surface and run parallel to the length of the finger [37]. These vessels are the largest arteries in the finger and are the main source of the finger's blood supply. Thus, the pulsatile blood waveform is strongest in these vessels. Since the pulsatile signal acquired using the transmittance configuration is believed to primarily come from the digital arteries as opposed to the peripheral capillary beds, it should ultimately be less susceptive to the motion artifacts related to changes in the peripheral vasculature. In the transmittance configuration, the percentage of the measured signal within the monitored control volume does not significantly change when peripheral capillary beds are collapsed since the majority of the pulsatile signal is based on volumetric changes within the digital artery. In particular, this

configuration should be much less sensitive to external pressures changes caused by finger flexion, which can significantly change the distribution of blood near the periphery of the skin.

Given that the digital arteries are located deep to the surface and have walls which are much thicker than the capillaries, pressure changes resulting from finger flexion should be much less influential on the output of the sensor unit. The changes in pressure near the surface, which can occlude the peripheral vessels, will not occlude the thicker digital arteries. Moreover, occlusion of the peripheral vasculature will not significantly affect the relative distributions of blood within the transmittance configuration's control volume since the main pulsatile contribution is from the digital arteries. Since a much greater control volume is utilized and since the pulsatile changes in blood volume mainly come from arterial pulsations, small changes in blood distribution have less of an affect on the measured PPG signal. Based on these hypotheses, we believe that a transmittance configuration should, overall, be less susceptive to applied motions.

Experiments, conducted in our lab, have demonstrated that a transmittance sensor configuration is less susceptive to motions involving both finger flexion and quick, vertical accelerations [38] (Figure 4-1, Figure 4-2). These results coincide with similar findings by other research groups that suggest a transmittance sensor configuration is less susceptible to motion artifacts [35], [39], [40]. Although the results of these experiments are quite promising, they are achieved at the cost of a higher power requirement for the optoelectronics. The existing reflectance configuration requires around 2 mA per LED for the driving current, while the transmittance configuration requires over 10 mA per LED to produce comparable signal amplitudes. A new driving circuit has been designed to achieve the increased LED driving current (Figure 4-5).

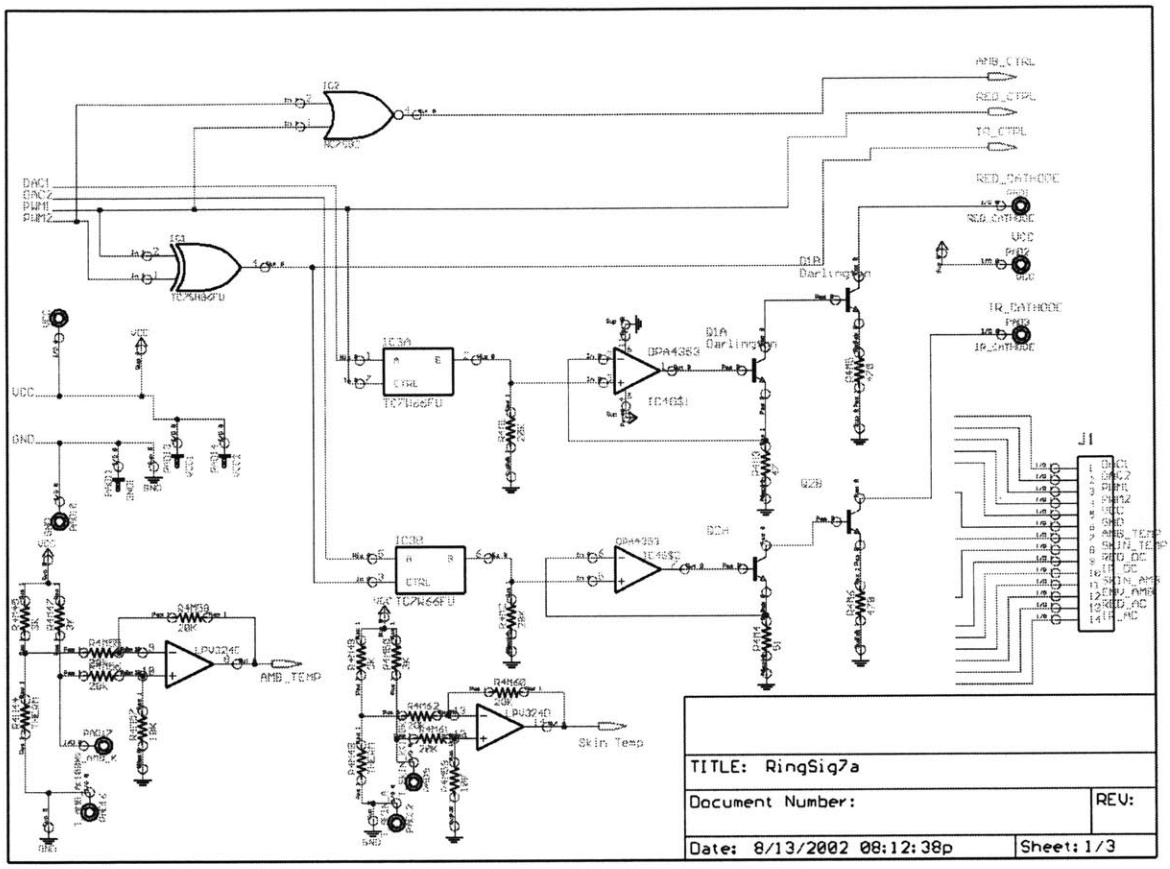

Figure 4-5: Schematic diagram of the LED current amplification circuit used by the new Ring Sensor.

The circuit is a standard current amplifier consisting of two cascaded Darlington transistors. The main advantage of using Darlington-type transistors is that they offer a significant increase in the current amplification for each stage, while requiring very little base current to be supplied by the microprocessor. For wearable sensors, power consumption is an extremely important design constraint. Thus, a transmittance sensor configuration is only acceptable if the required power can be reduced.

4.4 Signal Enhacnement with Increased Transmural Pressure

As was discussed in section 3.3, increasing the detected amplitude of arterial pulsations, i.e. the AC component in Figure 1, improves the signal-to-noise ratio of PPG. It is well understood that the application of an external pressure on the tissue surrounding the artery will increase the pulsatile amplitude. Such a pressure reduces the transmural pressure, that is, the pressure difference between inside and outside of the blood vessel. The pulsatile amplitude becomes a maximum when the transmural pressure approaches zero, since the arterial compliance becomes maximal with zero transmural pressure [17,41]. As was previously suggested, applying a pressure may interfere with tissue perfusion. Since the device is worn for long periods of time, the pressure must be kept such that it does not exceed levels that could damage other vasculature [42]. Thus, the mechanism for holding the LED and PD must be designed such that it provides a safe level of continuous pressure, well below the established clinical threshold.

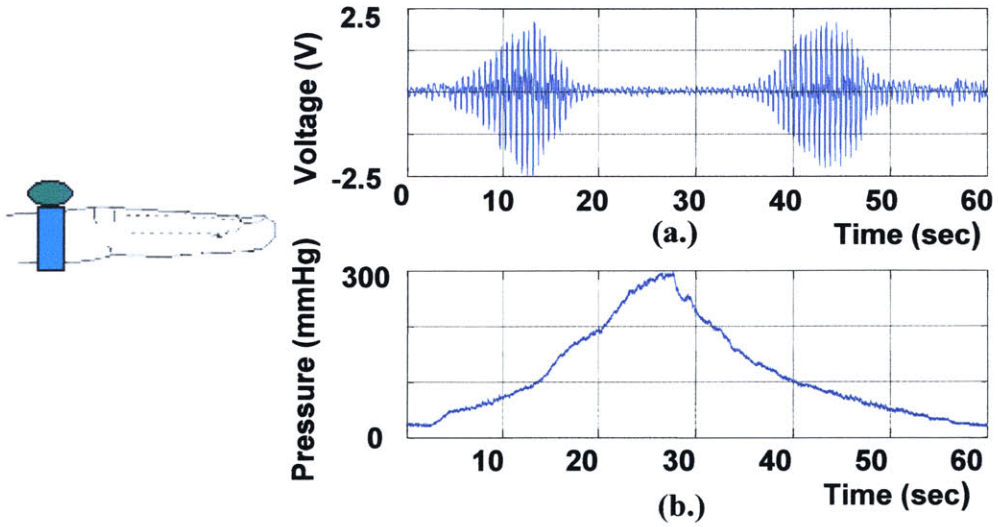

Figure 4-6: (a.) PPG signal amplitude (b.) Pressure at the photodetector.

Figure 4-6 shows the pulsatile amplitude of a finger base PPG for varied pressures generated by a finger cuff. Increases in cuff pressure lead to an increase in the PPG amplitude until a maximum value is reached. After the maximum oscillation value has been reached, further increases in pressure will actually lead to decreases in pulsation amplitude, due to occlusion of the blood vessels. The cuff pressure yielding the largest PPG amplitude, generally near the mean arterial pressure [43], is too high to apply for a long period of time. To prevent the capillary beds from being collapsed, though, the cuff pressure must be on the order of 10 mmHg, which is too low to obtain motion tolerant PPG waveforms.

A solution to this problem is to apply the pressure only at a local spot near the photodetector. When using a cuff, or any of the devices that provides uniform surface pressure onto the finger or the arm, it constricts the blood vessels, thus limiting or significantly impeding the amount of blood supplied downstream. However, by providing a local, non-circumferential increase in pressure near the sensor's optical components, it is possible to amplify the plethysmograph waveform while avoiding the potentially dangerous situation of long-term flow obstruction. As shown in Figure 4-7, the tissue pressure in the vicinity of one of the arteries can be increased with through the use of a special mechanism pushing Photodetector A towards the skin. This mechanism, which is attached to the sensor band, changes the pressure distribution such that the transmural pressure of one of the arteries could be high enough to obtain a large pulsatile signal while keeping the pressure low elsewhere to allow for sufficient blood perfusion. As long as the pressurized area is small enough to allow perfusion to the surrounding tissue, the local pressurization causes no major complications, even when the pressure is applied for many days.

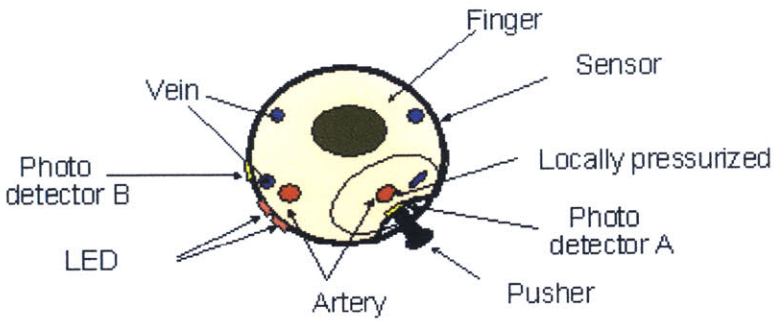

Figure 4-7: The schematic of a locally pressurized sensor band.

Based on this analysis, we find that the design of the Ring Sensor should incorporate a motion tolerant transmittance sensor configuration with an additional local pressure mechanism for optimal performance. Using these results, a new, more robust version of the Ring Sensor will be achieved.

Chapter 5 Power Saving High-Speed Modulation

5.1 Description of the Modulation Algorithm

Previous Ring Sensor designs used relatively slow optoelectronic components, making it impossible to implement a high-speed modulation methodology. Thus, the LED was 'turned on' for a relatively long interval of time. While the LED was on, the photodetector, having a much slower response time, would increase gradually to a maximum value. Once the output was at a maximum the value of the signal would be sampled (Figure 5-1a). If we use a high-speed photodetector with a short response time, it is possible to have the LED 'on' for a much shorter period of time and still sample a maximum intensity at the photodetector (Figure 5-1b.).

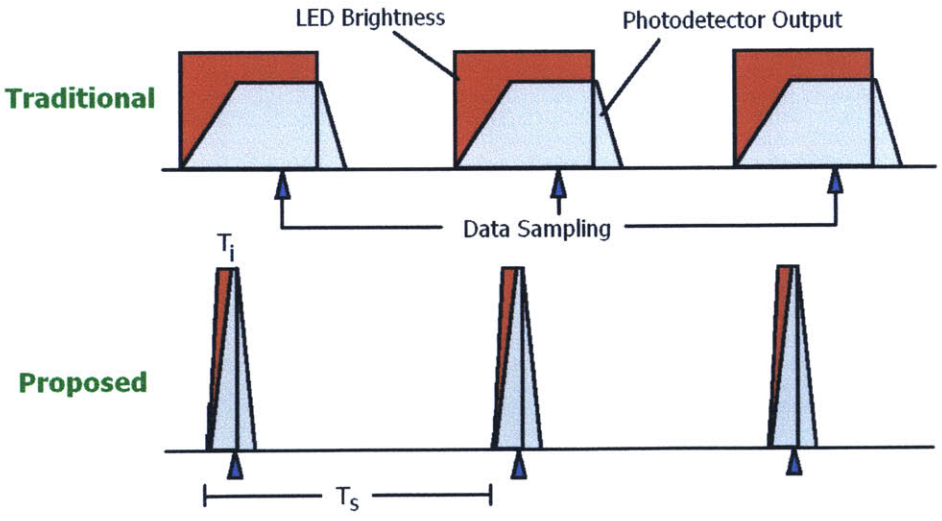

Figure 5-1: (a.) The slow response time of the photodetector meant that the LED had to be modulated at lower frequencies for data sampling. (b.) Faster photodetector response times makes it possible to increase the modulation frequency of the LED.

Using these assumptions as the basis for component selection, we have settled on optical components, made by Elekon industries, which are capable of a modulation frequency of 1 kHz with a duty ratio of 0.1% (i.e. the optical components have reported rise and fall times significantly faster than 1μs). The current modulation frequency and duty ratio were determined as an acceptable modulation pair for proof-of-concept. At this point, it should also be mentioned that an increase in modulation frequency would necessarily require an increase in onboard CPU clock speed. As the onboard clock speed increases, power consumption will also increase. Therefore, an optimization of CPU clock speed against LED modulation frequency must be performed. Additionally, as the modulation frequency is increased different components may be necessary to achieve required component rise times. These results for LED modulation can be shown mathematically as follows. If we define,

$$\text{Sampling Rate} = \frac{1}{T_s} = s \tag{8}$$

$$\text{Duty Ratio} = \frac{T_I}{T_s} = r \tag{9}$$

where T_s is the sampling period and T_I is the LED illumination time. The time for each LED illumination must therefore be,

$$T_I = \frac{r}{s} \tag{10}$$

This means that for a constant duty ratio, as the sampling rate increases the illumination time for the LED decreases. Thus, LEDs and photodetectors with faster response times may be necessary.

In theory, if the LEDs are modulated at a frequency of 1 kHz and have a duty cycle of 0.1%, the power consumption should be approximately 1/1000 of the power consumption for the same set-up with no LED modulation. The derivation for this power savings result is as follows: assuming we know the instantaneous power, P_{inst}, which is approximately constant throughout the sampling interval, and using the variables defined above in equations (8), (9), and (10) we can calculate the average power, P_{av}, for a circuit with no modulation and for a circuit modulated at 1 kHz with a 0.1% duty ratio (r = 0.001) as follows:

No Modulation:

$$P_{av} = \frac{1}{T_s - 0}\left[\int_0^{T_s} P_{inst}\,dt\right] = \frac{P_{inst}}{T_s}\int_0^{T_s} dt = P_{inst}\left(\frac{T_s}{T_s}\right) = P_{inst} \qquad (11)$$

$$\therefore P_{av} = P_{inst}$$

Modulation:

$$P_{av} = \frac{1}{T_s - 0}\left[\int_0^{T_s}\left(P_{on} + P_{off}\right)dt\right] = \frac{1}{T_s}\left[\int_0^{T_I} P_{inst}\,dt + \int_{T_I}^{T_s} 0\,dt\right] = P_{inst}\left(\frac{T_I}{T_s}\right) = P_{inst} * r \qquad (12)$$

$$\therefore P_{av} = 0.001 * P_{inst}$$

Thus, we find that for this example, modulation should lead to an average power consumption that is approximately 1/1000 of the power consumption measured for a circuit with no modulation.

Since the circuit is mounted on a micro-PCB, it is difficult to directly measure the power that is consumed only by the LEDs. However, we can estimate the average power consumed by the LEDs by first measuring the current drawn from the power supply with the LEDs in the circuit and by then measuring the current drawn without the LEDs in the circuit. The difference of these two measurements, multiplied by the average supplied voltage, provides a good estimate for the average power consumed by only the LEDs. By then comparing the measured power

consumed both with modulation and without modulation, we can quantify the actual power savings afforded by modulation. These direct measurements of the voltage and current used by the LEDs for the circuit appear to be in good agreement with our theoretical calculations for the power savings as shown below (Figure 5-2). It should be noted that the measurements were made with a 16-bit data acquisition board and sampled at a rate of 5 MHz.

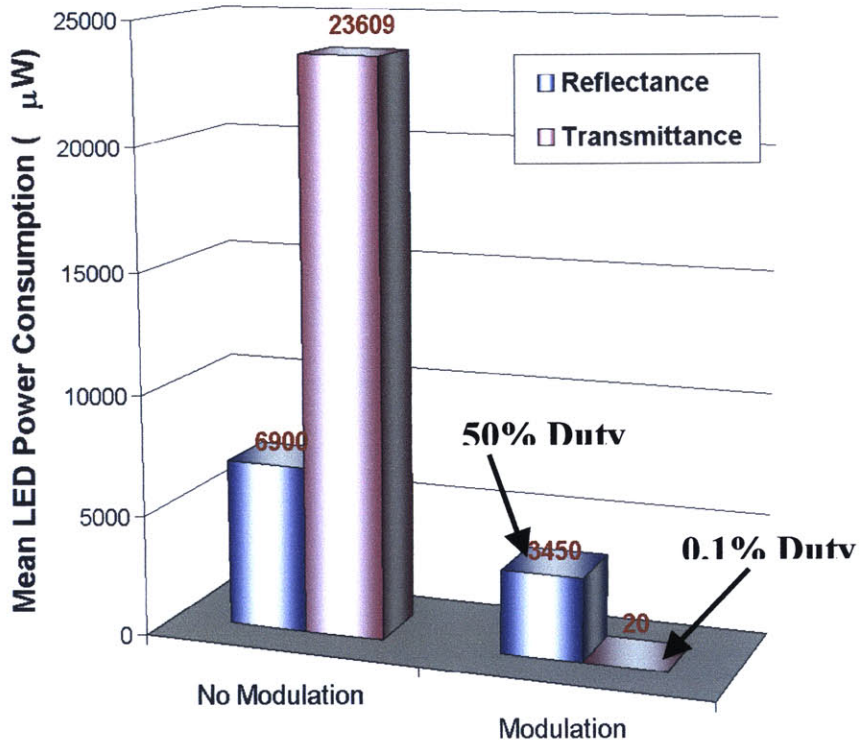

Figure 5-2: A comparison of the mean LED power consumption for both the reflectance and transmittance configurations with and without modulation. High-speed modulation makes it possible to significantly reduce the power consumption of the LEDs.

In addition to measuring the relative power consumption of the high-speed modulation in the transmittance configuration, we also compared this power consumption to the power consumption of the LEDs on previous models of the Ring Sensor (denoted as reflectance on the graph). We found that, as predicted, for a situation with no modulation, the power consumption of the LEDs in the new configuration was significantly more than the power consumption using

the reflectance method. However, as the duty cycle was lowered, we found that it is possible to decrease the power consumption to a level previously unattainable by the Ring Sensor. Since the Ring Sensor was not able to modulate the LEDs at low duty cycles, this level of power savings was previously unachievable.

A further consideration associated with implementing a high-speed modulation algorithm is waveform stability. In particular, it is important to determine whether or not an extremely short LED "on time" will affect the overall shape of the waveforms. We found that although the LED is on for only 1/1000th of the entire modulation cycle, the frequency of the modulation is high enough to acquire enough points to maintain smooth pulse waveforms (Figure 5-3). Stability of output waveforms is essential for oxygen saturation measurements as will be discussed in a later section of this report.

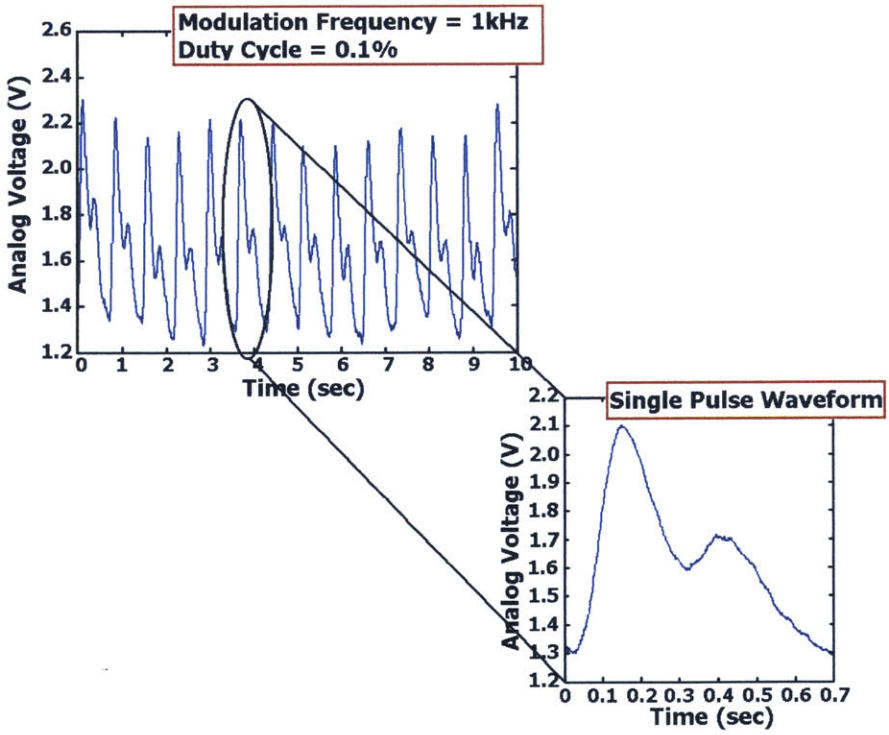

Figure 5-3: A single waveform from the pulsatile signal measured using high-speed modulating. Note that the overall waveform is still quite smooth even though we have the LEDs on for a very short period of time. Note also that a second peak likely resulting from vasoconstriction can be seen on the waveform.

5.1.1 Limitations of High-Speed Modulation

Although it appears that it is possible to acquire the pulsatile PPG component using high-speed modulation, there are limitations to this method that must be addressed. In particular, as the modulation frequency is increased beyond the bandwidth limits of the optical devices, we have found that the stability of our pulsatile signal significantly decreases (Figure 5-4). The photodetector response (i.e. rise time) presented earlier is quite fast. However, as we approach the upper limits of the response time, the quality of the measured signals degrades.

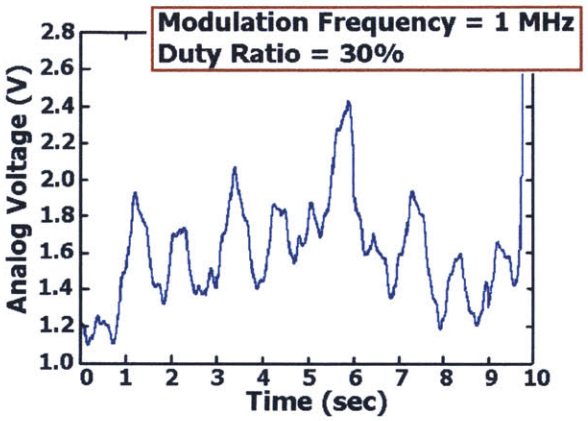

Figure 5-4: Plot of the pulsatile PPG signal captured using a very high modulation frequency. The quality of the detected signal has significantly decreased.

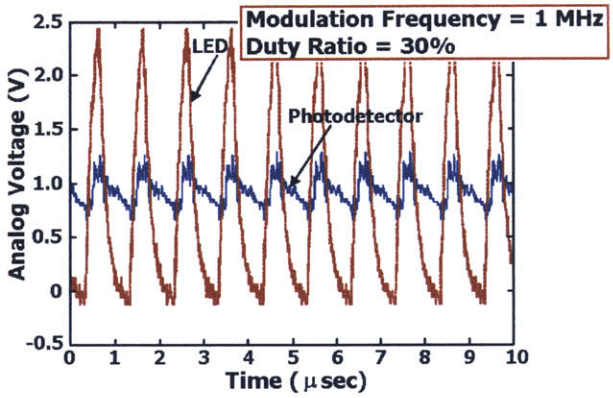

Figure 5-5: Comparison of the input LED modulation waveform and the waveform acquired by the photodetectors.

The major cause of the signal's deterioration is likely due to the response time of the photodetector. As was previously described, when the modulation frequency approaches the maximum frequency limit of the photodetector, the stability of the sensor system should decrease. Figure 5-5 is a plot comparing the output of the photodetector to the actual LED input modulation supplied by a function generator. At this higher frequency we find that the response of the photodetector is significantly degraded. Therefore, careful attention must be paid to the response time of the optical components for successful implementation of any high-speed modulation algorithm.

5.2 Optimization of LED Modulation Rate with CPU Clock Cycle

As previously mentioned, an increase in the overall modulation frequency of the LEDs must, in general, be accomplished by an increase of the clock speed of the on-board CPU. As the clock speed of the CPU increases more power is consumed. Therefore, there is an important design tradeoff that must be addressed involving the optimization of the LED modulation frequency for minimum overall power consumption. To this end, there are at least two simple optimization methods which can be implemented, based on the chosen type of on-board microprocessor: (1) optimize the CPU clock speed directly against the LED duty cycle, or (2) operate the microprocessor at a much slower overall speed and use as a trigger to initiate a temporary high-speed CPU mode. The following sections provide simple examples that illustrate the differences between the two proposed optimization methods.

5.2.1 Optimization of CPU Directly Against LED Duty Cycle

Using the nomenclature and methods defined in [44], it has been shown that the power consumed by the CPU and LEDs can be expressed, respectively, as follows:

$$P_{CPU}(q) = aq + b \tag{13}$$

$$P_{LEDs}(q) = 2rP_{inst} = \left(\frac{6f}{q}\right)P_{inst} \tag{14}$$

where,

q = CPU clock speed

r = LED duty cycle

a,b = empirically determined constants

f = sample and hold frequency

$\mathbf{P_{inst}}$ = instantaneous LED power consumption

By summing equations (13) and (14) and by then setting the resulting summation's derivative, as a function of clock speed, equal to zero, we find the optimal clock speed is given as,

$$\frac{dP_{inst}(q)}{dq} = 0 \Rightarrow q = \sqrt{\frac{.006 f P_{inst}}{a}} \tag{15}$$

which results in an optimal clock-speed of q_{opt} = 13.4 kHz. Additionally, if we use the results of the methodology described in [11], we find that the total power consumed per clock cycle is:

$$P_{tot}(q) = 37.7 \mu A$$

This result compares quite favorably to the previous achievable optimized power consumption for the Ring Sensor that was given as $P_{tot}(q)$ = 0.365 mA. Thus, optimization of the high-speed modulation algorithm leads to an ***89.7%*** reduction in the total power as compared to previous versions of the Ring Sensor.

5.2.2 Optimization with a Software Driven, Digitally Controlled, High-Speed Oscillator

As was previously mentioned, certain microprocessor models are available which allow alternative clock speed optimization methods to be implemented. For example, certain microprocessors contain software driven, digitally controlled, high-speed oscillators. Therefore, the CPU can be operated at a slow frequency $\sim T_s^{-1}$ while the LEDs are triggered with digitally

controlled, short bursts of high-speed operation. Modifying the previously used method we find that the power consumption per CPU clock cycle can be expressed as the sum of the following:

$$P_{slow-CPU}(q_2) = a\left(\frac{3f}{q_2 T_I}\right) + b \quad (\text{on } 99.9\% \text{ of the time}) \tag{16}$$

$$P_{fast-CPU}(q_2) = aq_2 + b \quad (\text{on } 0.1\% \text{ of the time}) \tag{17}$$

$$P_{LEDs} = \left(\frac{6f}{q_2}\right) P_{inst} \quad (\text{on } 0.1\% \text{ of the time}) \tag{18}$$

Now, if we set the derivative of the total power consumed per cycle relative to the fast clock speed equal to zero and solve for this optimal clock speed, we find that the optimized modulation frequency should be,

$$\frac{dP_{tot}(q_2)}{dq_2} = 0 \quad \Rightarrow \quad q_2 = \sqrt{\frac{2.997af + 0.999b + 0.006fP_{inst}T_I}{0.001aT_I}} = 2.512\ MHz$$

Also, since the slow clock speed is equal to T_s^{-1}, we can calculate the optimal slow clock speed as,

$$q_1 = \frac{3f}{q_2 T_I} = 1.194 \text{ kHz}$$

Based upon these results, the total power consumed per slow CPU clock cycle is now,

$$P_{tot}(q_2) = 13.9\mu A$$

Therefore, by implementing a multi-clock speed method, we can reduce the total power consumed by the Ring Sensor by as much as ***96.2***%.

Chapter 6 Signal Processing Optimization

6.1 Filter Order Analysis

An important design consideration for pulse oximeters is the type and order of the analog filtering that will be used to capture the pulsatile waveform. A particularly important consideration is the order of the high pass filter used to eliminate signal frequencies below 0.5Hz. As the order of the filter increases, the slope of the filter cutoff will become sharper (Figure 6-1). The sharper cutoff can improve the resolution of the pulsatile waveform. However, as the order increases the settling time of the filter's impulse response also increases (Figure 6-2). As the impulse response settling time increases, oscillations in the non-pulsatile part of the signal caused by any motion disturbance will increase in length of time. This important insight makes it necessary to study the tradeoffs between highpass filter order and non-pulsatile signal component oscillations.

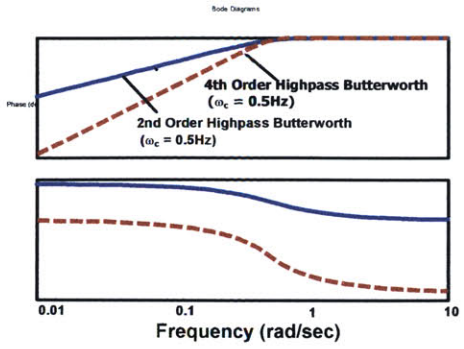

Figure 6-1: Bode plot of the magnitude and phase of both a 2nd order and a 4th order high pass Butterworth filter (0.5 Hz cutoff).

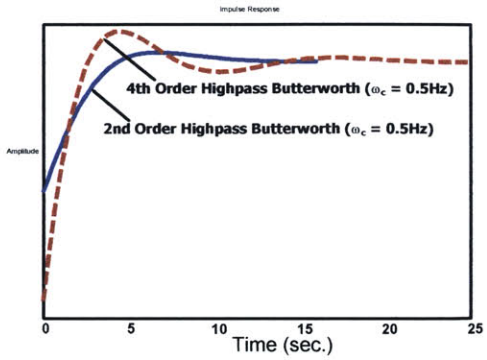

Figure 6-2: Impulse response plot for both a 2nd order and a 4th order high pass Butterworth filter (0.5 Hz cutoff).

Since we expect some patient movement to affect the DC component of the Ring Sensor's signal, we require that the filters that are used not add DC fluctuations to the existing signal. To better understand this design tradeoff, the signals detected after being passed through both a second order high pass filter and a fourth order high pass filter were studied under various monitoring conditions (Figure 6-3). It should be noted that both signals are originally passed through the previously described 4th order low pass filter.

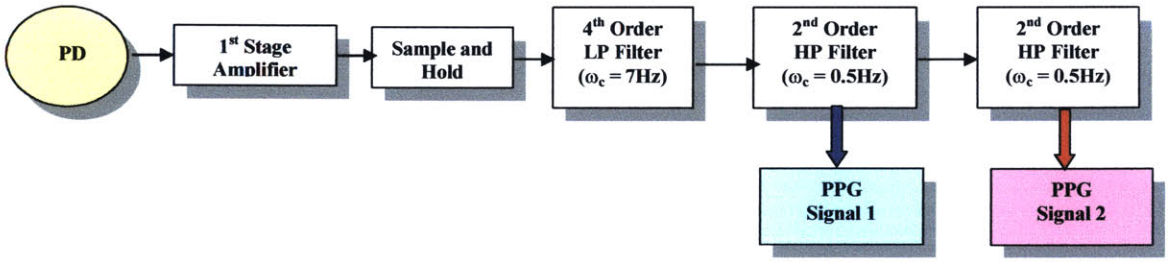

Figure 6-3: Block diagram representation of the Ring Sensor set-up utilized for the filter order analysis experiment.

We found that the optimal high pass filter for the Ring Sensor should be a 2nd order Butterworth filter [45]. A lower order filter was found to maintain sufficient waveform resolution (Figure 6-4) while requiring a far shorter overall settling time (Figure 6-5).

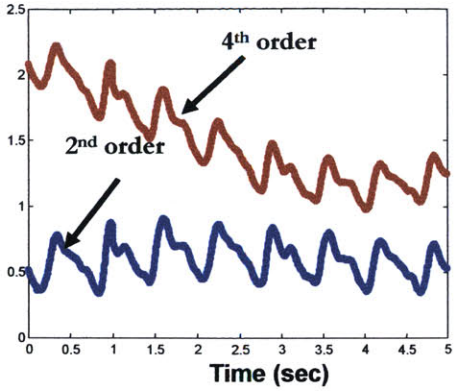

Figure 6-4: Comparison of the PPG waveforms after both 2nd order and 4th order filtering. Note that there appears to be no difference between the two waveforms.

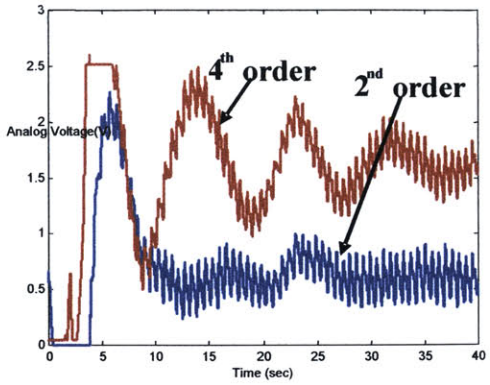

Figure 6-5: Comparison of the impulse responses of both the 2nd order and 4th order high pass filters. Note that the 4th order filter has a much longer settling time. The high frequency component is the plethysmograph

Based upon the results of this filter analysis it appears that the optimal layout for the front-end signal processing of the Ring Sensor should consist of a 2nd order high pass filter. To this end the signal processing circuit has been designed as shown in Figure 6-6 and Figure 6-7. The basic components of the analog circuitry consist of a voltage-to-current stage with amplification, a sample and hold stage, a 4th order low pass Butterworth filter (ω_c = 20 Hz), a 2nd order high pass Butterworth filter (ω_c = 0.1 Hz), and finally an inversion stage with additional signal amplification. The entire analog processing section of the circuit amplifies the measured signal approximately 1000 times before acquisition by the microprocessor.

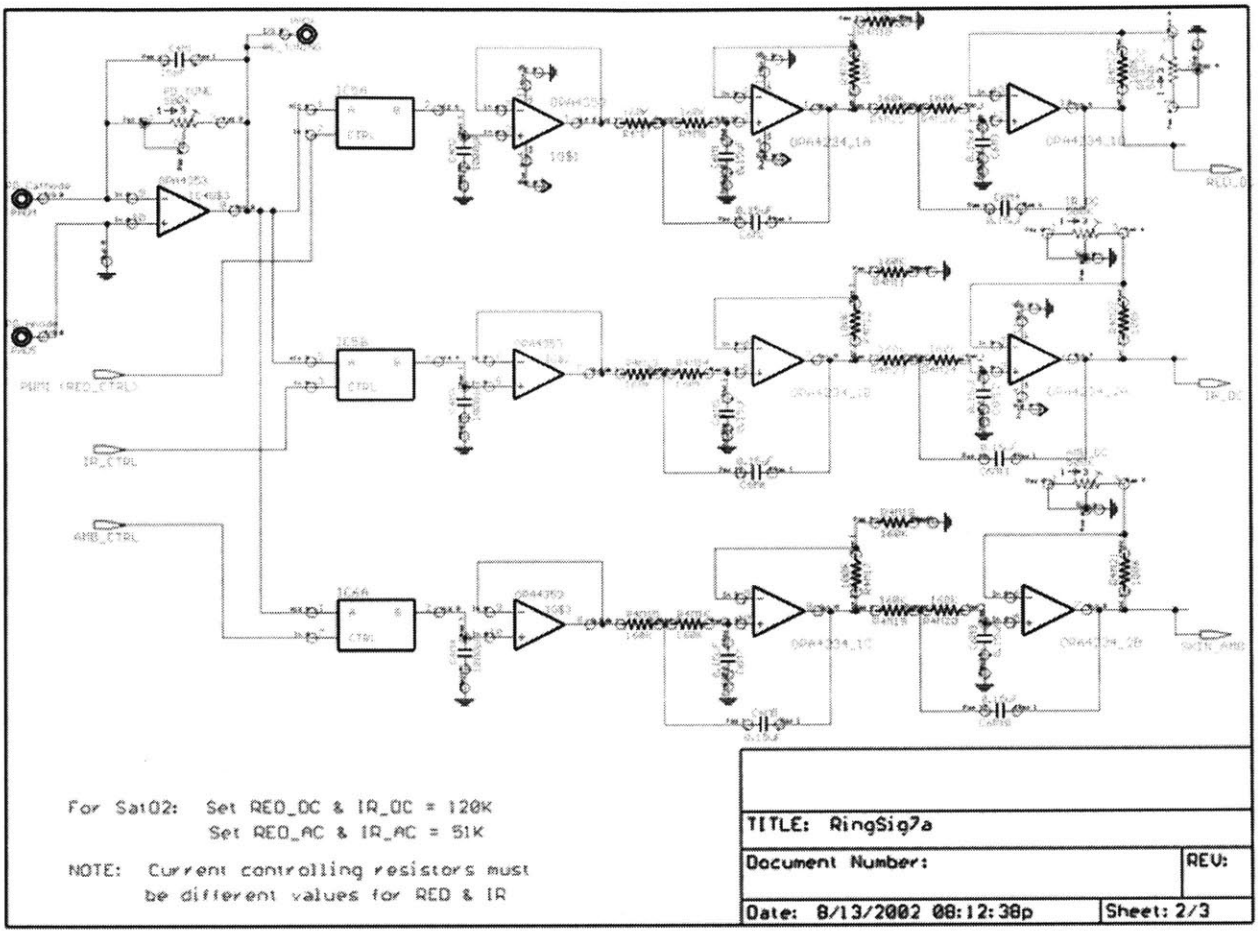

Figure 6-6: Analog signal processing circuit for the Ring Sensor.

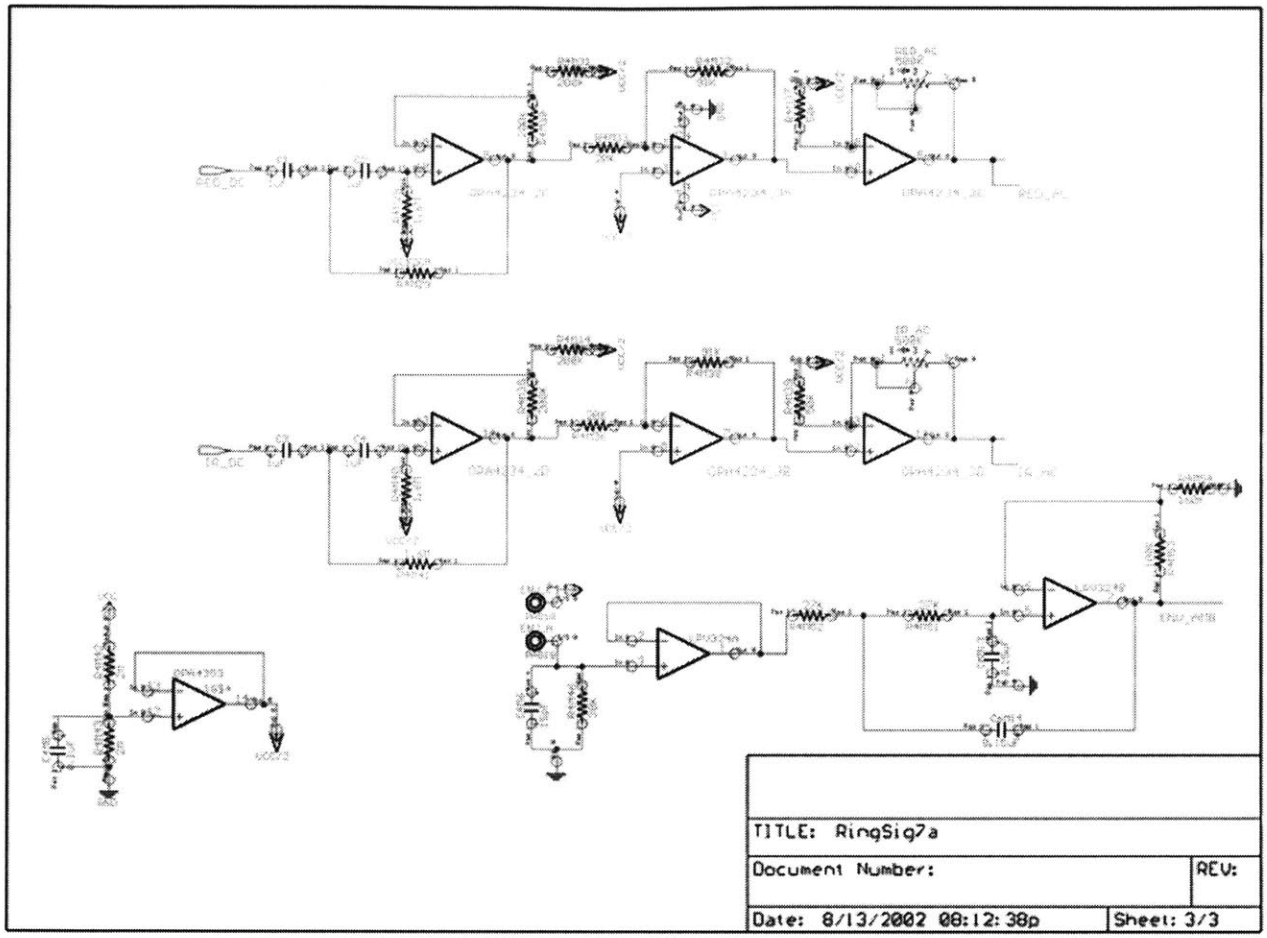

Figure 6-7: Schematic with 2nd order high pass filter for signal conditioning

6.2 Sampling Frequency Analysis

One of the most important considerations in sensor design is the determination of an optimal sampling rate. There are several factors that can affect detected signals and that can consequently lead to erroneous measurements. For example, from the sampling theorem, a signal f(t) cannot be reconstructed from its samples f(nt) if the sampling period T is greater than π/ω_{max}, where ω_{max} is the frequency of the highest frequency component in f(t). In this case, if the sampling period is greater than π/ω_{max} aliasing will occur [46]. Since we are modulating the

LEDs, and consequently the plethysmograph waveform at frequencies around our sampling frequency, it is possible that the wrong sampling frequency could lead to aliasing of the pulsatile waveform.

6.2.1 Sampling Frequency Minimization

The "optimal" sampling frequency has been determined by first comparing each modulated waveform with the baseline waveform. Next, the power spectra of both the modulated and modulated waveforms were compared with an emphasis on low frequency noise influences. In general, for sampling frequencies as low as 50 Hz, we found that aside from the expected loss of signal resolution as the sampling rate was decreased, there was no noticeable change in the acquired signal (Figure 6-8).

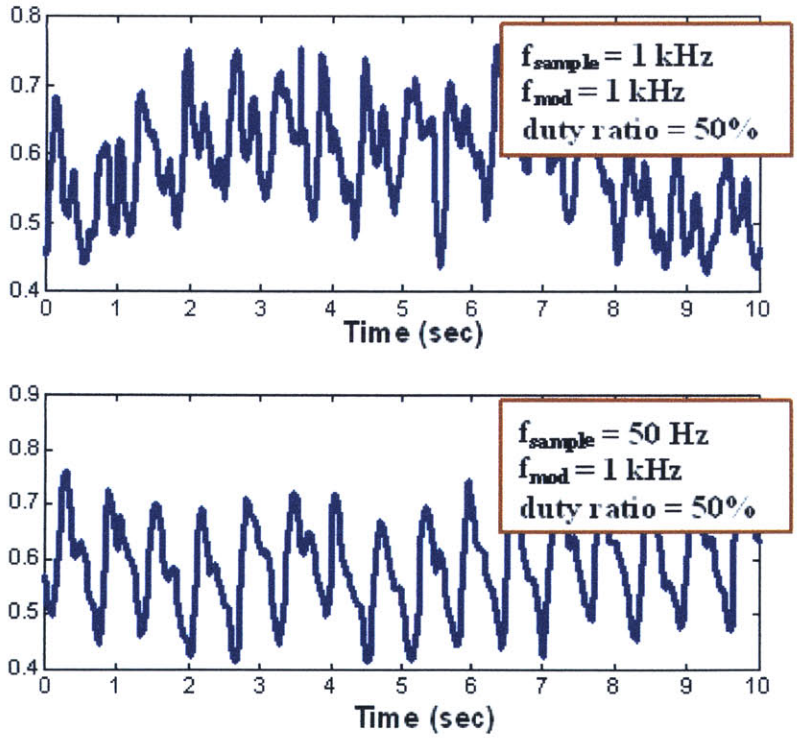

Figure 6-8: Comparison of the PPG waveforms sampled at (from top to bottom) 1kHz and 50Hz, respectively.

The first peak, resulting from peripheral wave reflections, and the other noticeable features of the waveform (caused by wave reflection from vasodilation) are still visible for the lower resolution signal. Although certain high frequency features that are visible on the waveform acquired at 1 kHz are no longer visible on the 50 Hz waveform, it is believed that these components add little information to the signal.

6.2.2 Signal Aliasing

Our research results indicate that there are no discernable aliasing effects for modulation rates over 50 Hz. However, for sampling rates less than 50 Hz, we found that the detected signal appeared to have extra high frequency components superimposed on the desired signal (Figure 6-9). Although the main PPG signal is still visible, the added high frequency components are undesirable. It is believed that the root cause of this signal corruption is a form of signal aliasing. It seems reasonable that the 30Hz sampling rate may be a frequency that accentuates or excites one of the frequencies contained within the plethysmograph signal. The excitation of the higher frequency component through aliasing leads to the 'corrupted' PPG waveform. The most likely explanation for this finding is that the low pass filter's cutoff is not sufficiently eliminating frequency components within this range. Consequently, the Nyquist criterion is not satisfied and aliasing is occurring. This extra corruption could be a problem for the signals of patients with low perfusion or high levels of vasoconstriction. If the reflected wave is not very prominent, as could be the case for the aforementioned patients, it could be easily lost amongst the aliasing effects.

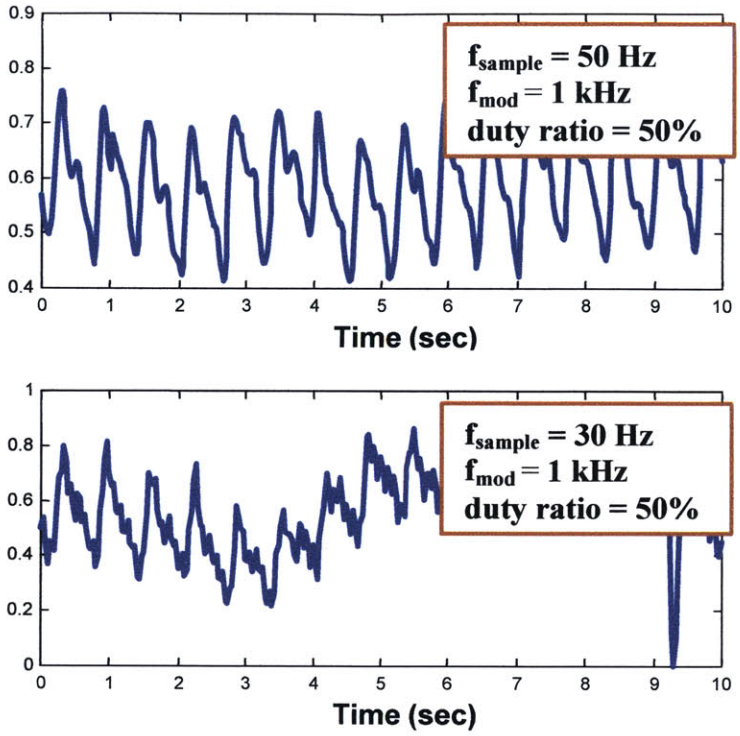

Figure 6-9: Comparison of the PPG waveforms acquired at sampling rates of (from top to bottom) 50 Hz and 30 Hz, respectively. Note the extra high frequency components on the 30 Hz waveform.

Based on our results, we recommend that for high-speed LED modulation situations, a minimum sampling rate of 50 Hz should be used. Since signal resolution improves as sampling frequency increases, we recommend the implementation of a sampling rate of 100 Hz for normal monitoring situations. The higher sampling rate provides added resolution and should not require too much free space for situations where patients are monitored for several hours.

Chapter 7 Oxygen Saturation Measurement Algorithm

7.1 Oxygen Saturation Calculation Method

During this research significant work has focused on incorporating oxygen saturation measurements (S_aO_2) into the array of measurements obtainable by the Ring Sensor. Oxygen saturation provides valuable information regarding blood oxygenation and can be obtained completely noninvasively. If two wavelengths of monochromatic light alternately illuminate a pulsating bed of vessels (generally in either the finger or ear), the percentage ratio between the concentration of oxyhemoglobin [O_2Hb] and the sum of the concentration of oxyhemoglobin and reduced hemoglobin [HHb] can be calculated. This ratio is commonly referred to as the oxygen saturation level of the finger (19).

$$SpO_2 = \frac{[O_2Hb]}{[O_2Hb]+[HHb]} \times 100 \qquad (19)$$

Once the theoretical oxygen saturation calculation has been described, its incorporation into the software design of the Ring Sensor will be described. Initial work has focused on the calculation of oxygen saturation from the traditional Beer-Lambert law.

$$I_{out} = I_{in} e^{-Cd(S\beta_o + (1-S)\beta_R)} \qquad (20)$$

where S is the saturation, β_o is the extinction coefficient for oxyhemoglobin, and β_R is the extinction coefficient for reduced hemoglobin. If the ratio of light intensity measured at two

times with two different wavelengths is calculated, it can be shown that the Lambert-Beer Law can be written independent of both absorber concentration and path length.

$$R = \frac{\ln\left(\frac{I_{out}(t_1)}{I_{out}(t_2)}\right)_{red}}{\ln\left(\frac{I_{out}(t_1)}{I_{out}(t_2)}\right)_{IR}} = \frac{-\Delta Cd\left(S\beta_{ored} + (1-S)\beta_{Rred}\right)}{-\Delta Cd\left(S\beta_{oIR} + (1-S)\beta_{RIR}\right)} \tag{21}$$

For the above expression, $I_{out}(t_1)_{red}$ indicates the red light intensity exiting through the finger during systole, $I_{out}(t_2)_{red}$ is the red light intensity exiting the through the finger during diastole, with similar definitions for the intensities of infrared light noted in the denominator. If equation (21) is rewritten as an expression for S (the saturation), we find that

$$S = \frac{\beta_{Rred} - R\beta_{RIR}}{R[\beta_{oIR} - \beta_{RIR}] - \beta_{ored} + \beta_{Rred}} \tag{22}$$

From an absorption spectra table, we can determine the appropriate extinction coefficients for oxyhemoglobin and reduced hemoglobin illuminated with both red and infrared light (table 1).

	RED	IR
β_R	0.812 ± 0.006	0.181 ± 0.003
β_o	0.080 ± 0.005	0.294 ± 0.002

Table 1: Extinction coefficients for [O_2Hb] and [HHb] for both red and infrared light [47].

Using the quoted extinction coefficients we can obtain an expression for the saturation in terms of only the light intensity ratios.

$$S = \frac{0.812 - (0.181)\mathbf{R}}{0.113\mathbf{R} + 0.732} \tag{23}$$

Therefore, by using red and infrared light and by taking the ratio of the detected pulsatile signal at the maxima and the minima we should be able to estimate the oxygen saturation of the monitored patient.

7.2 Ring Sensor S_aO_2 Calculation Algorithm

The ratio calculation is very susceptive to motion artifacts [48], [49]. Any large corruption of the non-pulsatile component can easily affect the saturation ratio. Therefore, it is necessary to stabilize the calculation by using a moving average window. The first step in determining the oxygen saturation is to define the sampling window (ie: the number of samples used for each calculation). The sampling window used for the oxygen saturation calculations is the same as the window used for the heart rate calculations. For our calculations, the width of the sampling window, N, is defined to be the number of data points acquired in ten seconds. Once the prescribed number of data points has been sampled, several calculations are executed. First, the Fast Fourier Transform (FFT) of the sampled data set is taken using the standard FFT equation,

$$\overline{F_m} = \sum_{n=0}^{N-1} W_N^{mn} f_n \tag{24}$$

where $\overline{F_m}$ is the FFT of the sampled signal, fn is the signal, and

$$W_N = e^{-j(2\pi mn/N)} \tag{25}$$

Once the FFT has been calculated for the 10-second window, the power spectrum is calculated using equation (26).

$$P = \left| \left(\sum_{n=-\infty}^{\infty} f_n e^{-jn\omega T} \right) \right|^2 \tag{26}$$

The power spectrum shows the relative strengths of oscillating signals contained within a given input signal. Under ideal conditions, the heart rate can be calculated from the first peak of the

power spectrum. The measured heart rate is equal to the frequency of the first peak times 60 (converts beats/sec to beats/min),

$$HR = \omega_1 \left[\frac{\text{beats}}{\text{sec}} \right] * 60 \left[\frac{\text{sec}}{\text{min}} \right] \tag{27}$$

Since the FFT uses the entire 10-second window for the frequency determination, the heart rate calculation is essentially an average of the beat-to-beat changes in heart rate during the 10-second sampling period (Figure 7-1).

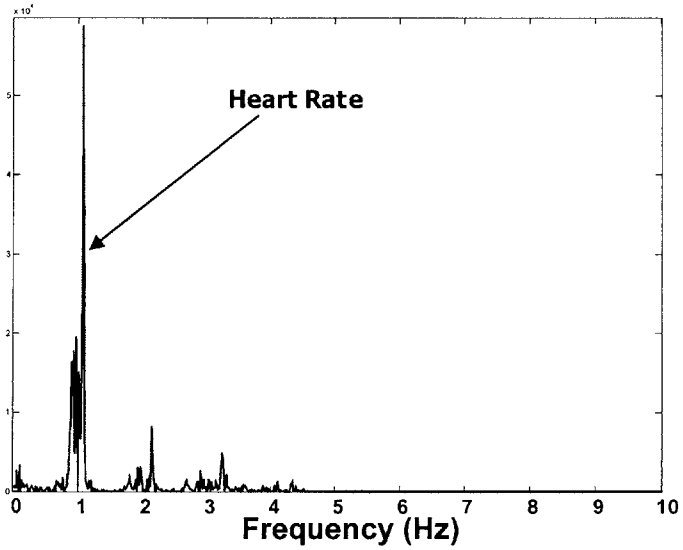

Figure 7-1: Standard power spectrum of Ring Sensor PPG signal. The first peak is used to estimate the patient's heart rate.

After the heart rate is calculated, the frequency used for the calculation (ω_1) is used to find each of the maximum and minimum parts of the plethysmograph waveform (Figure 7-2).

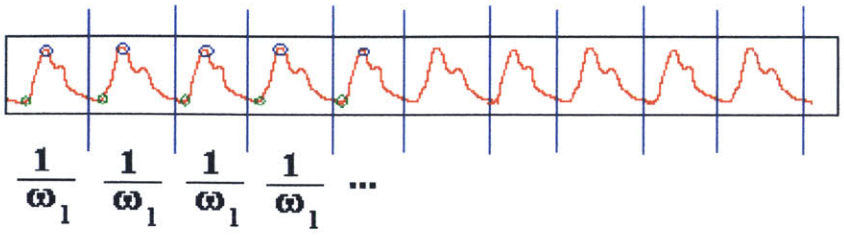

Figure 7-2: Graphical representation of how the windowed data is subdivided for oxygen saturation calculations. Each bin has a width of $1/\omega_1$, the heart rate of the patient. Once the 10-second window has been subdivided, each max and min is located and an R-value is calculated

The inverse of the frequency (i.e.: period) defines the local window used to determine each point corresponding to systole (local max) and each point corresponding to diastole (local min). Each set of max and min pairs is used for an individual oxygen saturation ratio calculation. Once all of the ratios within the main 10-second window have been calculated, they are averaged as follows,

$$R_{j-av} = \frac{1}{P}\sum_{i=1}^{P} r_i \qquad \textbf{(28)}$$

where P is the total number of ratios measured within the 10-second window, r_i is the i^{th} ratio of intensities, defined in (21). Next, the average oxygen saturation for the windowed set of data is calculated using equation (23). Finally, since this measurement is very susceptive to motion artifacts, each average oxygen saturation measurement is averaged with the average of the previous saturation readings. All of these calculations are made immediately after the data is acquired and the results are displayed in real-time.

Chapter 8 Sensor Validation and Benchmarking at MGH

8.1 Motion Artifact Reduction

Although continuous monitoring of arterial hemoglobin using pulse oximeters has become a universally accepted standard of care in the hospital, "...little progress has been made in reducing the incidence of failure to display valid data" [50]. As described earlier, situations in which there is a failure of valid data display generally occur because of either a physiologically based change or because of a change at the sensor. Therefore, proper sensor design is critical for minimizing motion artifact. However, most research in the field of wearable sensors has been focused on the post-processing of sensor data [51, 52, 53, 54] and not on the minimization of artifact through careful sensor design.

8.1.1 Previous Ring Sensor Monitoring Results

Research associated with the design of the Ring Sensor has focused on optimizing the sensor design before using any additional signal processing techniques. Although appropriate signal processing algorithms are important, their utility depends greatly upon the quality of signal that is provided. Thus, they do not fix the motion artifact problem; they merely provide an adjustment to the true data to make it more usable. Ring Sensor design efforts have focused on providing the highest quality of data before any processing, thus making it possible for clinicians to evaluate data that is as close to the "true signal" as possible. To this end, significant work

effort has been put into a design that decouples the monitored region of interest (the region surrounded by the sensor band) from external disturbances (Figure 8-1).

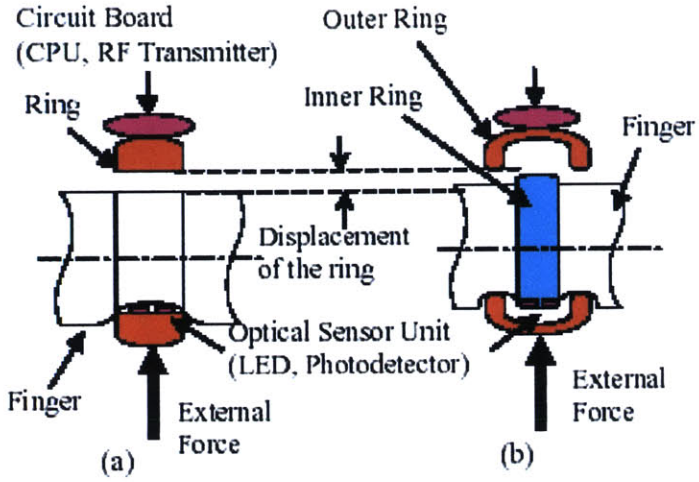

Figure 8-1: Dislocation of Ring Sensors due to external load (a) Traditional single body design under external force (b) New isolating Ring Sensor under external force [55].

Initial experimental results from laboratory tests on health volunteers indicated that the Ring Sensor was capable of continuously monitoring patients during a variety of activities [56]. At the time of this experiment, activities included walking, writing, typing, and running. It was found that a measurable signal was detected ~35% of the time (Figure 8-2).

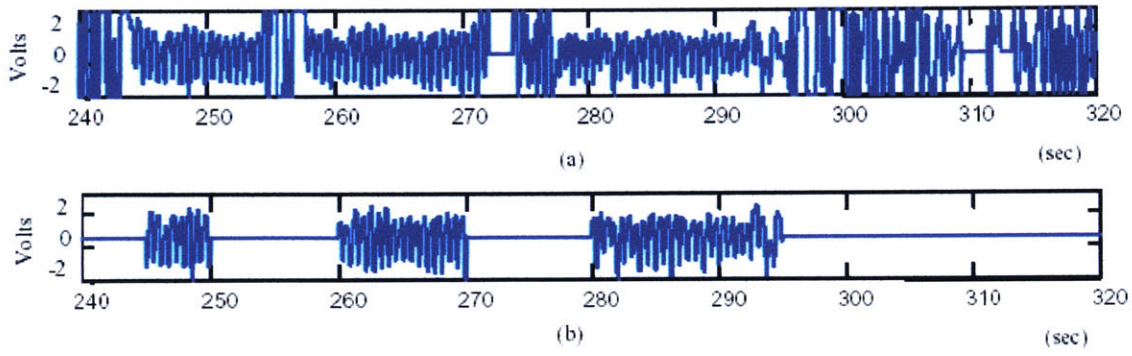

Figure 8-2: A part of the two-hour monitoring test result. The software detected motion artifact and removed the contaminated signal. (a) Raw data of the Ring Sensor (b) Data after artifact detection process.

It should be noted that the algorithm used for motion detection was rather conservative in that it defined a good signal to be a "clean signal" that lasted for duration of at least five seconds or more. Therefore, the measured signal result reported earlier should be considered to be a lower bound estimate for the artifact rejection potential of the Ring Sensor.

8.1.2 Revised Ring Sensor Laboratory Results

Continued research has been focused toward an improved mechanical design. A significant improvement in signal stability was realized by employing a transmittance optoelectronics sensor configuration (Figure 4-1). Further refinement has gone into the design of the sensor band. In particular, the attachment of the electronic components has been changed such that they no longer directly touch the wearer's skin (Figure 8-3).

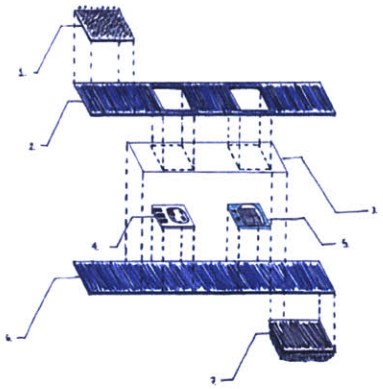

Figure 8-3: Redesigned sensor band. Protects optical components from direct contact with skin and hides wires from outside environment.

Additionally, as described earlier, the basic analog signal processing has been optimized for improved front-end signal stability (Figure 8-4, Figure 8-5).

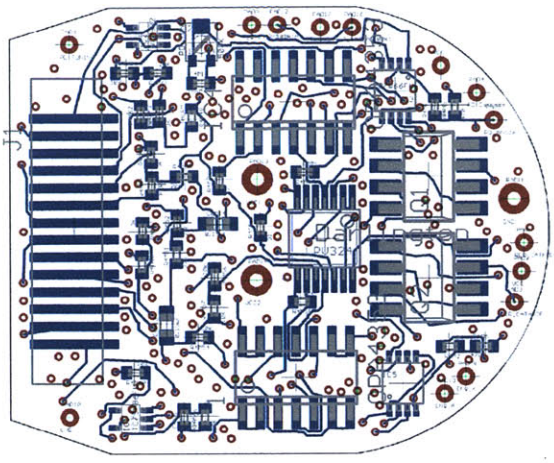

Figure 8-4: Top view of the analog signal processing board of Ring Sensor.

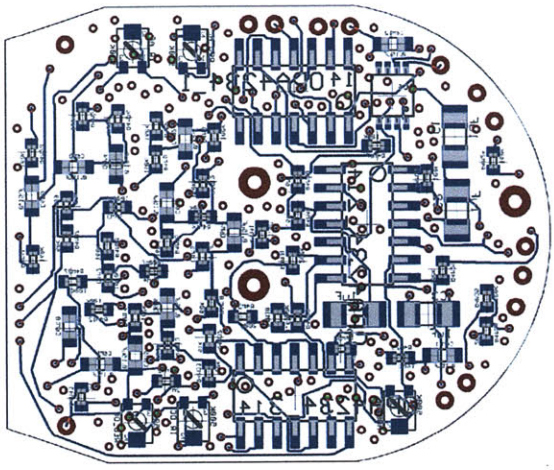

Figure 8-5: Bottom view of the analog signal processing board of the Ring Sensor.

These modifications greatly improved the ability of the device to measure traditionally difficult variables such as heart rate variability. Comparisons with other cardiovascular monitoring modalities indicate that the modifications to the Ring Sensor design have improved this measurement (Figure 8-6.)

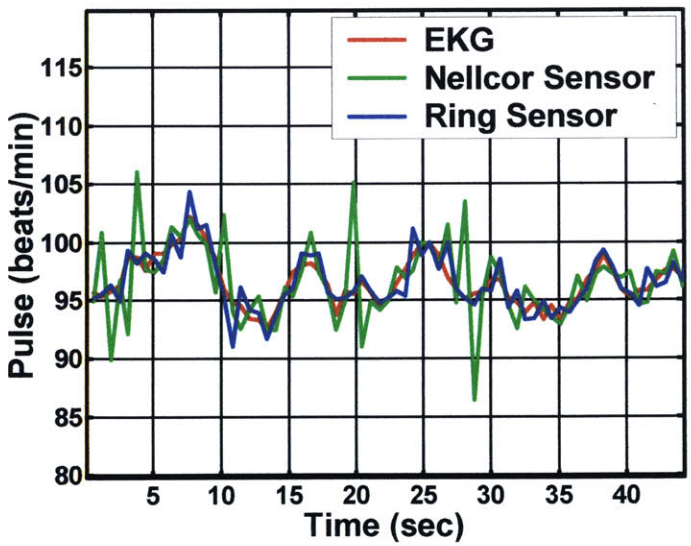

Figure 8-6: Beat-to-beat pulse rate of Prototype B Ring Sensor benchmarked with EKG and FDA approved fingertip PPG by Nellcor.

These improvements, along with the extensive advancements made in the early stages of the sensor design have prepared the sensor for more extensive benchmarking.

8.2 MGH Benchmarking

IRB approval was obtained to begin testing a tethered version of the Ring Sensor on patients in the Pulmonary Function Testing (PFT) laboratory at the Massachusetts General Hospital (Figure 8-7).

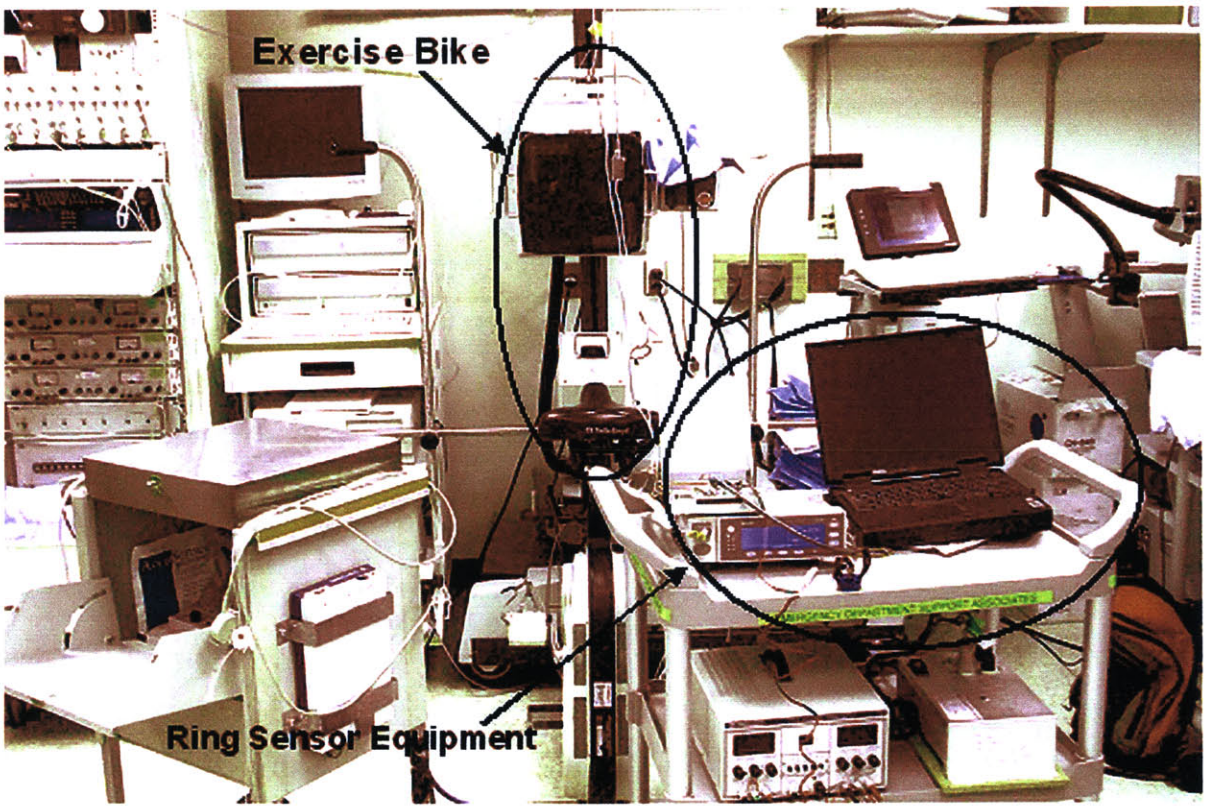

Figure 8-7: Pulmonary Function Testing laboratory with Ring Sensor monitoring equipment.

The Ring Sensor was successfully tested on 15 patients (7 male, 8 female) of various ages and with different morphologies and degrees of cardio-pulmonary related pathologies. All patients provided informed consent of our protocol. Informed consent consisted of first receiving and reviewing a standard form letter distributed by a third party individual to maintain complete

patient anonymity before the trial. The contents of the letter described the basic experimental protocol and additional considerations such as the potential for compensation and any possible hazards to the individual's health which might occur as a result of participation in the study (A.1). Once the protocol had been reviewed, each patient was asked to return an accompanying signed postcard, indicating whether or not they were willing to participate in the study (Figure 8-8).

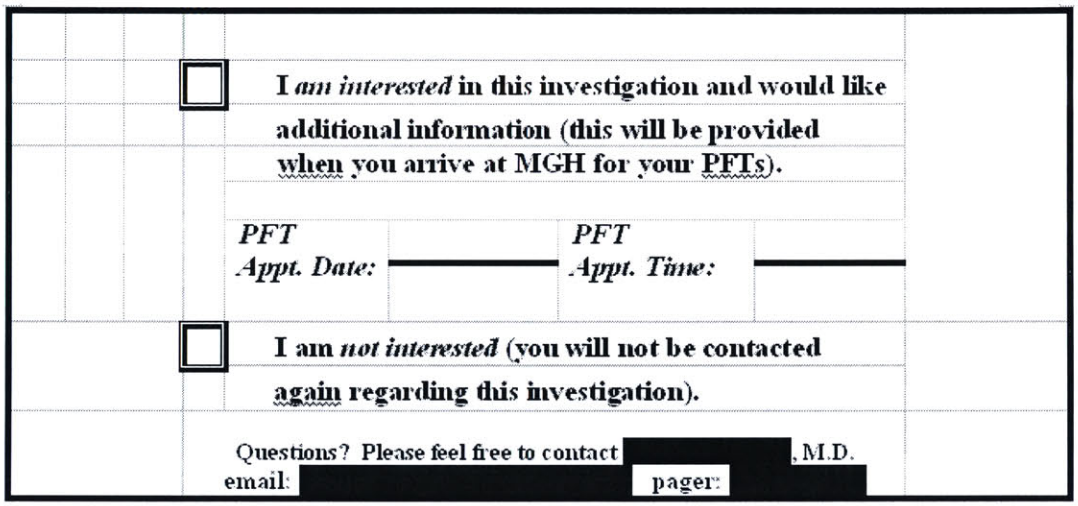

Figure 8-8: Copy of postcard each study subject was asked to return denoting interest in learning more about the study.

The patients who were interested in participating in the study were then contacted the day of the trial and were fully informed of the complete study protocol. All additional questions were answered at this time and the patients were once again asked if they would like to participate, with the option to end the study, for any reason, at any time during their normal PFT visit. For our study, the only aspects that differed from the PFT lab's normal protocol involved wearing the Ring Sensor and an FDA approved Nellcor N-395 pulse oximeter while performing their normal exercise test (Figure 8-9).

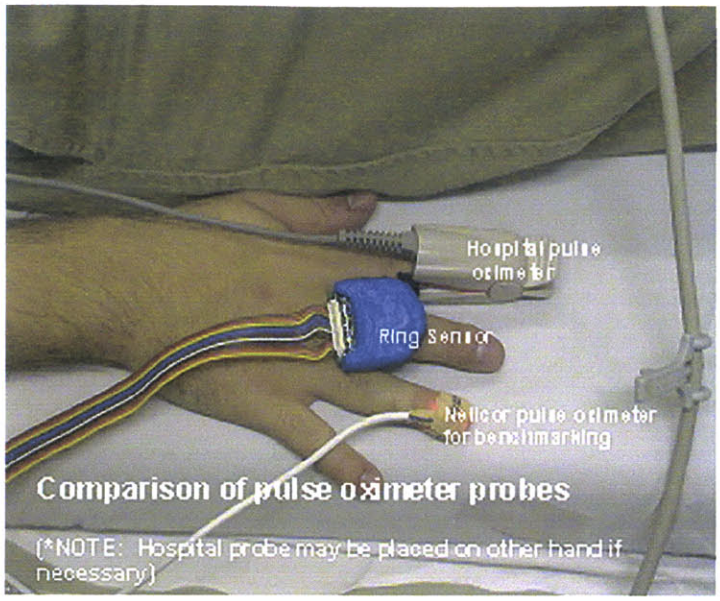

Figure 8-9: Comparison of pulse oximeter probes worn by patient during PFT lab testing. For all experiments, a tethered version of the Ring Sensor was used.

8.2.1 MGH Motion Artifact Benchmarking

The PFT lab's protocol consisted of obtaining resting blood gas and EKG data on the patient and then obtaining data while the patient rides a stationary bicycle against an increasing pedaling resistance until exhaustion. Throughout the protocol, PPG data was collected for both the Ring Sensor and the Nellcor fingertip pulse oximeter. Plethysmographs from both devices were sampled and recorded using a National Instruments DAQCard-6024E for PCMCIA data acquisition board at a sampling frequency of 1000 Hz, for a time of approximately 30 minutes. Data acquisition was performed with a custom graphical user interface designed using Labview® (Figure 8-10). Oxygen saturation measurements were additionally benchmarked with both the Nellcor sensor and with arterial blood gas samples analyzed by a CO-Oximeter. The Ring Sensor data used for comparison was the raw, unprocessed sensor data. No additional post-processing algorithms were used to improve the quality of the measured signals.

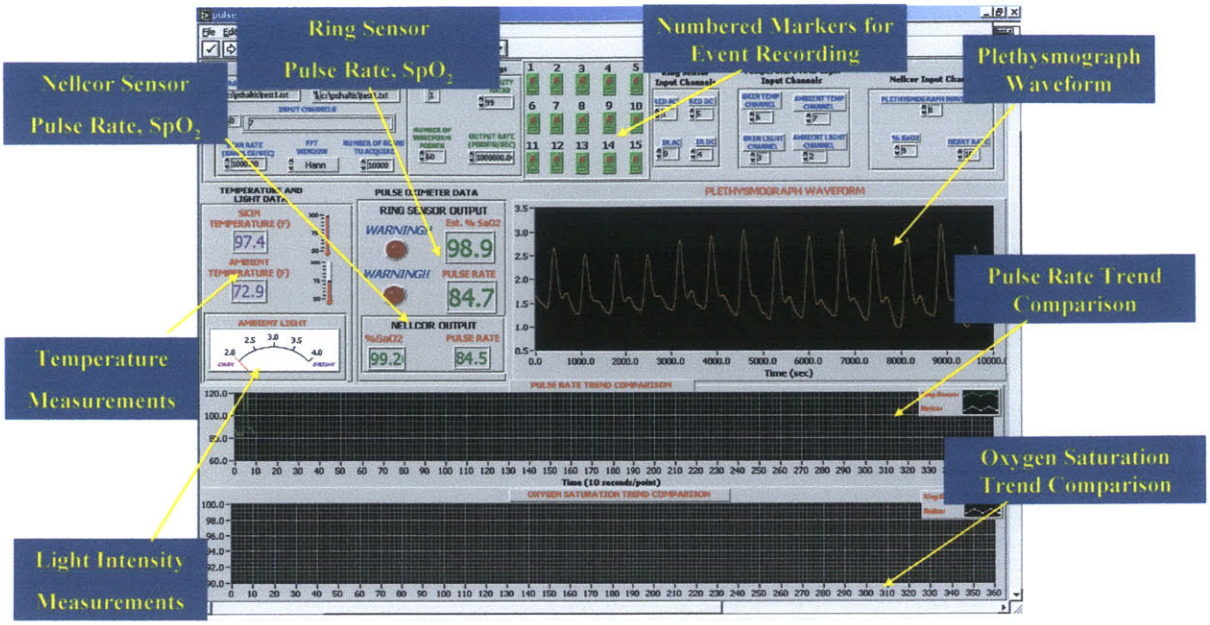

Figure 8-10: Windows-based, graphical user interface for the Ring Sensor. Note that both the buffered window of the PPG waveform and heart rate trend data are displayed.

In general, we found that the Ring Sensor matched the Nellcor sensor's signal stability during patient resting times (Figure 8-11a). More importantly, though, the Ring Sensor consistently provided a significantly more stable plethysmography waveform for ALL patients (Figure 8-11b). In fact, we found that the Ring Sensor's PPG signal was even generally unaffected by changes in sensor attachment. In nearly all cases, a useable signal was acquired while the patient was struggling to ride a bicycle. Perhaps even more promising is the fact the signals that were acquired, including those presented in this report, required no additional off-line signal post-processing for improvement. The raw signals obtained directly from the sensors were stable enough to utilize traditional oxygen saturation calculation algorithms. Additional post-processing can be added to better extrapolate particular waveform features such as heart rate variability, breathing rate, peripheral resistance, etc., but the raw waveforms are "clean" enough to calculate both heart rate and oxygen saturation even while the patient is riding a bicycle.

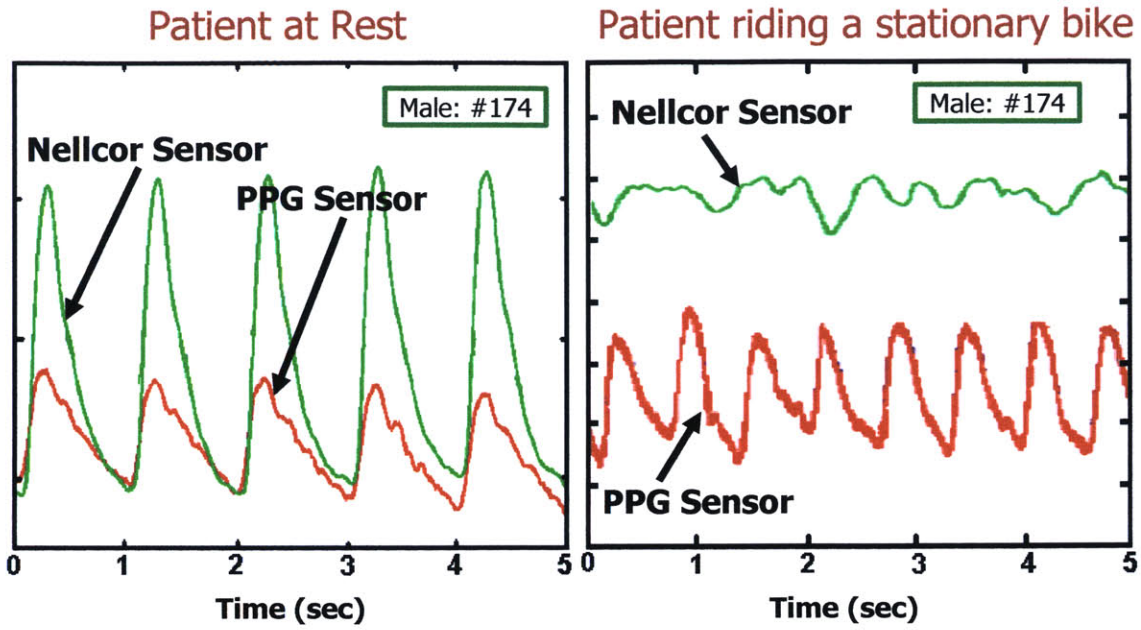

Figure 8-11: Representative example of PPG benchmarking data acquired while (a.) patient was at rest (b.) patient was riding a bicycle against a graded resistance.

An additional finding from our tests at the PFT lab was that the decoupled design of the Ring Sensor eliminated variations in signal magnitude caused by changes in bicycle handle grip pressure. As is well known, changes in transmural pressure can significantly change the magnitude of a PPG signal [57]. However, as was previously demonstrated by the double ring design, if the sensor unit is sufficiently decoupled from the mechanical interaction with the wearer's environment, no discernable changes in signal amplitude should occur. During our tests in the PFT lab, patient's frequently changed their grip pressure on the handlebars of the bicycle. These changes in grip pressure were expectedly detected by the Nellcor fingertip pulse oximeter. However, the decoupling design of the Ring Sensor prevented these noticeable changes in grip pressure, providing added assurance for the quality of the detected waveform (Figure 8-12).

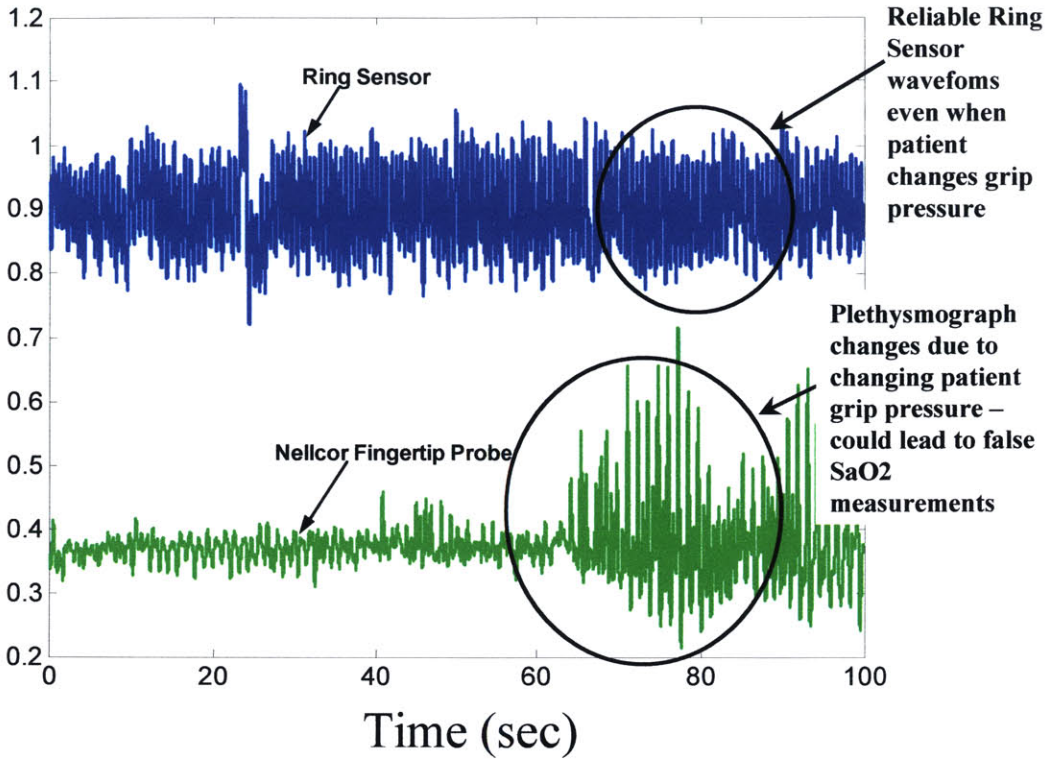

Figure 8-12: Decoupled Ring Sensor design leads to no significant change in signal magnitude during changes in patient grip pressure. Note the large changes in magnitude measured by the FDA approved Nellcor fingertip pulse oximeter.

Overall the results of our field testing and benchmarking at the Massachusetts General Hospital have demonstrated that the Ring Sensor's superior front-end mechanical sensor design have eliminated many of the traditional motion artifact problems associated with other wearable sensors. By focusing on first, developing an understanding of the mechanisms which lead to motion artifact and by then devising a mechanical and electrical system which minimizes their respective influences, the Ring Sensor has demonstrated a superior ability to reject motion artifact, independent of additional signal post-processing techniques. Consequently, unlike existing FDA approved devices, the Ring Sensor has demonstrated a potential for noninvasive monitoring patients both under low and high motion conditions.

8.2.2 MGH Oxygen Saturation Calibration and Benchmarking

It is well known that the Beer-Lambert law S_aO_2 calculation method provides only an estimate of the patient's true arterial saturation levels [58]. Therefore, there are several factors, resulting from assumptions made by the traditional calculation method, which necessitate the direct calibration of the sensor unit against a "gold standard" measure of the true arterial saturation level. These assumptions include:

- No light must be measured that has not passed through the pulsatile vascular bed
- The pulsatile changes in artery thickness must be the same for both wavelengths
- Valid measurement assumes that the pulsatile signal originates only from varying absorption by arterial oxygenated and reduced hemoglobin
- To simplify description of the principle behind measurement and its limitations, the Beer-Lambert law was assumed valid for the passage of light through tissue.

For these reasons, it was necessary to calibrate the Ring Sensor using blood gas samples taken from both normal and hypoxic patients. In addition to our motion artifact benchmarking tests conducted in the PFT lab, we have also collected blood sample data, using the FDA approved "gold standard" of blood gas monitoring, a CO-Oximeter. The CO-Oximeter is an off-line machine which is capable of measuring the constituents of either arterial or venous blood samples taken directly from lines inserted into the patient. Consequently, blood gas samples measured from this device are not continuous, but discrete measurements of the true saturation of the arterial blood. Since all non-invasive pulse oximeters are guaranteed to be accurate to within ±4% of the true saturation level [3], it is necessary to use the discrete samples measured by the CO-Oximeter for calibration.

Our measurement protocol dictated that only patients who, as part of their regular clinician prescribed lab work, would have an arterial line placed into their radial artery for blood gas data. Following the PFT prescribed protocol, time stamps were marked in our data set to indicate when blood samples were acquired. Therefore, we were able to mark the times for

which we had "true" arterial saturation measurements. As per the PFT protocol, baseline blood gas samples were drawn ~five minutes before the patient began pedaling, against no resistance, on the bicycle. Once the patient was instructed to pedal, blood gas samples at 1 and 3 minutes were drawn and sent to the lab for analysis. After pedaling for 3 minutes without resistance, a motor was activated which slowly added resistance to the bicycle's pedals. The patient was then instructed to pedal for as long as they could against the increasing resistance until they reached exhaustion. Blood was sampled once per minute while the patient continued to pedal. When the patient indicated exhaustion, they were asked to continue for a little while longer, and when instructed a "peak" desaturation blood was drawn from the patient. After the "peak" blood gas had been taken, the pedaling resistance was turned off and the patient was instructed to continue pedaling until an EKG-determined heart rate baseline was reached. At this time, a final blood sample was drawn to ensure that the patient was returning to a state of homeostasis.

As was mentioned earlier, both the Ring Sensor and Nellcor Sensor were attached to the patient throughout the aforementioned exercise test. Continuous PPG, heart rate, and oxygen saturation measurements were acquired during this time for further offline analysis. During our tests, a total of four patients desaturated to a level below 85% (defined to be a significant desaturation for our protocol). The data acquired for these patients has been used to construct a calibration curve for the Ring Sensor (Figure 8-13).

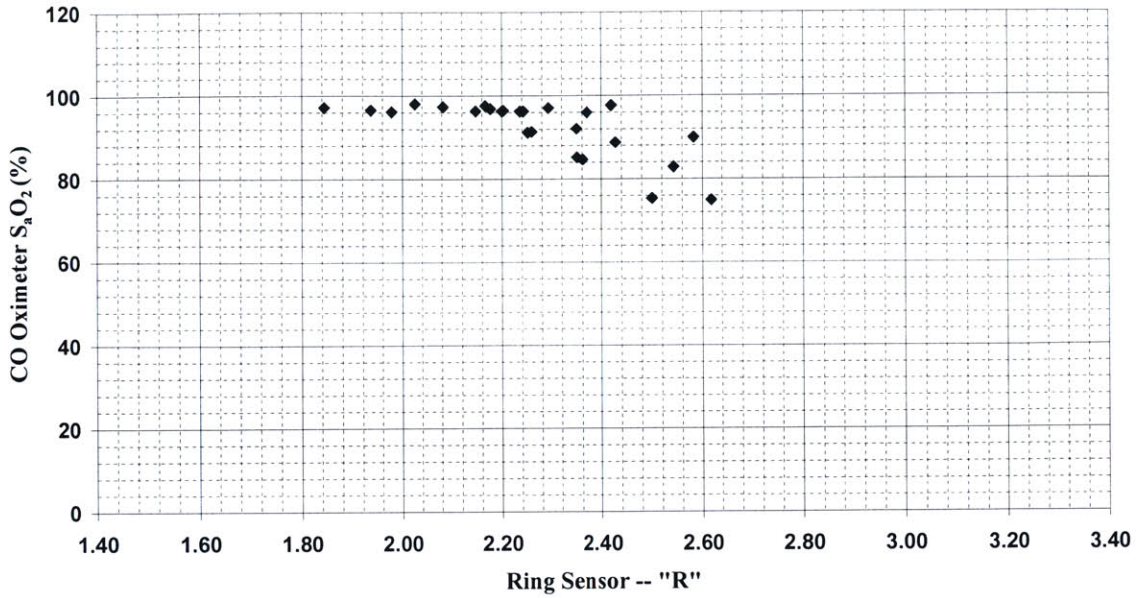

Figure 8-13: Experimentally determined calibration curve for the Ring Sensor. Each data point represents an average of approximately 10 data points sampled by the Ring Sensor during a sampling of arterial blood from the patient.

In addition to the calibration data that was collected for each patient, trend data from long-term monitoring of oxygen saturation was also calculated for each patient. Thus, we were able to develop saturation and heart rate trend comparisons for several minutes worth of data. As described in an earlier section, the Ring Sensor had a significantly more stable plethysmograph signal during patient testing. The superior stability of the signal translated into fewer false desaturation measurements for the Ring Sensor (Figure 8-14). In general, patient motion led to falsely low measurements of S_aO_2 for the Nellcor Sensor. However, since the Ring Sensor's plethysmography waveform was generally more stable, fewer false alarms were measured. It is important to note that the S_aO_2 levels estimated by the Ring Sensor are based on beat-to-beat calculations and consequently, do not involve any buffering of the data. Again, we find that by eliminating the causes of motion artifact through the mechanical design of the wearable sensor, we are able to obtain a more reliable estimate of the true oxygen saturation of the patient, even in

situations when there is patient motion. A complete data record for each patient can be found in the accompanying Appendix (A.2).

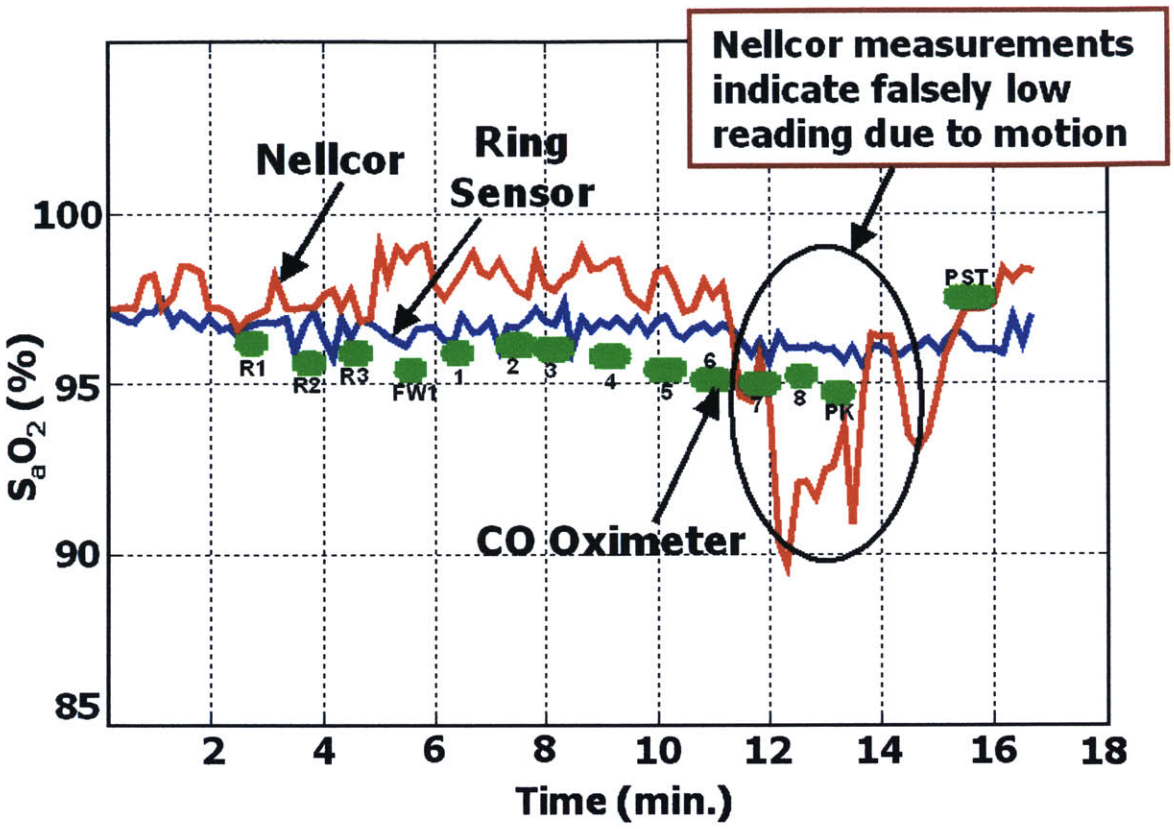

Figure 8-14: Oxygen saturation trend comparison. Discrete blood samples were drawn for measurement with an FDA approved CO-Oximeter. These samples represent the "true" arterial oxygen saturation level. It is important to note that when the patient was exerting maximum effort (near exhaustion), the Nellcor fingertip pulse oximeter recorded a falsely low arterial saturation level, while the Ring Sensor matched the true value.

8.3 Patient Comfort Survey

After gaining consent from the patients that were being tested in the PFT lab, we also conducted a short survey of overall sensor comfort to help determine the long-term wearability of the current Ring Sensor design. Our survey consisted of asking the patient about their discomfort associated with the Ring Sensor before, during, and after the exercise test. In particular, each patient was asked to describe the relative level of comfort/discomfort associated

with the Ring Sensor. For comparison purposes, the rating system was between 1 and 6 as follows (1 = no discomfort, 6 = complete discomfort):

1. Can barely notice
2. Can feel sensor but no real discomfort (like wearing a hat)
3. Slightly uncomfortable but not too bad (like wearing a hat a little too tight)
4. Irritating (like a hat much too tight or an itchy sweater)
5. Painful (like getting a shot with a needle)
6. Worse than getting a shot with a needle

The following three bar charts show the responses of the patients (Figure 8-15):

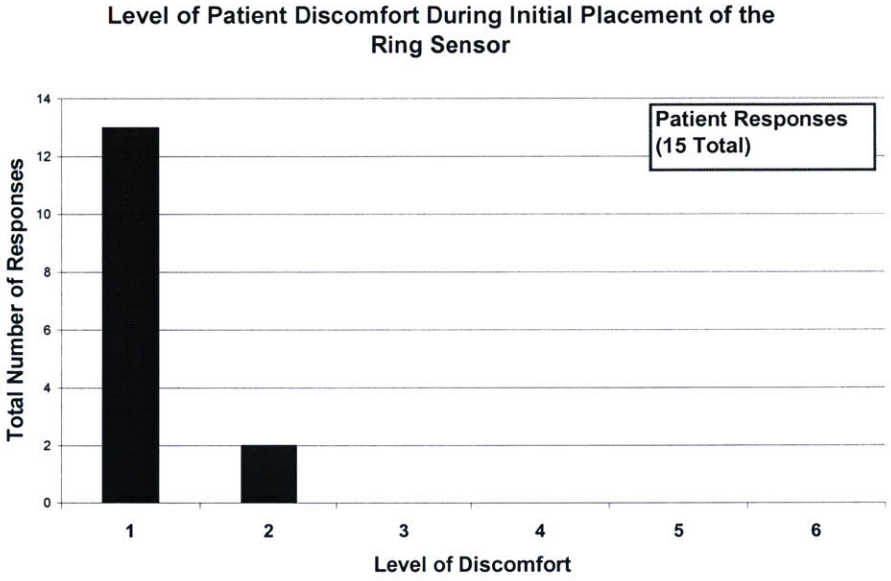

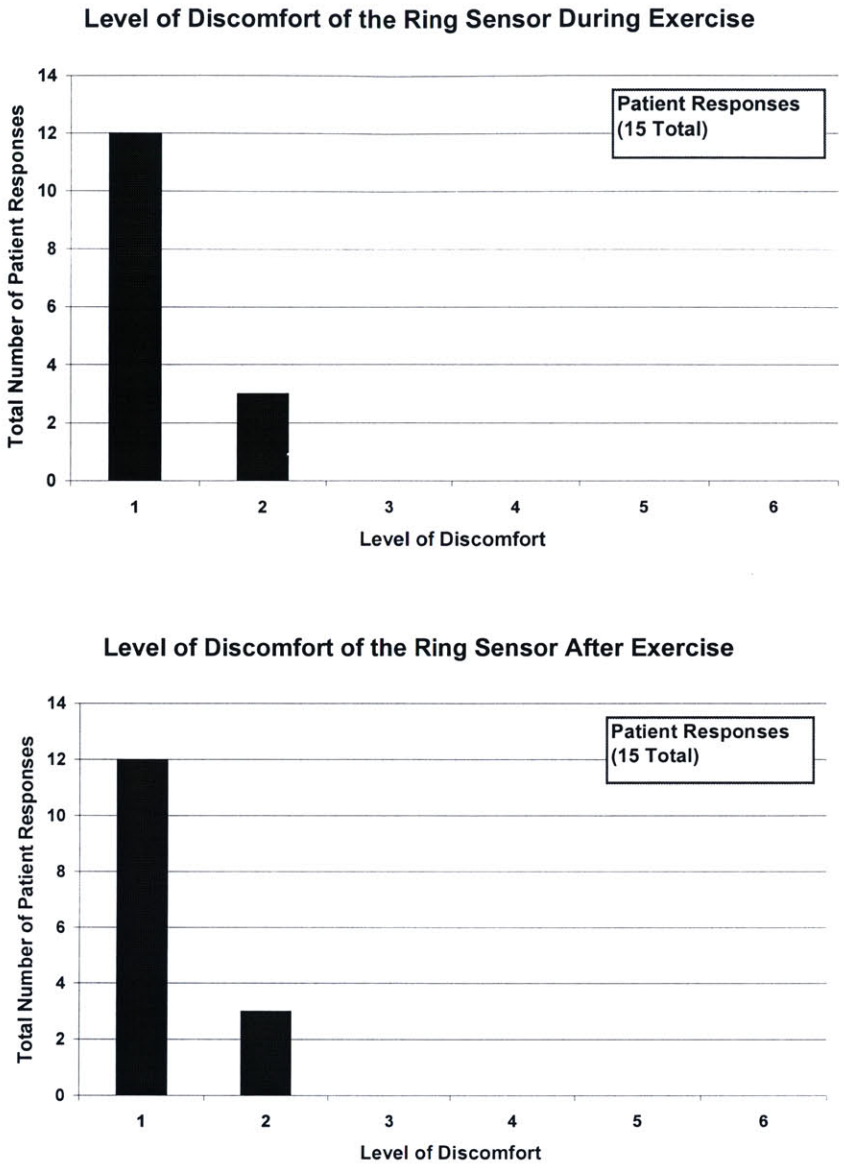

Figure 8-15: Patient responses regarding the relative discomfort of the Ring Sensor before , during, and after exercise. It is important to note that all patients have indicated that wearing the Ring Sensor is no worse than wearing a hat. These responses suggest the Ring Sensor may be an acceptable accessory for long-term monitoring.

As is demonstrated by the figure presented above, all of the patients tested to date have felt that the Ring Sensor is reasonably comfort and is, at worst, no more unacceptable than wearing a hat. These results, although simple, are important evidence that the Ring Sensor design is an

acceptable accessory for long-term, daily wear. Additionally, they demonstrate the first proof that the Ring Sensor is a publicly acceptable wearable sensor.

Chapter 9 Conclusions

Throughout the duration of this research we have strived to complete the motion artifact minimization work achieved in the previous embodiments of the Ring Sensor. We have improved the overall signal stability to the point that the Ring Sensor, without additional post-processing, is more reliable and more robust than existing FDA approved pulse oximeters in several different monitoring environments. In particular, we have shown that the Ring Sensor is able to monitor several different types of patients, reliably, even during situations when extreme motion exists. It is extremely important to emphasize that the Ring Sensor's signal stability exists without any additional post-processing. By engineering the mechanical and electrical components of the Ring Sensor to eliminate the causes of motion artifact, we have significantly enhanced the robustness of the sensor unit. Additionally, through a careful patient survey conducted at MGH, we have shown that the Ring Sensor is a comfortable accessory that should be acceptable for long-term patient use.

Appendix A. Opt-Out Letter

Dear Mr./Ms. _____,

We are mailing this letter to MGH patients scheduled for pulmonary function testing, to inform them about a medical study that we are conducting. This letter will briefly describe the study. Also enclosed is an addressed, stamped postcard. If, after you read about this study, you decide you are not interested in participating, you can check off the box that says "Not interested" and you will not be contacted again about this matter. You should feel very comfortable in saying this, since it will in no way alter the treatment and testing you receive at the pulmonary function testing (PFT's) clinic. In fact, we appreciate the time you are taking to read this letter, even if you decide you do not care to be in this study.

If you do NOT mail in the card, you can make a decision about being in this study on the day you come for pulmonary function testing. If we do not hear from you, we may approach you on the day you come in to the MGH PFT lab and provide you with additional information on this study. You will have a chance to ask any questions, and then you can make a decision about being in this study. You will not offend anybody if you don't want to be in the study; you should feel very comfortable saying "no" at that time if you are not interested. If you are uncertain if you want to be in the study, we will NOT enroll you in the study. Only people who say very clearly that yes, they want to be in the study, can be in the study.

Who is conducting this study?

This study is being conducted by several doctors from the MGH, in collaboration with several engineers from the Massachusetts Institute of Technology. The primary investigator at MGH is Andrew Reisner, MD, of the Department of Emergency Medicine. Also participating are William Hurford, MD, of the Department of Anesthesia, and David Systrom, MD, of the MGH PFT lab.

What are we testing in this study of MGH PFT patients?

A machine called a "pulse oximeter" measures how much oxygen is in your blood after the blood passes through your lungs. It is a safe, very common medical device that works by shining light through part of the body, usually a fingertip. In this study, we are testing a investigational pulse oximeter developed at the Massachusetts Institute of Technology. It is new in that it is very very low power, which means that it may be able to function using a low power watch battery (only 2.5% of the voltage of a standard pulse oximeter).

Diagram Illustrating Three Kinds of Pulse Oximeters:

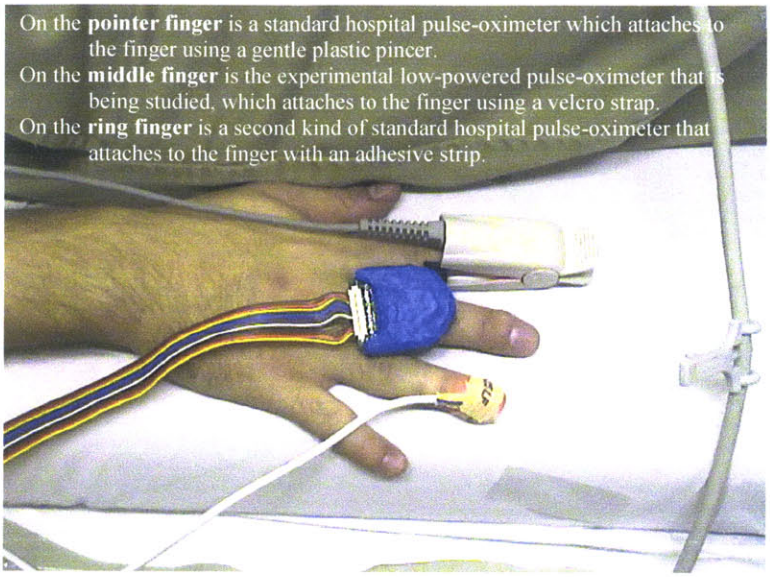

Will all PFT patients be approached for this study?

Even if you receive this letter, you may not be approached about this study since the study investigators will not be available every day to collect data. We are sending this letter only to PFT patients whose doctors have already decided that the testing should include testing samples of arterial blood.

Overall, we expect to approach less than half of all patients who come in for pulmonary function testing.

What will this study involve?

We need data on two issues. The first is how accurate the readings are from the investigational sensor compared to a standard pulse oximeter. The second issue is if the investigational Ring Sensor, which goes around your finger and is held in place by two cloth straps, is uncomfortable. We have designed these straps so that they should be comfortable, but now we need to test out if in fact the sensor is as comfortable as we want it to be. Therefore, we will ask participants to rate the comfort of the sensor as the study goes on. IF at any time you do think the sensor is uncomfortable and you want to take it off, it is very important that you tell us. If we learn that the sensor is uncomfortable when people are trying it out, we will then re-examine the design of the sensor to make it fit more comfortably.

At the same time, we will also place a regular commercial pulse oximeter (this is the kind used used commonly in hospitals throughout the United States). We will use a Nellcor brand pulse oximeter. We will collect data while you go through all the routine procedures that are part of your regularly scheduled pulmonary function testing. For our analysis of this investigational pulse oximeter, we will also use the information that is collected as part of your regularly scheduled pulmonary function testing, including the results of any blood tests performed and other basic information about you (such as your age and why you were scheduled for PFT's).

At the end of your regularly scheduled pulmonary function testing, if you are willing, we will collect an additional 5 – 10 minutes of pulse oximeter information.

Costs

There is no cost to you for enrolling in this study.

Risks and discomforts

We do not anticipate any risks nor discomfort as a result of this study.

The Ring Sensor's ring is constructed from fabric bought in a normal fabric store, and it also has common Velcro in it. The sensor is encased in common plastics (Polyurethane, epoxy, and Plasti-Dip) which can be found in such common products as finish for a wooden floors, and dried super-glue.

BURN FROM THE SENSOR: The sensor uses nothing more than a small light bulb. It does not produce enough heat to cause a burn. In laboratory tests, the light bulb does not even feel warm to the touch. It does not generate other forms of dangerous radiation, either.

INFECTION: The sensor will be used on multiple people. Therefore, each person will have their finger very well cleaned before the sensor is placed, to make sure that germs are reduced before the sensor is put in place. After each use, the sensor itself will be cleaned. We expect that the sensor will be as safe to use as any other piece of reused hospital equipment (regular pulse oximeter, blood pressure cuff, doctor's stethoscope, and so on).

ELECTRICAL SHOCK / BURN DUE TO SHORT CIRCUIT: This device runs using 4 volts, which is only about 3% of the voltage used by a light bulb plugged in to the wall. Also, in the event of a short circuit, a fuse in the circuitry will prevent excess current from flowing.

BLOOD DRAW: No additional blood will be drawn for this study.

Benefits

There are no benefits for the people who participate in this study.

Alternatives

Your alternative is to decide you are not interested in being a part of this medical study.

If you are not interested in learning more about this study, you can take the enclosed postcard, check off the box that says "Not interested" and drop the postcard in the mail, and you will not be contacted again about this matter.

If you are interested in learning more about this study, you can take the enclosed postcard, check off the box that says "I am interested in this study" and drop the postcard in the mail. If we know you are interested, we will make special attempts to be present on the day you come in for pulmonary function testing. EVEN if you ARE interested, we will provide you with additional information on the day you come in for pulmonary function testing. You WILL NOT BE ASKED to make a final decision about whether or not to be in the study until after we have provided you with additional information.

If you are not sure, or if we do not hear from you, we may approach you on the day you come in for pulmonary function testing. At that time, you can decide to not be in the study, or you may choose to receive additional information about the study.

If you have questions or concerns in the meantime, please contact [redacted], MD: email [redacted], or else page on weekdays 12pm – 5pm by calling [redacted].

Appendix B. MGH Patient Data

The following tables contain complete blood gas information obtained from each patient who participated in the Ring Sensor study.

Date:	9-Jul-02
Gender:	Female
Time:	14:00
Subject No.:	3775
MGH ID:	[redacted]
Data File(s):	7_9_02raw
	7_9_02raw1
	7_9_02trend
	7_9_02trend1
Sampling Rate:	1000 Hz
Room Temp (C)	24

Questionnaire Informatic	
Question No.	*Rating*
1	1
2	1
3	2

Additional Info: [redacted]

Patient Arterial Data

Time Stamp	File	Sample ID	Time	Condition	pO2	pCO2	pH	HCO3	Hb	O2Hb	COHb	O2ct
1	raw	SS	15:36	steady state	87.0	36.7	7.43	24.4	10.8	**93.5**	2.5	14.1
1	raw1	R1	15:48	rest	100.0	27.0	7.43	18.0	7.9	**95.9**	1.1	10.6
2	raw1	R3	15:50	rest	92.0	36.8	7.43	24.5	10.4	**94.3**	1.7	13.6
3	raw1	R5	15:51	rest	86.0	38.2	7.42	24.9	40.5	**93.7**	1.9	13.6
5	raw1	FW1	15:55	free wheel	93.0	37.5	7.42	24.7	11.1	**94.2**	2.1	14.5
6	raw1	FW2	15:57	free wheel	95.0	34.9	7.42	22.7	10.1	**94.1**	1.9	13.2
7	raw1	1	16:00	exercise	98.0	35.5	7.41	22.9	9.6	**94.6**	2.8	12.6
8	raw1	2	16:02	exercise	99.0	35.7	7.41	22.6	8.0	**94.5**	1.9	10.5
9	raw1	3	16:04	exercise	103.0	35.5	7.41	22.7	8.2	**96.9**	0.0	11.1
10	raw1	PK	16:05	peak	108.0	34.1	7.40	21.5	11.1	**95.3**	1.4	14.7
12	raw1	PT	16:06	post	113.0	34.6	7.35	19.4	10.8	**95.0**	1.8	14.3

Additional time stamps:

2	raw	starting bike
4	raw1	starts pedaling
11	raw1	stops pedaling

Date:	10-Jul-02
Gender:	Female
Time:	11:50
Subject No.:	386
MGH ID:	[redacted]
Data File(s):	7_10_02raw
	7_10_02raw1
	7_10_02trend
	7_10_02trend1
Sampling Rate:	1000 Hz
Room Temp (C)	24

Questionnaire Informatic	
Question No.	*Rating*
1	1
2	1
3	1

Additional Info:

Patient Arterial Data

Time Stamp	File	Sample ID	Time	Condition	pO2	pCO2	pH	HCO3	Hb	O2Hb	COHb	O2ct
1	raw	SS	11:52	steady state	73.0	38.3	7.40	23.8	11.8	**91.9**	1.1	15.1
1	raw1	R1	12:04	rest	80.0	32.7	7.41	20.8	11.4	**92.7**	1.2	14.7
2	raw1	R3	12:06	rest	80.0	34.5	7.41	22.4	12.1	**93.1**	0.8	15.7
3	raw1	R5	12:08	rest	78.0	37.4	7.40	23.7	12.2	**92.6**	1.3	15.7
4	raw1	FW1	12:10	free wheel	80.0	34.2	7.41	22.0	11.8	**92.8**	1.4	15.2
5	raw1	FW2	12:12	free wheel	79.0	34.8	7.40	21.9	11.8	**92.8**	1.0	15.2
6	raw1	1	12:13	exercise	77.0	35.9	7.40	22.4	12.1	**92.3**	0.9	15.5
7	raw1	2	12:17	exercise	74.0	37.3	7.39	22.9	12.3	**91.9**	1.1	15.7
8	raw1	3	12:21	exercise	75.0	37.5	7.38	22.2	12.6	**91.5**	1.0	16.1
9	raw1	4	12:23	exercise	76.0	38.6	7.35	21.4	12.3	**91.5**	0.6	15.7
10	raw1	PK	12:25	peak	75.0	39.9	7.31	20.2	12.4	**90.7**	0.5	15.7
11	raw1	PT	12:28	post	95.0	36.2	7.28	17.1	12.5	**93.5**	0.5	16.3

Additional time stamps:

2	raw	moving to bike

Date:	11-Jul-02
Gender:	Male
Time:	10:30
Subject No.:	174
MGH ID:	
Data File(s):	174raw
	174raw1
	174trend
	174trend1
Sampling Rate:	1 kHz
Room Temp (C)	20

Questionnaire Information	
Question No.	*Rating*
1	1
2	1
3	1

Additional Info:

Patient Arterial Data

Time Stamp	File	Sample ID	Time	Condition	pO2	pCO2	pH	HCO3	Hb	O2Hb	COHb	O2ct
1	174raw	SS	10:34	steady state	72.0	41.5	7.43	27.9	14.3	**94.2**	2.1	18.8
1	174raw1	R1	10:44	rest	80.0	39.1	7.44	27.1	14.4	**95.5**	2.2	19.1
2	174raw1	R1	10:46	rest	77.0	41.5	7.42	27.3	14.4	**94.9**	2.2	18.9
3	174raw1	R2	10:48	rest	79.0	41.3	7.43	27.6	14.6	**95.5**	1.9	19.4
4	174raw1	FW2	10:50	free wheel	76.0	42.8	7.42	27.9	14.7	**94.5**	2.0	19.3
5	174raw1	1	10:53	exercise	80.0	43.5	7.41	27.9	14.9	**95.4**	2.1	19.8
6	174raw1	2	11:01	exercise	82.0	42.4	7.41	27.2	14.4	**95.6**	2.2	19.1
7	174raw1	3	11:03	exercise	81.0	43.9	7.41	28.0	14.9	**95.7**	2.0	19.8
8	174raw1	4	11:04	exercise	80.0	43.1	7.40	27.3	14.6	**95.5**	1.7	19.3
9	174raw1	5	11:06	exercise	78.0	44.5	7.39	27.3	14.7	**94.8**	2.1	19.4
10	174raw1	6	11:08	exercise	77.0	44.1	7.38	26.5	16.4	**94.5**	1.7	21.5
11	174raw1	7	11:12	exercise	76.0	42.6	7.38	25.6	15.1	**94.2**	1.7	19.8
12	174raw1	8	11:14	exercise	78.0	42.3	7.37	24.9	15.8	**94.6**	1.5	20.7
13	174raw1	PK	11:17	peak	75.0	42.1	7.37	24.5	15.7	**94.2**	1.8	20.5
14	174raw1	PT	11:19	post	105.0	39.8	7.35	22.4	15.7	**97.6**	1.9	21.3

Date:	11-Jul-02
Gender:	Male
Time:	14:00
Subject No.:	604
MGH ID:	
Data File(s):	604raw
	604trend
Sampling Rate:	1000 Hz
Room Temp (C)	21

uestionnaire Informati	
Question No.	*Rating*
1	1
2	1
3	1

Additional Info:

Patient Arterial Data

Time Stamp	File	Sample ID	Time	Condition	pO2	pCO2	pH	HCO3	Hb	O2Hb	COHb	O2ct
1	raw	SS	14:51	steady state	92.0	37.9	7.40	23.7	12.2	**96.7**	2.1	16.4
2	raw	R1	14:55	rest	100.0	32.5	7.41	20.8	10.9	**97.8**	1.7	14.9
3	raw	R3	14:57	rest	101.0	34.8	7.42	23.0	12.2	**97.5**	2.3	16.5
4	raw	R5	15:00	rest	101.0	34.9	7.42	22.9	12.0	**97.9**	1.8	16.4
5	raw	FW1	15:02	free wheel	93.0	37.5	7.39	23.0	12.0	**96.9**	2.0	16.2
6	raw	FW2	15:04	free wheel	94.0	377.0	7.38	22.8	12.3	**96.7**	2.0	16.6
7	raw	1	15:06	exercise	96.0	39.2	7.38	23.6	12.4	**97.2**	1.9	16.7
8	raw	2	15:08	exercise	92.0	39.9	7.38	23.9	12.4	**96.8**	2.0	16.7
9	raw	3	15:09	exercise	92.0	41.1	7.37	23.9	12.6	**96.6**	1.9	16.9
10	raw	4	15:13	exercise	90.0	39.8	7.35	22.2	12.6	**96.2**	2.1	16.8
11	raw	5	15:15	peak	93.0	37.3	7.33	20.0	11.6	**96.5**	1.7	15.5
12	raw	PT	15:22	post	109.0	36.1	7.31	18.3	13.1	**97.5**	1.8	17.7

Date:	8-Aug-02
Gender:	Male
Time:	9:00
Subject No.:	746
Data File(s):	f746raw
	f746trend
	f746raw1
	f746trend1
Sampling Rate:	1000 Hz
Room Temp (C)	23-25

Questionnaire Informati	
Question No.	*Rating*
1	1
2	1
3	1

Additional Info:

Patient Arterial Data

Time Stamp	File	Sample ID	Time	Condition	pO2	pCO2	pH	HCO3	Hb	O2Hb	COHb	O2ct
1 - long		SS		steady state - on O_2	58.0	34.6	7.44	23.5	14.8	**91.3**	2.4	18.7
2 - off O_2		R1		rest - off O_2	56.0	34.3	7.43	22.9	15.6	**90.2**	2.4	19.3
4		R3		rest	55.0	35.6	7.42	23.1	15.8	**89.4**	2.4	19.6
5		R5		rest	55.0	34.6	7.42	22.8	15.8	**89.4**	2.3	19.7
6		FW1		free wheel	52.0	34.8	7.42	23.0	16.1	**87.6**	2.1	19.6
7		FW2		free wheel	52.0	36.3	7.42	23.7	15.6	**87.5**	1.8	19.0
8		1		exercise	51.0	34.7	7.41	22.4	15.5	**86.6**	1.7	18.7
9		2		exercise	50.0	37.4	7.40	23.6	15.8	**85.3**	1.9	18.7
10		PK		exercise	46.0	37.9	7.39	22.8	15.7	**80.7**	1.0	17.9
11		CHECK		recovery - O_2 1L/mi	68.0	38.9	7.41	25.0	14.9	**93.8**	2.1	19.4
12		POST 2.5		post	57.0	35.4	7.39	21.8	16.0	**89.6**	2.0	19.8

Additional time stamps:

1 short -- mistake
3 long -- mistake

	f93trend
Sampling Rate:	1000 Hz
Room Temp (C)	22

Patient Arterial Data

Time Stamp	File	Sample ID	Time	Condition	pO2	pCO2	pH	HCO3	Hb	O2Hb	COHb	O2ct
1		SS		steady state	105.0	35.1	7.44	24.2	14.7	**97.9**	1.3	20.1
2		R1		rest	98.0	38.1	7.43	25.7	14.9	**97.5**	1.7	20.1
3		R3		rest	104.0	38.0	7.42	24.8	14.7	**97.8**	1.6	20.0
4		FW1		rest	106.0	34.8	7.44	23.7	14.7	**97.9**	1.4	20.0
5		FW2		free wheel	104.0	34.8	7.45	24.5	14.7	**97.9**	2.0	20.0
6		1		free wheel	109.0	34.2	7.45	23.9	14.8	**98.1**	2.1	20.1
7		2		exercise	110.0	34.8	7.45	24.6	14.6	**98.1**	2.1	19.8
8		3		exercise	101.0	36.5	7.44	25.3	14.8	**97.7**	2.6	20.0
9		4		exercise	105.0	36.4	7.44	24.9	14.7	**97.9**	1.6	20.1
10		5		exercise	102.0	37.4	7.43	24.8	14.6	**97.9**	1.5	19.8

Additional time stamps:

Date:	9-Aug-02
Gender:	Female
Time:	9:00
Subject No.:	977
Data File(s):	f977raw
	f977trend
Sampling Rate:	1000 Hz
Room Temp (C)	20

uestionnaire Informati

Question No.	*Rating*
1	1
2	1
3	1

Additional Info:

Patient Arterial Data

Time Stamp	File Sample ID	Time	Condition	pO2	pCO2	pH	HCO3	Hb	O2Hb	COHb	O2ct
1	SS		steady state	86.0	37.0	7.43	25.0	15.2	**96.8**	2.0	20.4
2	SS		steady state	76.0	35.1	7.47	25.7	14.0	**96.0**	2.2	18.6
3	R1		rest	79.0	33.6	7.46	24.3	13.4	**96.3**	2.9	17.7
4	R3		rest	87.0	35.0	7.48	26.1	14.0	**97.2**	2.8	18.6
5	R5		rest	84.0	30.9	7.51	25.0	13.7	**97.2**	2.5	18.3
6	FW1		free wheel	67.0	30.3	7.51	24.6	13.8	**95.1**	2.9	18.0
7	FW2		free wheel	61.0	31.9	7.50	25.3	13.9	**93.6**	2.5	17.8
8	2		exercise	56.0	35.3	7.47	25.7	14.1	**91.1**	2.3	17.5
9	3		exercise	57.0	33.9	7.46	24.3	16.4	**91.4**	2.0	20.6
10	4		exercise	54.0	33.7	7.45	23.7	13.9	**89.7**	2.5	17.1
11	5		exercise	54.0	34.6	7.43	23.1	14.2	**89.2**	1.7	17.4
12	6		exercise	51.0	34.6	7.42	22.5	15.5	**86.9**	0.7	18.8
13	PK		peak	48.0	34.3	7.40	21.6	14.7	**83.8**	2.3	16.9
14	PT		post	86.0	29.8	7.40	18.6	14.5	**96.7**	2.6	19.3

Date:	20-Aug-02
Gender:	Female
Time:	9:30
Subject No.:	418
Data File(s):	f418raw
	f418trend
	f418raw1
	f418trend1
Sampling Rate:	1 kHz
Room Temp (C)	20

uestionnaire Informati

Question No.	*Rating*
1	1
2	1
3	1

Additional Info:

Patient Arterial Data

Time Stamp	File Sample ID	Time	Condition	pO2	pCO2	pH	HCO3	Hb	O2Hb	COHb	O2ct
----	SS		steady state	104.0	33.7	7.47	24.6	11.1	**98.0**	2.5	15.0
1	R1		rest	86.0	40.4	7.41	26.1	11.2	**96.6**	2.3	14.9
2	R3		rest	100.0	37.6	7.44	25.9	10.5	**97.7**	1.7	14.3
3	R5		rest	101.0	35.2	7.46	25.5	11.2	**97.8**	2.8	14.9
4	FW1		free wheel	95.0	35.5	7.46	25.5	11.3	**97.5**	2.5	15.1
5	FW2		free wheel	100.0	34.7	7.46	24.8	11.0	**97.8**	2.6	14.8
6	1		exercise	78.0	41.9	7.41	26.5	11.1	**95.6**	2.5	14.6
7	2		exercise	82.0	42.9	7.39	26.4	11.9	**95.9**	2.3	15.7
8	3		exercise	96.0	39.0	7.42	25.4	11.9	**97.4**	2.3	15.9
9	4		exercise	101.0	35.8	7.43	24.2	11.6	**97.7**	2.1	15.6
10	PK		peak	98.0	34.0	7.43	22.6	11.6	**97.6**	2.6	15.6
11	PT		post	110.0	36.0	7.37	21.2	11.5	**97.8**	2.3	15.4

Date:	20-Aug-02
Gender:	Female
Time:	12:00
Subject No.:	85
Data File(s):	f85raw
	f85trend
Sampling Rate:	1kHz
Room Temp (C)	22

Questionnaire Information	
Question No.	*Rating*
1	1
2	1
3	1

Additional Info:

Patient Arterial Data

Time Stamp	File	Sample ID	Time	Condition	pO2	pCO2	pH	HCO3	Hb	O2Hb	COHb	O2ct
---		SS		steady state	100.0	35.1	7.42	22.8	9.3	**97.6**	2.1	12.4
1		R1		rest	89.0	42.4	7.40	26.4	10.3	**96.8**	2.3	13.5
2		R2		rest	90.0	42.0	7.40	26.4	10.2	**96.9**	2.3	13.4
3		FW1		free wheel	94.0	41.0	7.40	26.0	10.3	**97.2**	2.4	13.6
4		FW2		free wheel	96.0	41.4	7.40	25.7	13.7	**97.3**	2.2	18.2
5		1		exercise	94.0	40.9	7.40	25.4	9.4	**97.2**	2.2	12.4
6		2		exercise	84.0	42.7	7.38	25.7	11.5	**96.1**	2.4	15.0
7		3		exercise	94.0	42.0	7.38	25.3	10.9	**97.0**	2.3	14.3
8		4		exercise	99.0	42.2	7.37	24.9	11.1	**97.3**	2.5	14.7
9		5		exercise	102.0	39.9	7.36	22.9	10.6	**97.4**	2.1	14.1
10		6		exercise	109.0	38.9	7.36	22.0	11.1	**97.7**	1.9	14.7
11		PK		peak	108.0	35.0	7.36	20.2	11.0	**97.7**	2.0	14.6
12		PT		post	121	30.3	7.32	15.9	10.6	**98.1**	2.1	14.1

Additional time stamps:

Date:	20-Aug-02
Gender:	Male
Time:	3:15
Subject No.:	949
Data File(s):	f949raw
	f949trend
Sampling Rate:	1kHz
Room Temp (C)	21

Questionnaire Information	
Question No.	*Rating*
1	1
2	1
3	1

Additional Info:

Patient Arterial Data

Time Stamp	File	Sample ID	Time	Condition	pO2	pCO2	pH	HCO3	Hb	O2Hb	COHb	O2ct
1		SS		steady state	91.0	38.8	7.39	23.6	13.0	**96.9**	3.2	17.3
2		R1		rest	92.0	42.3	7.39	26.0	14.2	**97.0**	3.1	18.9
3		R2		rest	95.0	36.8	7.38	22.1	12.1	**97.2**	3.1	16.2
4		R5		rest	94.0	39.5	7.31	20.3	16.1	**96.6**	2.8	21.5
5		FW1		free wheel	95.0	39.8	7.38	23.8	14.0	**97.1**	3.1	18.7
---		FW2		free wheel	101.0	39.2	7.41	24.9	14.5	**97.6**	3.0	19.5
---		1		exercise	99.0	39.6	7.39	24.5	14.3	**97.4**	3.1	19.2
6		2		exercise	124.0	37.0	7.40	23.1	13.5	**98.3**	2.9	18.3
7		3		exercise	100.0	40.1	7.38	24.2	15.1	**97.4**	3.2	20.2
8		4		exercise	100.0	41.1	7.37	23.9	15.2	**97.4**	3.1	20.3
9		5		exercise	105.0	40.8	7.35	22.8	14.0	**97.5**	2.8	18.8
10		PK		peak	96.0	37.7	7.33	20.2	14.6	**96.9**	2.9	19.5
11		PT		post	117.0	34.7	7.27	16	15.7	**97.7**	2.6	21.2
12		PT		post	110	34.1	7.26	15.3	14.9	**97.4**	2.6	50
---		PT		post	107	34.3	7.28	16.4	14.8	**97.3**	2.6	19.8

Date:	22-Aug-02
Gender:	Male
Time:	10:00
Subject No.:	877
Data File(s):	f877raw
	f877trend
Sampling Rate:	1 kHz
Room Temp (C)	21

Questionnaire Information	
Question No.	*Rating*
1	1
2	1
3	1

Additional Info:

Patient Arterial Data

Time Stamp	File	Sample ID	Time	Condition	pO2	pCO2	pH	HCO3	Hb	O2Hb	COHb	O2ct
1		SS		steady state	65.0	32.3	7.44	22.3	17.9	**93.7**	2.4	23.2
2		R1		rest	67.0	32.3	7.44	22.2	17.9	**94.2**	2.6	23.1
3		R3		rest	70.0	33.2	7.43	22.3	17.8	**94.7**	2.3	23.2
4		R5		rest	71.0	32.0	7.44	22.1	18.1	**95.0**	2.6	23.7
5		FW1		free wheel	58.0	31.4	7.45	22.2	18.2	**91.7**	3.0	23.0
6		FW2		free wheel	58.0	32.3	7.44	22.4	18.2	**91.4**	2.8	23.0
7		1		exercise	54.0	31.7	7.45	22.4	18.6	**89.8**	2.7	23.0
8		2		exercise	53.0	32.3	7.44	22.3	18.0	**89.0**	2.6	22.1
9		3		exercise	50.0	31.1	7.44	21.4	18.3	**87.1**	2.6	22.0
10		4		exercise	47.0	31.8	7.44	21.8	18.3	**84.7**	2.4	21.5
11		5		exercise	43.0	30.8	7.44	21.0	18.0	**80.8**	2.1	20.4
12		PK		peak	42.0	32.6	7.41	21.1	18.7	**78.0**	2.9	20.4
13		PT		post	70.0	29.8	7.40	18.8	18.3	**94.4**	2.4	23.7

Date:	22-Aug-02
Gender:	Female
Time:	12:00
Subject No.:	404
Data File(s):	f404raw
	f404trend
Sampling Rate:	1 kHz
Room Temp (C)	22

Questionnaire Information	
Question No.	*Rating*
1	2
2	2
3	2

Additional Info Viagra Study

Patient Arterial Data

Time Stamp	File	Sample ID	Time	Condition	pO2	pCO2	pH	HCO3	Hb	O2Hb	COHb	O2ct
1		SS		steady state	81.0	41.6	7.44	28.8	12.6	**96.3**	1.6	16.6
2		R1		rest	101.0	36.2	7.48	27.6	13.1	**97.9**	1.6	17.6
3		R2		rest	91.0	42.7	7.44	29.2	13.7	**97.2**	2.1	18.1
4		FW1		free wheel	99.0	37.0	7.49	28.4	13.6	**97.8**	1.8	18.3
5		FW2		free wheel	106.0	32.2	7.53	27.2	13.4	**98.2**	2.0	18.0

Date:	22-Aug-02
Gender:	Female
Time:	15:30
Subject No.:	228
Data File(s):	f228raw
	f228trend
Sampling Rate:	1 kHz
Room Temp (C)	22

Questionnaire Information

Question No.	*Rating*
1	1
2	1
3	1

Additional Info:

Patient Arterial Data

Time Stamp	File	Sample ID	Time	Condition	pO2	pCO2	pH	HCO3	Hb	O2Hb	COHb	O2ct
1		SS		steady state	87.0	45.3	7.40	28.6	12.4	**96.5**	2.9	16.1
2		R1		rest	86.0	45.0	7.40	28.5	12.3	**96.5**	2.8	16.2
3		R2		rest	86.0	46.1	7.40	28.8	12.2	**96.4**	2.9	16.0
4		FW1		free wheel	125.0	45.4	7.41	29.0	12.4	**98.3**	2.4	16.7
5		FW2		free wheel	91.0	44.3	7.41	28.6	12.6	**97.0**	2.8	16.6
6		1		exercise	108.0	44.1	7.41	28.6	12.5	**97.8**	2.4	16.7
7		2		exercise	93.0	45.2	7.40	28.6	12.6	**97.1**	2.1	16.7
8		3		exercise	75.0	45.1	7.39	27.9	12.6	**94.9**	2.5	16.5
9		4		exercise	102.0	44.6	7.40	27.9	12.6	**97.6**	2.8	16.7
10		5		exercise	109.0	39.9	7.41	25.8	12.8	**97.9**	2.5	17.1
11		6		exercise	117.0	37.7	7.39	23.2	12.6	**98.1**	2.2	16.9
12		PK		peak	106.0	35.3	7.39	21.7	13.1	**97.7**	2.0	17.7
13		PT		post	111.0	38.6	7.32	20	12.8	**97.6**	2.0	17.1

Date:	23-Aug-02
Gender:	Male
Time:	10:45
Subject No.:	499
Data File(s):	f499raw
	f499trend
Sampling Rate:	1 kHz
Room Temp (C)	20

Questionnaire Information

Question No.	*Rating*
1	1
2	1
3	1

Additional Info New sensor

Patient Arterial Data

Time Stamp	File	Sample ID	Time	Condition	pO2	pCO2	pH	HCO3	Hb	O2Hb	COHb	O2ct
1		R1		rest	57.0	33.7	7.46	24.4	15.7	**91.4**	2.7	19.9
2		R3		rest	58.0	32.2	7.47	23.7	15.4	**92.1**	2.6	19.7
3		R5		rest	56.0	34.0	7.47	25.0	15.9	**91.2**	3.0	20.2
4		FW1		free wheel	52.0	35.6	7.46	25.4	16.1	**88.8**	3.0	19.9
5		FW2		free wheel	48.0	36.8	7.44	25.0	15.9	**85.2**	2.6	19.0
6		1		exercise	48.0	37.9	7.43	25.3	16.3	**84.7**	2.6	19.3
7		2		exercise	47.0	39.5	7.41	25.4	15.9	**82.9**	2.9	18.4
8		3		exercise	41.0	41.7	7.40	25.8	16.1	**75.4**	2.5	17.3
9		PK		peak	41.0	40.8	7.39	24.7	16.0	**74.9**	2.3	16.9
10		PT		post	93.0	37.0	7.39	22.6	16.0	**97.1**	2.7	21.5

Date:	27-Aug-02
Gender:	Male
Time:	15:30
Subject No.:	454
Data File(s):	f454raw
	f454trend
Sampling Rate:	1 kHz
Room Temp (C)	21

Questionnaire Information

Question No.	*Rating*
1	1
2	1
3	1

Additional Info level 3 -- not viagra

Patient Arterial Data

Time Stamp	File	Sample ID	Time	Condition	pO2	pCO2	pH	HCO3	Hb	O2Hb	COHb	O2ct
1		SS		steady state	87.0	39.9	7.38	24.1	11.1	**96.5**	1.2	14.9
2		R1		rest	88.0	38.8	7.39	23.5	11.3	**96.6**	2.1	15.1
3		R2		rest	91.0	38.8	7.39	23.5	11.3	**96.9**	2.0	15.1
4		FW1		rest	97.0	36.4	7.40	22.9	10.0	**97.4**	5.2	13.1
5		FW2		free wheel	86.0	40.8	7.37	23.9	11.5	**96.2**	2.0	15.4
6		1		free wheel	101.0	35.0	7.41	22.7	14.7	**97.6**	2.1	19.9
7		2		exercise	96.0	39.4	7.38	23.8	12.0	**97.2**	2.2	16.2
8		3		exercise	85.0	38.3	7.39	23.2	14.8	**96.3**	2.5	19.7
9		4		exercise	86.0	37.6	7.39	22.9	11.4	**96.4**	2.2	15.3
10		5		exercise	85.0	37.6	7.39	22.8	10.7	**96.3**	3.4	14.2
11		6		exercise	83.0	37.8	7.38	22.7	14.5	**96.0**	2.4	19.3
12		7		peak	86.0	35.6	7.38	21.2	12.1	**96.4**	1.9	16.2
13		8		post	106.0	34.0	7.37	20	12.6	**97.7**	2.3	17.1
14		PK		post	90.0	33.1	7.37	19.4	11.7	**90**	2.4	15.6
15		PT		post	120	33.9	7.34	18.6	11.7	**98.1**	2.3	15.9

Date:	26-Sep-02
Gender:	Female
Time:	10:00
Subject No.:	119
Data File(s):	f119raw
	f119trend
Sampling Rate:	1 kHz
Room Temp (C):	

Questionnaire Information

Question No.	*Rating*
1	2
2	2
3	2

Additional Info:

Patient Arterial Data

Time Stamp	File	Sample ID	Time	Condition	pO2	pCO2	pH	HCO3	Hb	O2Hb	COHb	O2ct
1		SS		steady state	40.0	32.8	7.50	25.9	14.1	**79.7**	2.2	15.4
2		R1		rest	71.0	34.9	7.43	23.6	13.9	**94.8**	2.2	18.0
3		R2		rest	77.0	37.8	7.43	25.5	13.8	**95.7**	2.5	18.1
4		FW1		free wheel	73.0	36.2	7.43	24.5	14.0	**95.2**	2.3	18.3
5		FW2		free wheel	64.0	34.5	7.45	24.3	14.4	**93.6**	2.4	18.4
6		1		exercise	63.0	35.1	7.43	23.7	14.2	**92.9**	2.2	18.1
7		PK		peak	61.0	34.9	7.43	23.6	14.7	**92.3**	1.9	18.5
8		PT		post	45.0	28.5	7.47	21	14.3	**84.3**	1.0	16.4

References

[1] David, D., Michelson, E.L., and Dreifus, L.S., "Ambulatory Monitoring of the Cardiac Patient," Chapter 1, Philadelphia, U.S., F. A. Davis Company, 1988.

[2] Rhee, S., Yang, B-H., and Asada, H., "Artifact-Resistant, Power-Efficient Design of Finger-Ring Plethysmographic Sensors, Part I : Design and Analysis," 22nd Annual International Conference of the IEEE Engineering in Medicine and Biology Society, Chicago IL USA, Jul 23-28, 2000.

[3] http://www.mallinckrodt.com

[4] Tremper, K., Barker, S., "Pulse Oximetry," Anesthesiology, **70**, pp. 98-108, 1989.

[5] Katcher, ML., Shapiro, MM., and Guist, C., "Severe injury and death associated with home infant cardiorespiratory monitors," Pediatrics, vol. **78**(5), pp. 775-779, Nov. 1986.

[6] Hayes, M.J. and P.R. Smith, "Quantitative Evaluation of Photoplethysmographic Artefact Reduction for Pulse Oximetry in Biomedical Sensors, Fibers and Optical Delivery Systems," Stockholm, Sweden: SPIE, 1999.

[7] Barreto, A.B., Vicente, L.M., Taberner, A., "Adaptive Pre-Processing of Photoplethysmographic Blood Volume Pulse Measurements," Biomedical Engineering Conference, Proceedings of the 1996 Fifteenth Southern, pp. 114-117, 1996.

[8] Lictenthal P.R., Wade, L.D., "Evaluation of signal extraction technology (SET) in preventing false alarms when using pulse oximetry in the recovery room," Anesthesiology, vol. **86**(2S), pp. S278, 1996.

[9] Kestin, IG., Miller, BR., and Lockhart, CH., "Auditory alarms during anesthesia monitoring," Anesthesiology, vol. **69**(1), pp. 106-109, Jul. 1988.

[10] Bentt, LR., Santora, TA., et al., "Accuracy and utility of pulse oximetry in the surgical intensive care unit," Curr Surg., vol. **47**(4), pp. 267-268, Jul-Aug. 1990.

[11] Lanza, GA., Lucente, M., et al., "Accuracy in clinical arrhythmia detection of a real-time Holter system," J. Electrocardiol, vol. **23**(4), pp. 301-306, Oct. 1990.

[12] Cooper, DH., Kennedy, HL., et al., "Holter triage ambulatory ECG analysis. Accuracy and time efficiency," J. Electrocardiol, vol. **29**(1), pp. 33-38, Jan. 1996.

[13] Holter, N.J., "New method for heart studies : Continuous electrocardiography of active subjects over long periods is now practical," Science, vol. **134**, pp. 1214, 1961.

[14] Zimetbaum PJ, Josephson, ME., "The evolving role of ambulatory arrhythmia monitoring in general clinical practice," Ann of Intern Med, vol. **130**(10), pp. 848-856, May. 1999.

[15] Bellet, S., Roman, L., et al., "Continuous electrocardiographic monitoring during automobile driving," Am J Cardiol vol. **22**, pp. 856, 1968.

[16] McGrath BP, "Ambulatory blood pressure monitoring.," Med J Aust., vol. **176**(12), pp. 588-592, June 17, 2002.

[17] Wesseling, K. H., de Wit, B., et al., "Physiocal, Calibrating Finger Vascular Physiology for Finapres," Homeostatis, vol. **36**(2-3), pp. 67-82, 1995.

[18] http://www.finapres.com/portapres.pdf

[19] http://www.seiko-pgt.or.jp/english_k.html

[20] http://www.life-assist.com/nonin/onyx.html

[21] Mascaro, S., Chang, K.-W. and Asada, H., "Photo-Plethysmograph Nail Sensors for Measuring Finger Forces Without Haptic Obstruction," Proceedings of the IEEE International Conference on Robotics and Automation, vol. **2**, pp. 962-967, 1999.

[22] Blalock, A., "Shock: further studies with particular reference to the effects of hemorrhage," Arch Surg., vol. **29**, pp. 837-846, 1937.

[23] Clayton DG, "Pulse oximeter probes. A comparison between finger, nose, ear and forehead probes under conditions of poor perfusion," Anaesthesia, vol. **46**(4), pp. 260-265, Apr. 1991.

[24] Guyton, A., Hall, J., "Textbook of Medical Physiology," 9th ed., Philadelphia: W.B. Saunders Company, pp. 199-218, 1996.

[25] Shaltis, P., Rhee, S., Asada, H., "Artifact-Resistant, Power-Efficient, High-Speed Modulation Design for Photo Plethysomographic Ring Sensors," Annals of Biomedical Engineering Conference, Durham, NC USA, Oct 4-7, 2001.

[26] Rhee, S., Yang, B-H. and Asada, H., "The Ring Sensor: a New Ambulatory Wearable Sensor for Twenty-Four Hour Patient Monitoring," Proc. of the 20th Annual International Conference of the IEEE Engineering in Medicine and Biology Society, Hong Kong, Oct, 1998.

[27] Rhee, S., "Design and Analysis of Artifact-Resistive Finger Photoplethysmographic Sensors for Vital Sign Monitoring," Thesis (Ph.D.), Massachusetts Institute of Technology, Dept. of Mechanical Engineering, 2000.

[28] Rhee, S., Yang, B-H and Asada, H., "Artifact-Resistant, Power-Efficient Design of Finger-Ring Plethysmographic Sensors" IEEE Transactions on Biomedical Engineering, vol. **48**(7), pp. 795-805, 2001.

[29] Severinghaus, JW., Honda, Y., "Pulse Oximetry," Int. Anesthesiol Clin., vol. **25**(4), pp. 205, 1987.

[30] Goldie, E.A.G., "A Device for the Continuous Indication of Oxygen Saturation of Circulating Blood in Man," J. Scient. Instruments, vol. **19**, pp. 23-25, 1942.

[31] http://www.masimo.com (2004.)

[32] Zhang, Y., "Multi-channel Blind System Identification for Central Hemodynamic Monitoring," Thesis (Ph.D.), Massachusetts Institute of Technology, Dept. of Mechanical Engineering, 2002.

[33] Higgins, J. L. and Fronek, A., "Photoplethysmographic Evaluation of the Relationship between Skin Reflectance and Skin Blood Volume," Journal of Biomedical Engineering, vol. **8**, pp.130-136, Apr. 1986.

[34] Berne, Robert M. and Levy, Matthew J., "The Cardiovascular System." Physiology, 4th ed. St. Louis: Mosby, Inc., 1998.

[35] Mendelson, Y. and Ochs, B.D., "Noninvasive Pulse Oximetry Utilizing Skin Reflectance Photoplethysmography," IEEE Transactions on Biomedical Engineering, vol. **35**(10), pp. 798-805, 1988.

[36] Mascaro, S., Chang, K.-W. and Asada, H., " Photo-Plethysmograph Nail Sensors for Measuring Finger Forces Without Haptic Obstruction," Proceedings of the IEEE International Conference on Robotics and Automation, vol. **2**, pp. 962-967, 1999.

[37] Guyton, A., Hall, J., "Textbook of Medical Physiology," 9th ed., Philadelphia: W.B. Saunders Company, pp. 199-218, 1996.

[38] Shaltis, P., Rhee, S., Asada, H., "Artifact-Resistant, Power-Efficient, High-Speed Modulation Design for Photo Plethysomographic Ring Sensors," Annals of Biomedical Engineering Conference, Durham, NC USA, Oct 4-7, 2001.

[39] Feng, W., Haishu, D., Fenghua, T., et. al., "Influence of Overlying Tissue and Probe Geometry on the Sensitivity of a Near-Infrared Tissue Oximeter," Physiological Measurement, vol. **22**, pp. 201-208, 2001.

[40] Kumar, G., Schmitt, J.M., "Optimal Probe Geometry for Near-Infrared Spectroscopy of Biological Tissue," Applied Optics, vol. **36**(10), pp. 2286-2293, April 1997.

[41] Yamakoshi, K., Shimazu, H., et al., "New Oscillometric Method for Indirect Measurement of Systolic and Mean Arterial Pressure in the Human Finger. Part 1: Correlation Study," Medical & Biological Engineering & Computing, vol. 20, pp. 307-313, 1982.

[42] R. K. Daniel, D. L. Priest, and D. C. Wheatley, "Etiologic factors in pressure sores: An experimental model," Arch. Physical Med. Rehab., vol. 62, pp. 492–498, 1981.

[43] Shimazu, H., Kawarada, A., et al., "Electric Impedance cuff for the indirect measurement of blood pressure and volume elastic modulus in human limb and finger arteries," Medical & Biological Engineering & Computing, vol. 27, pp. 477-483, 1989.

[44] Asada, H., Rhee, S., "Design and Analysis of Artifact-Resistant Finger Photoplethysmographic Sensors for Vital Sign Monitoring," Phase 2: Final Report, HAHC, 2000.

[45] Asada, H., Shaltis, P., Rhee, S., "Validation and Benchmarking of a High-Speed Modulation Design For Oxygen Saturation Measurement Using Photo Plethysmographic Ring Sensors," Progress Report 3-2, HAHC, 2001.

[46] Stearns, S. and Hush, D., "Digital Signal Analysis," 2nd ed., New Jersey: Prentice Hall, 1999.

[47] Zijlstra, W. G., Buursma, A., and Meeuwsen-van der Roest, W. P., "Absorption Spectra of Human Fetal and Adult Oxyhemoglobin, De-Oxyhemoglobin, Carboxyhemoglobin, and Methemoglobin," Clin. Chem., 37/9:1633-1638, 1991.

[48] Barker, S., Shah, N., "The Effects of Motion on the Performance of Pulse Oximeters in Volunteers," Anesthesiology, 86:101-108, 1997.

[49] Plummer, J. L., Zakaria, A. Z., Ilsley, A. H., Fronsko, R. R. L., and Owen, H., "Evaluation of the influence of movement on saturation readings from pulse oximeters," Anaesthesia, 50: 423-426, 1995.

[50] Barker, S., Shah, N., "The Effects of Motion on the Performance of Pulse Oximeters in Volunteers," Anesthesiology, 86:101-108, 1997.

[51] Hayes, M., Smith, P., "A New Method for Pulse Oximetry Possessing Inherent Insensitivity to Artifact," IEEE Transactions on Biomedical Engineering, 48(4):452-461, 2001.

[52] Widrow, B., Glover, J., McCool, J., Kaunitz, J., et al, "Adaptive Noise Cancelling: Principles and Applications," Proc. IEEE, 63(12): 1692-1716, 1975.

[53] Vicente, L., Barreto, A., and Taberner, A., "Adaptive Pre-Processing of Photoplethysmographic Blood Volume Pulse Measuremments," Proceedings of the 1996 Fifteenth Southern Biomedical Engineering Conference, 114-117, 1996.

[54] Hayes, M., Smith, P., "Artifact Reduction in Photoplethysmography," Applied Optics, 37(31): 7437-7446, 1998.

[55] Rhee, S. Yang B-H and Asada, H., "Design of a Artifact-Free Wearable Plethysmographic Sensor," 21st Annual International Conference of the IEEE Engineering in Medicine and Biology Society, Atlanta GA USA, Oct 13-16, 1999.

[56] Rhee, S., Yang, B-H and Asada, H., "Design and Evaluation of Artifact-Resistant Finger-Ring Plethysmographic Sensors," 2000 ASME International Mechanical Engineering Congress and Exposition, Orlando, Florida, November 5-10, 2000.

[57] Rhee, S. Yang B-H and Asada, H., "Theoretical Evaluation of the Influence of Displacement on Finger Photoplethysmography for Wearable Health Monitoring Sensors," Symposium on Dynamics, Control, and Design of Biomechanical Systems ASME International Mechanical Engineering Congress and Exposition, Nashville, Tennessee, November 14-19, 1999.

[58] König, V., Huch, R., and Huch, A., "Reflectance Pulse Oximetry – Principles and Obstetric Application in the Zurich System," Journal of Clinical Monitoring and Computing, 14: 403-412, 1998.